Department of Energy
Washington, DC 20585

QA: N/A
DOCKET NUMBER 63-001

March 4, 2009

ATTN: Document Control Desk
John H. (Jack) Sulima, Project Manager
Project Management Branch Section B
Division of High-Level Waste Repository Safety
Office of Nuclear Material Safety and Safeguards
U.S. Nuclear Regulatory Commission
EBB-2B2
11545 Rockville Pike
Rockville, MD 20852-2738

YUCCA MOUNTAIN – REQUEST FOR ADDITIONAL INFORMATION – SAFETY EVALUATION REPORT, VOLUME 3, CHAPTER 2.2.1.2.1 (SCENARIO ANALYSIS), THIRD SET (DEPARTMENT OF ENERGY'S SAFETY ANALYSIS REPORT SECTION 2.2, Table 2.2-5)

Reference: Ltr, Sulima to Williams, dtd 02/04/09, "Yucca Mountain – Request for Additional Information – Safety Evaluation Report, Volume 3, Chapter 2.2.1.2.1 (Scenario Analysis), 3rd Set (Department of Energy's Safety Analysis Report Section 2.2, Table 2.2-5)"

The purpose of this letter is to transmit the U.S. Department of Energy's (DOE) responses to the Request for Additional Information (RAI) identified in the above-referenced letter regarding DOE's License Application Section 2.2, Table 2.2-5. The initial set of eleven RAIs was e-mailed by the Nuclear Regulatory Commission (NRC) on January 23, 2009. As stated in the above-referenced letter, NRC would not require DOE to respond to RAI #5. Each RAI response is provided as a separate enclosure. Any DOE references cited in the RAI responses, which have not been previously provided to the NRC, are included with this submittal. All references are available on the Licensing Support Network.

There is one commitment in the enclosed RAI responses under RAI #9. If you have any questions regarding this letter, please contact me at (202) 586-9620, or by email to jeff.williams@rw.doe.gov.

Jeffrey R. Williams, Supervisor
Licensing Interactions Branch
Regulatory Affairs Division
Office of Technical Management

OTM: SEG-0513

Printed with soy ink on recycled paper

Enclosures (17):

Enclosures 1 through 10
Responses to 10 Requests for Additional Information
Volume 3, Chapter 2.2.1.2.1, Set 3, Numbers 1 through 4 and 6 through 11

Enclosures 11 through 17
References cited in the RAI responses that have not been previously provided to the NRC

11. BSC (Bechtel SAIC Company) 2004. *Structural Stability of a Drip Shield Under Quasi-Static Pressure*. 000-00C-SSE0-00500-000-00A. Las Vegas, Nevada: Bechtel SAIC Company. ACC: ENG.20040830.0032.
12. BSC 2005. *Creep Deformation of the Drip Shield*. CAL-WIS-AC-000004 REV 00A. Las Vegas, Nevada: Bechtel SAIC Company. ACC: DOC.20050830.0007.
13. BSC 2008. *Structural Stability of a Drip Shield Under Quasi-Static Pressure*. 000-00C-SSE0-00500-000-00A CACN 001. Las Vegas, Nevada: Bechtel SAIC Company. ACC: ENG.20080312.0017.
14. SNL (Sandia National Laboratory) 2007. *Irrigation Recycling Model.* MDL-MGR-HS-000001 REV 00. Las Vegas, Nevada: Sandia National Laboratories. ACC: DOC.20071105.0005.
15. SNL 2007. *Irrigation Recycling Model.* MDL-MGR-HS-000001 REV 00 ACN 01. Las Vegas, Nevada: Sandia National Laboratories. ACC: DOC.20080117.0001.
16. SNL 2007. *Irrigation Recycling Model.* MDL-MGR-HS-000001 REV 00 ERD 01. Las Vegas, Nevada: Sandia National Laboratories. ACC: LLR.20080414.0002.
17. SNL 2008, *General and Localized Corrosion of the Drip Shield*. ANL-EBS-MD-000004 REV 02 ADD 01 ERD 02. Las Vegas, Nevada: Sandia National Laboratories. ACC: DOC.20081209.0001.

EIE Document Components:

Enclosure #	File Name	File Size, kB
N/A	001_NRC_Transmittal Letter_3.2.2.1.2.1_Set_3.pdf	
1 through 10	002_Enclosures_1_through_10_3.2.2.1.2.1_Set_3.pdf	9,767
11	003_ENG.20040830.0032_00000CSSE00050000000A.pdf	6,519
12	004_DOC.20050830.0007_CALWISAC000004R0A.pdf	4,245
13	005_ENG.20080312.0017_00000CSSE00050000000AC1.pdf	249
14	006_DOC.20071105.0005_MDLMGRHS000001R0.pdf	36,712
15	007_DOC.20080117.0001_MDLMGRHS000001R0ACN1.pdf	3,322
16	008_LLR.20080414.0002_MDLMGRHS000001R0ERD1.pdf	3,907
17	009_DOC.20081209.0001_ANLEBSMD000004R2AD1E2.pdf	14,115

cc with Enclosures 1 through 10:

B. J. Benney, NRC, Rockville, MD
J. C. Chen, NRC, Rockville, MD
J. R. Davis, NRC, Rockville, MD
A. S. Mohseni, NRC, Rockville, MD
N. K. Stablein, NRC, Rockville, MD
D. B. Spitzberg, NRC, Arlington, TX
J. D. Parrott, NRC, Las Vegas, NV
L. M. Willoughby, NRC, Las Vegas, NV
Jack Sulima, NRC, Rockville, MD
Christian Jacobs, NRC, Rockville, MD
Lola Gomez, NRC, Rockville, MD
W. C. Patrick, CNWRA, San Antonio, TX
Budhi Sagar, CNWRA, San Antonio, TX
Bob Brient, CNWRA, San Antonio, TX
Rod McCullum, NEI, Washington, DC
B. J. Garrick, NWTRB, Arlington, VA
Bruce Breslow, State of Nevada, Carson City, NV
Alan Kalt, Churchill County, Fallon, NV
Irene Navis, Clark County, Las Vegas, NV
Ed Mueller, Esmeralda County, Goldfield, NV
Ron Damele, Eureka County, Eureka, NV
Richard Cervantes, Inyo County, Independence, CA
Chuck Chapin, Lander County, Battle Mountain, NV
Connie Simkins, Lincoln County, Pioche, NV
Linda Mathias, Mineral County, Hawthorne, NV
Darrell Lacy, Nye County, Pahrump, NV
Jeff VanNeil, Nye County, Pahrump, NV
Joe Kennedy, Timbisha Shoshone Tribe, Death Valley, CA
Mike Simon, White Pine County, Ely, NV
K. W. Bell, California Energy Commission, Sacramento, CA
Barbara Byron, California Energy Commission, Sacramento, CA
Susan Durbin, California Attorney General's Office, Sacramento, CA
Charles Fitzpatrick, Egan, Fitzpatrick, Malsch, PLLC

RAI Volume 3, Chapter 2.2.1.2.1, Third Set, Number 1:

Provide a technical basis for exclusion of FEP 1.1.03.01.0A, Error in Waste Emplacement, that is consistent with a screening decision of low consequence. This information is needed to verify compliance with 10 CFR 63.114 (e), (f).

Basis: In SAR Table 2.2-5 the FEP 1.1.03.01.0A is classified as excluded based on low consequence. Table 2.2-5 refers to SNL (2008) for further discussion of the technical bases for screening decision. The document SNL (2008, p. 6-39) states that FEP 1.1.03.01.0A is excluded by regulation. The version ERD 01 of the SNL (2008) corrects the screening decision as excluded on the basis of low consequence (in consistency with SAR Table 2.2-5). However, the screening argument was not updated to address consequence of errors in waste emplacement.

1. RESPONSE

The exclusion justification for FEP 1.1.03.01.0A, Error in Waste Emplacement, states the possible types of waste emplacement errors as: (1) emplacement of waste packages closer to each other than in the design specification and (2) emplacement of a waste package so that it straddles a known Quaternary fault with the potential for significant displacement (SNL 2008). In general, waste package emplacement errors can be defined as departures from specified requirements. Examples could include: not emplacing waste packages in conformance with the emplacement drift loading plan, emplacing waste packages too far apart, emplacing a waste package outside the waste package end points in a drift, and emplacing waste packages on faults encountered during excavation. Specifically with respect to postclosure repository performance, the relevant requirements for waste emplacement are summarized by the parameters that require controls to ensure the postclosure performance assessment analytical bases are established and maintained during design, construction, procurement, operations, and closure. Those postclosure control parameters relevant to waste package emplacement are identified and described in Table 1, which is adapted from SAR Tables 1.3.3-8 and 1.3.4-5, and Table 2, which is adapted from SAR Table 1.3.4-5. Each control parameter has either a control parameter value or range of values or a constraint relevant to the as-emplaced design configuration or emplacement operations. Some of the controls are related to controlled interface parameters. These represent parameters that are controlled through the configuration management system presented in SAR Chapter 5. Some control parameters are related to procedural safety controls, which apply when there are specific and unique operator, inspector, or verification activities required by the control parameter that are not addressed by standard administrative controls such as those management systems identified in SAR Chapter 5. Both the procedural safety controls and design configuration are controlled by management systems identified in SAR Chapter 5.

Effective implementation of these management systems will ensure that potentially significant waste package emplacement errors will be detected, evaluated, and mitigated as necessary during the operational period. Therefore, it is the potential consequences of undetected and unmitigated waste emplacement errors that must be considered further. Errors resulting in damage to waste

packages, errors in emplacement spacing, and possible emplacement on faults are discussed below.

The potential that a waste package is subjected to handling damage during emplacement without the damage being detected is considered as part of included FEP 2.1.03.08.0A (Early Failure of Waste Packages). Handling damage is defined as any visible gouging or denting of the waste package surface that may jeopardize the performance of the Alloy 22 outer corrosion barrier. As described in SAR Section 2.3.6.6.3.2, the analysis considered possible damage between receipt and final inspection at the time of emplacement, including but not limited to possible damage associated with tilting to upright position, downending, and placement on the pallet. The mean and median probabilities of improper waste package handling causing damage and not being detected are 9.63×10^{-7} and 7.71×10^{-7} per waste package, respectively. This probability distribution was considered along with probability distributions for improper base material selection, improper heat treatment of the outer shell and lid, improper weld filler material, and improper low-plasticity burnishing, to develop an overall distribution for the probability of early waste package failure per waste package, which is characterized by a lognormal distribution with a mean of 1.13×10^{-4} and an error factor of 8.17 (SNL 2007, Section 6.5.1). For the repository inventory of approximately 11,600 waste packages, the mean number of early-failed waste packages is slightly more than one. While the damage mechanisms leading to early failure are expected to result in enhanced probability of stress corrosion cracking, the waste packages are treated as completely failed at the time of repository closure.

The potential that waste package emplacement errors could result in a violation of thermal line loading requirements per the approved emplacement drift loading plan (SAR Section 1.3.1.2.5) is also relevant to this FEP. Thermal management of the waste packages is required to maintain the integrity of engineered barrier components and to ensure that natural or altered conditions of the host rock conform to conditions analyzed for long-term repository performance (see SAR Section 2.3.5.4.3). The emplacement of waste packages is controlled through a loading plan that determines waste package loading sequences and interfaces with the repository operations to maintain temperatures within prescribed limits during the preclosure period. In the preclosure period, these operations establish the initial conditions for closure so that, upon termination of ventilation at closure, the thermal loading in the repository results in temperature transients during the thermal pulse that are consistent with the conditions analyzed in the repository performance assessment.

The probability of waste package misplacement and the probability that such misplacement may result in violation of the thermal limits for the repository have been calculated. The probability associated with placing a waste package in the wrong location is 4.0×10^{-6} per demand. The probability of placing a waste package in the right location, but with the wrong thermal load is 2.6×10^{-5} per demand. The combined probability of either placing a waste package in the wrong location, or emplacing with the wrong thermal load, is:

$$4.0 \times 10^{-6} + 2.6 \times 10^{-5} = 3.0 \times 10^{-5}$$

For the repository inventory of approximately 11,600 waste packages, the mean number of misplaced waste packages is considerably less than one. A misplaced waste package does not

affect the performance of adjacent waste packages. The possible consequences of errors in waste emplacement spacing are therefore bounded by the already low consequences of the waste package early failure modeling case included in the performance assessment (SAR Figure 2.4-18 and SAR Figure 2.4-35), which considers consequences of failures due to undetected manufacturing defects and handling damage that are assumed conservatively to fully compromise the flawed package.

Table 1. Summary of Conformance of Subsurface Facility Design to Postclosure Control Parameters Relevant to Waste Package Emplacement Spacing

Postclosure Control Parameter Number and Title	**Postclosure Control Parameter Value, Range of Values or Constraints**	**Design Criteria/Configuration**	**Postclosure Procedural Safety Control**
02-01, As-Emplaced Waste Configuration (Controlled Interface Parameter);	The configuration for the emplaced waste packages shall be controlled through the configuration management system (Section 5).	The process for emplacing the waste packages and maintaining the configuration of their emplacement are described in Section 1.3.4.8.2. This process includes the operational and monitoring controls related to the in-drift positioning of the waste packages. Design considerations for emplacement of sequences of waste packages in a drift for thermal management purposes are described in Section 1.3.1.2.5.	NA
03-21 Waste package handling	The waste package shall be handled in a controlled manner during fabrication, handling, transport, storage, emplacement, installation, operation, and closure activities to minimize damage; surface contamination; and exposure to adverse substances.	NA (Background information: Criteria and design considerations for safe handling of the waste package from the surface facilities to the emplacement areas underground are described in Section 1.3.3.5. The waste package, when being transported in the TEV, rests on its pallet, and the surfaces of the waste package do not contact any other surfaces other than the pallet supports. Speed of travel of the TEV is designed and controlled to a slow rate and the pallet is restrained inside the shielded compartment so that its load is prevented from moving and incurring).	The waste package emplacement procedures will include handling requirements to limit activities that could physically degrade, contaminate and limit exposure of adverse substances to the surface of the waste package. Inspection procedures will be developed to identify damage, surface contamination or exposure to adverse substances at the time of waste package emplacement. The TEV will have adequate means to inspect visible waste package surfaces. The operational and monitoring controls applicable to the TEV when handling the waste package on its pallet from the surface facilities to the underground turnouts are described in Section 1.3.3.5.2.3. Travel and movements of the TEV are controlled, and documented by remote operators from the CCCF.

Table 1. Summary of Conformance of Subsurface Facility Design to Postclosure Control Parameters Relevant to Waste Package Emplacement Spacing (continued)

Postclosure Control Parameter Number and Title	Postclosure Control Parameter Value, Range of Values or Constraints	Design Criteria/Configuration	Postclosure Procedural Safety Control
03-22 Waste package handling and emplacement	Waste package handling and emplacement activities shall be monitored through equipment with resolution capable of detecting waste package damage. An operator and an independent checker shall perform the operations.	NA (Background Information: In order to minimize damage, the pallet carrying the waste package is restrained inside the shielded compartment of the TEV and there is no movement or handling of the waste package inside the TEV when in transit. Handling of the pallet holding the waste package during emplacement is limited to lowering of the loaded pallet on to the emplacement).	The operational and monitoring controls on the waste package emplacement system are presented in Sections 1.3.4.8.2.3 and 1.3.4.8.2.4, respectively. Procedures will be used to control the inspection by an operator and independent checker of the handling of the loaded pallet during emplacement. This inspection will be conducted remotely from the CCCF, using high-resolution cameras and by monitoring and verification of operational steps. The TEV operational steps are described in Sections 1.3.3.5.2.1 and 1.3.4.8.2.2.
05-01, Waste Package Handling and Emplacement	Waste package handling and emplacement activities shall be monitored through appropriate equipment. An operator and an independent inspector shall verify proper waste package installation.	NA (Background information: The operational and monitoring controls on the waste package emplacement system are presented in Sections 1.3.4.8.2.3 and 1.3.4.8.2.4, respectively. Design of monitoring equipment, instrumentation, and sensors that are part of the transport and emplacement vehicle and that are needed to satisfy this requirement is described in Section 1.3.4.8.2.5.)	The waste package handling and emplacement procedures will be developed and include requirements for monitoring during handling. Verification of waste package handling will be done by an operator from the remote CCCF location with the use of high-resolution cameras and electronic sensors. An independent inspector will verify the adequacy of the emplacement.
05-02, Waste Package Spacing	Adjacent waste packages in a given emplacement drift shall be emplaced 0.1 m (nominal) apart, from the top surface of the upper sleeve of one waste package to the bottom surface of the lower sleeve of the adjacent waste package.	NA (Background information: The design of the TEV is to emplace a waste package at a nominal spacing of 10 cm from a previously emplaced waste package as presented in Section 1.3.4.8.2.1.)	The waste package emplacement procedures will be developed and include emplacement limitations to be met. Monitoring equipment, instrumentation, and sensors that are part of the TEV are used to control this operation. The controls and instrumentation needed to satisfy this requirement are described in Section 1.3.4.8.2.5.

Source: Adapted verbatim from SAR Tables 1.3.3-8 and 1.3.4-5.

The postclosure control parameter relevant to waste package emplacement on a Quaternary fault with potential for significant displacement is identified and described in Table 2, which is adapted from SAR Table 1.3.4-5.

Table 2. Summary of Conformance of Subsurface Facility Design to Postclosure Control Parameters Relevant to Waste Package Emplacement on a Fault

Postclosure Control Parameter Number and Title	Postclosure Control Parameter Value, Range of Values or Constraints	Design Criteria/ Configuration	Postclosure Procedural Safety Control
01-05 Repository Standoff from Quaternary Fault*	The emplacement drifts shall be located a minimum of 60 m from a Quaternary fault with potential for significant displacement*	The repository design has located the emplacement openings with a minimum standoff of 60 m from a Quaternary Fault with potential for significant displacement* (Section 1.3.2.2.1).	NA

Source: Adapted verbatim from SAR Table 1.3.4-5 (except for * note).

* There are two known Quaternary faults with potential for significant displacement in the immediate vicinity of the repository area: the Solitario Canyon Fault and the Bow Ridge Fault (SAR Section.3.4.2.2).

Quaternary faults other than the Solitario Canyon Fault and the Bow Ridge Fault exist within the general area of the repository block (as shown in SAR Figure 1.1-73). Some Quaternary faults are expected to be encountered during construction (e.g., SAR Figure 1.1-61), some of which may not be known at present. For postclosure, the potential for fault displacement (offset) along unknown faults/splays and its potential impact on waste packages are explicitly included in the TSPA as described in included FEP 1.2.02.03.0A (Fault Displacement Damages EBS Components). As discussed in SAR Section 2.3.4.5.5.1, postclosure fault displacement could impact key Engineered Barrier System (EBS) components by causing mechanical damage to the waste packages and drip shields. Potential faulting within the emplacement drifts generally results in small displacements along the faults. With the exception of the Solitario Canyon Fault and the Ghost Dance Fault, which are immediately outside the western and eastern boundaries of the emplacement drifts, a fault displacement of greater than 0.1 cm is associated with a mean annual exceedance frequency of less than 10^{-5} per year (SNL 2007, Section 6.11). In addition, only the small number of waste packages located directly above faults is subject to damage from fault displacement. The small contribution to mean annual dose from emplacement of waste packages on faults is calculated in the seismic fault displacement modeling case in the performance assessment (SAR, Section 2.4.1.2.4), and need not be further considered in this FEP exclusion justification.

CONCLUSIONS

Proposed 10 CFR 63.114(e) provides that "Specific features, events, and processes must be evaluated in detail if the magnitude and time of the resulting radiological exposures to the reasonably maximally exposed individual, or radionuclide releases to the accessible environment, would be significantly changed by their omission." Conversely, a FEP may be excluded from the TSPA if radiological exposures to the reasonably maximally exposed

individual, or radionuclide releases to the accessible environment, would not be significantly changed by its omission.

In addition to the operational requirements and safety controls to avoid waste emplacement errors described above, postclosure control parameters will be subject to quality assurance controls applied in accordance with 10 CFR 63.142, as discussed in the exclusion justification for FEP 1.1.08.00.0A, Inadequate Quality Control and Deviations from Design. Through the application of the controls, the analytical bases of the performance assessment will be established and maintained during the preclosure period. As discussed in SAR Section 1.9.2, the use of appropriate management systems will ensure that postclosure control parameters will be maintained during design, construction, procurement, operations, and closure. Effective implementation of these controls and management systems will ensure that potentially significant waste package emplacement errors will be detected, evaluated, and mitigated as necessary during the operational period. There are no reasonably foreseeable emplacement errors that might remain undetected and unmitigated at the time of closure that would result in fully compromising a waste package, and the consequences of undetected and unmitigated emplacement errors are therefore bounded by the already low consequences of the waste package early failure modeling case included in the performance assessment (SAR Figure 2.4-18 and SAR Figure 2.4-35), which considers consequences of failures due to undetected manufacturing defects that are assumed conservatively to fully compromise the flawed package. As a result, the magnitude and time of the resulting radiological exposures to the reasonably maximally exposed individual, or radionuclide releases to the accessible environment, would not be significantly changed by the exclusion of FEP 1.1.03.01.0A.

2. COMMITTMENTS TO NRC

None.

3. DESCRIPTION OF PROPOSED LA CHANGE

None.

4. REFERENCES

SNL (Sandia National Laboratories) 2007. *Seismic Consequence Abstraction.* MDL-WIS-PA-000003 REV 03. Las Vegas, Nevada: Sandia National Laboratories. ACC: DOC.20070928.0011.

SNL 2008. *Features, Events, and Processes for the Total System Performance Assessment: Analyses*. ANL-WIS-MD-000027 REV 00. Las Vegas, Nevada: Sandia National Laboratories. ACC: DOC.20080307.0003; DOC.20080407.0009; LLR.20080522.0166.

RAI Volume 3, Chapter 2.2.1.2.1, Third Set, Number 2:

Evaluate the effect of other credible groundwater flow lines on the capture zone geometry and well recapture fraction or justify why other likely alternatives should not be analyzed. For example, nonparallel flow lines that converge near the compliance boundary may imply a capture zone that widens with upstream distance from the well. This information is needed to verify compliance with 10 CFR 63.114 (e).

Basis: The capture zone geometry of the irrigation recycling model to support the FEP screening argument (Sandia National Laboratories, 2008) is based on an idealized system of a pumping well applied to a background of uniform, parallel groundwater flow lines. Observations in northern Amargosa Valley indicate flow lines converge near the compliance boundary and may support a different shape of the well capture zone that widens with increasing upstream distance from the well. A wider capture zone may increase the well recapture fraction compared to the assumed capture zone geometry for uniform, parallel groundwater flow lines. Increasing the well recapture fraction increases both the amount of recycling and estimated concentrations of radionuclides in groundwater.

1. RESPONSE

The response to this RAI demonstrates that the well capture zone analysis based on uniform, parallel groundwater flow lines used in support of the screening decision for FEP 1.4.07.03.0A, Recycling of Accumulated Radionuclides from Soils to Groundwater, provides an adequate evaluation of the well recapture fraction, relative to uncertainties and conservative assumptions utilized in the irrigation recycling model. An analysis using convergent groundwater flow lines that are representative of conditions near the compliance boundary is documented in this response for comparison to the cumulative distribution function (CDF) of recapture fraction upon which the irrigation recycling model is based. As shown in the following discussion, the simpler approach of uniform, parallel flow lines used in *Irrigation Recycling Model* (SNL 2007a), has only a small effect on uncertainty in the recapture fraction, and does not significantly impact the screening justification.

The convergence of groundwater flow in the saturated zone in the area near the compliance boundary is quantified using the results of *Saturated Zone Site-Scale Flow Model* (SNL 2007b). The average simulated values of specific discharge in two areas along the flow path from beneath the repository are compared for this purpose. The average specific discharge across the approximate width and depth of simulated particle paths from the repository at the compliance boundary is 4.31 m/yr. The corresponding average specific discharge from the model in an area 6-km upgradient is 3.03 m/yr. The specific discharge is evaluated at a distance of 6-km upgradient from the compliance boundary because the distribution of distances to fields associated with the pumping well in the irrigation recycling model is generally less than 6 km and because flow paths from beneath the repository are located within alluvium over this distance. The factor by which specific discharge increases over this representative 6-km distance (or the factor of groundwater convergence) is 1.42.

An approximate analytical solution is implemented for the delineation of the well capture zone for a convergent groundwater flow field in which the ambient groundwater specific discharge is assumed to decrease as a linear function of the distance upgradient from the pumping well. This solution calculates the width of the capture zone as a function of the local specific discharge at varying distance upgradient or downgradient from the pumping well. Example solutions of the well capture zones for a uniform flow field that is flowing from north to south (solid black line) and for a linear convergent flow field (dashed red line) are shown in Figure 1. The well capture zone for convergent flow shown in the figure is for a convergence factor of 1.42. As expected, the well capture zone for convergent flow widens with upstream distance from the well, relative to the capture zone for a uniform ambient flow field. The capture zone downgradient of the well is slightly smaller for convergent flow lines, relative to the uniform flow field, although the fact that the red dashed line in the figure is inside the black line is difficult to discern. In the example shown in Figure 1, even though the red dashed line and the black line appear to be the same, the stagnation point of the capture zone is 458.3-m downgradient of the well for the convergent flow field, compared to 475.8-m downgradient for the uniform flow field.

The Monte Carlo analysis of the recapture fraction performed to support the irrigation recycling model (SNL 2007a) is modified to incorporate the approximate solution for the well capture zone in a convergent flow field with a convergence factor of 1.42. The resulting CDF of recapture fraction for convergent flow conditions is plotted in Figure 2, along with the CDF for a uniform flow field. Comparison between the CDFs for convergent and uniform flow shows that the values of recapture fraction are somewhat higher for the convergent flow analysis. The mean value of the well recapture fraction for the uniform flow field is 0.122, and the mean value for the convergent flow case is 0.129. Although the area within the capture zone for the convergent flow case is significantly larger for regions more than about 2 km upgradient from the pumping well (see Figure 1), the CDF for the recapture fraction for the convergent flow case is not much higher than the CDF for the uniform flow case. This is because the density of potential irrigated field locations used in the analysis is much higher near the pumping well than for locations more distant from the well. Therefore, widening of the capture zone at greater distances upgradient from the pumping well has a lesser impact on the recapture fraction.

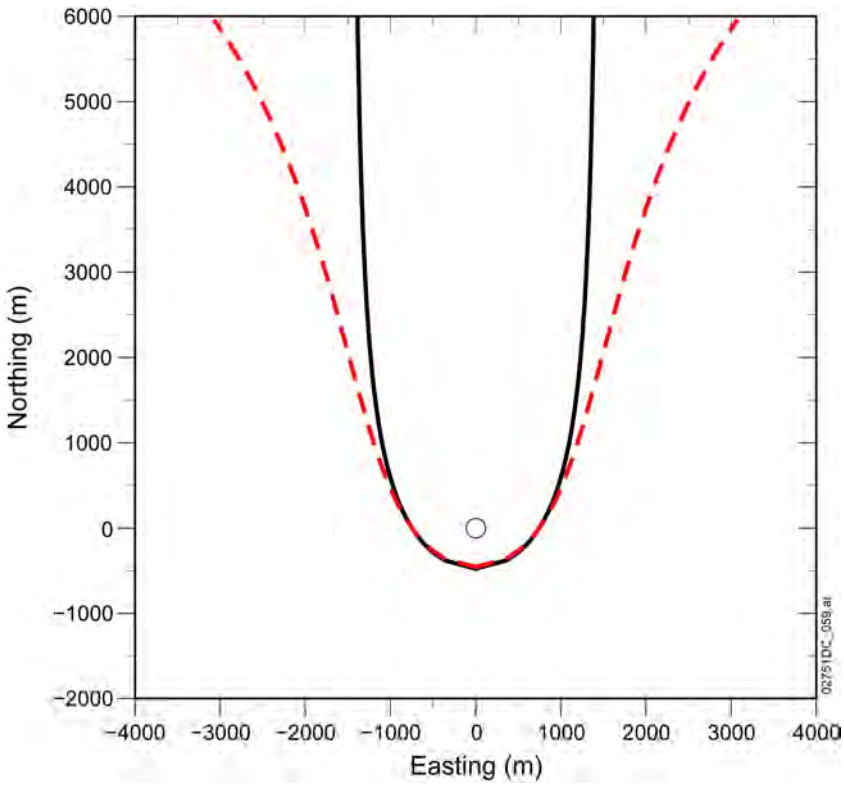

NOTE: Solid black line is the well capture zone for a uniform groundwater flow field and the dashed red line is the well capture zone for a convergent flow field.

Figure 1. Example Well Capture Zones for Uniform and Convergent Groundwater Flow Fields

Differences between the CDFs of recapture fraction for the convergent and uniform flow cases shown in Figure 2 are small relative to the overall uncertainty in the recapture fraction. The difference in the mean recapture fraction for convergent versus uniform groundwater flow is 0.007 (i.e., 0.129 to 0.122). The difference in recapture fraction over the uncertainty range from the 5th to the 95th percentile (i.e., corresponding to recapture fraction values of 0.068 and 0.255, respectively) from the Monte Carlo analysis for uniform groundwater flow that was used in the FEP screening justification is 0.187 (i.e., 0.255 to 0.068), which is much larger than the difference in the mean recapture fraction for convergent versus uniform groundwater flow.

The difference in the consequences for the recycling of accumulated radionuclides resulting from differences in the recapture fraction for the convergent and uniform flow cases is also small. A simple bounding method of evaluating the consequences of recycling is to calculate the equilibrium increased concentration of a contaminant in groundwater as a function of the recapture fraction using Equation 1:

$$\frac{C}{C_o} = \frac{1}{(1 - F_c)} \qquad \text{(Eq. 1)}$$

where C is concentration with recycling, C_0 is the initial concentration, and F_c is the recapture fraction. Using the mean values of the recapture fraction (0.122 and 0.129), the factors by which radionuclide concentrations would increase by recycling are 1.14 assuming the uniform flow field and 1.15 for the convergent flow field case. The difference between these factors is not significant.

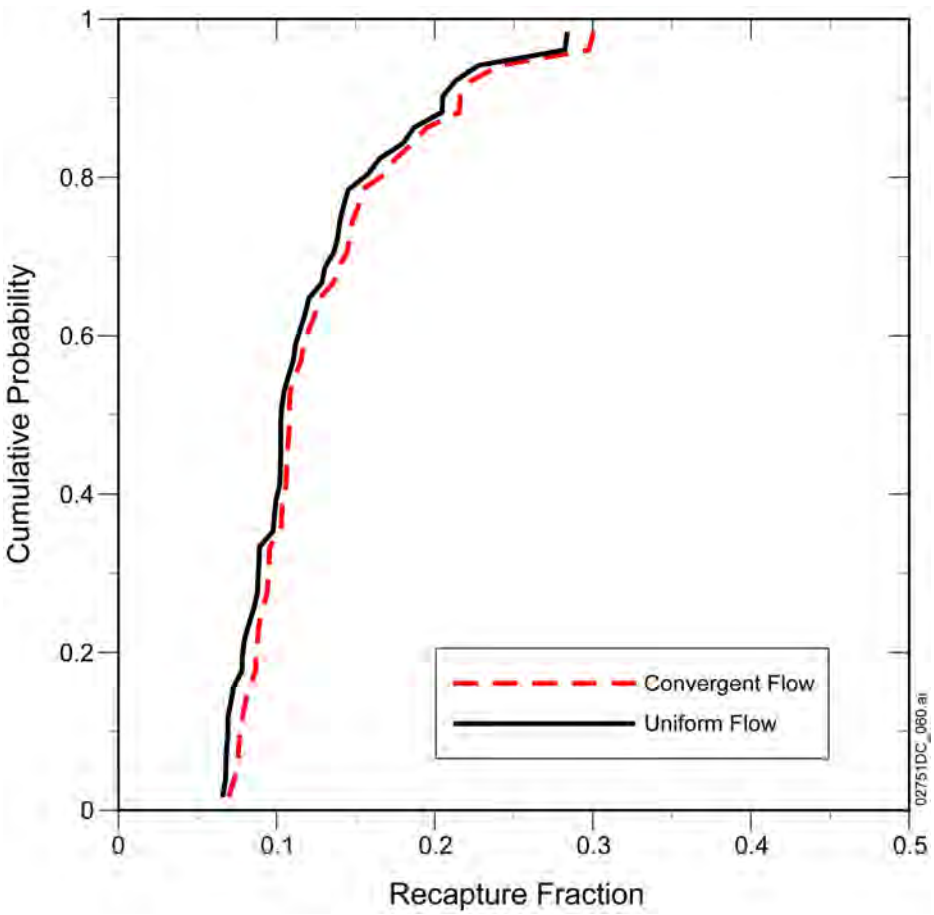

Figure 2. Cumulative Distribution Functions of Well Recapture Fraction for Uniform and Convergent Groundwater Flow Fields

Impacts of differences in the CDFs of recapture fraction for the convergent and uniform flow cases are small relative to the impacts of conservative assumptions incorporated in the irrigation recycling model (SNL 2007a). The regulations state that the reasonably maximally exposed individual lives above the highest concentration in the plume and uses well water with the average radionuclide concentrations in 3,000 acre-ft/yr (10 CFR 63.312 (a) and (c)) for the purposes of calculating dose. These assumptions have been carried forward into the irrigation recycling model, and the pumping well is assumed to operate continuously at a single location in the center of the contaminant plume. Continuous pumping at one location in the resulting model is inconsistent with current irrigation practices in the region, and is conservative with respect to assessments of the possible impacts of irrigation recycling of accumulated radionuclides. Pumping wells associated with irrigated agriculture in the region do not operate indefinitely at one location, but their operation varies in space and time in response to factors such as

economics and land ownership. A more realistic situation in which pumping wells operate at different locations relative to the contaminant plume and at different times would tend to result in lower consequences from the recycling of accumulated radionuclides, relative to the irrigation recycling model. Overall, the effects of the small change in the CDF of the recapture fraction due to convergent groundwater flow are not significant relative the conservative assumptions associated with the location and operation of the pumping well in the irrigation recycling model.

In conclusion, the analysis of the well recapture fraction assuming uniform and parallel groundwater flow lines provides an adequate basis for the uncertainty in this parameter in the irrigation recycling model and for the decision to exclude FEP 1.4.07.03.0A, Recycling of Accumulated Radionuclides from Soils to Groundwater. The modified analysis of the uncertainty in the well recapture fraction for a convergent groundwater flow field results in somewhat higher values of the recapture fraction. However, differences in the values of the recapture fraction for uniform and convergent flow fields are small, relative to the overall uncertainty in this parameter. The differences in the recapture fraction for uniform and convergent flow fields have only a minor impact on the equilibrium radionuclide concentration increases due to recycling. In addition, the impact on the CDF of well recapture fraction of assuming a uniform flow field is small, relative to conservative assumptions embodied in the irrigation recycling model.

2. COMMITMENTS TO NRC

None.

3. DESCRIPTION OF PROPOSED LA CHANGE

None.

4. REFERENCES

SNL (Sandia National Laboratory) 2007a. *Irrigation Recycling Model.* MDL-MGR-HS-000001 REV 00. Las Vegas, Nevada: Sandia National Laboratories. ACC: DOC.20071105.0005; DOC.20080117.0001; LLR.20080414.0002.

SNL 2007b. *Saturated Zone Site-Scale Flow Model.* MDL-NBS-HS-000011 REV 03. Las Vegas, Nevada: Sandia National Laboratories. ACC: DOC.20070626.0004.

RAI Volume 3, Chapter 2.2.1.2.1, Third Set, Number 3

Demonstrate that distributions of distances between a hypothetical well and irrigated fields are representative of actual distances of irrigation supply wells to irrigated fields, or justify the differences and assess the effect of those differences on the well recapture fraction. This information is needed to verify compliance with 10 CFR 63.114 (e).

Basis: Distributions of distances from wells to irrigated fields were developed to determine the well recapture fraction (Sandia National Laboratories, 2008). Based on current water usage in Amargosa Valley, about 90 percent of withdrawn water is used for irrigation. To quantify distances from the single hypothetical water supply well to the fields, the FEP screening analysis assumed that the well could be located anywhere within the community and calculated distributions of distances for the first, second, third, and fourth closest irrigated fields from the well for the set of random well locations. Because the placement of irrigation supply wells is not likely to be random, irrigation practices in Amargosa Valley may indicate that irrigation wells were closer to the field than modeled. In the DOE model, a reduction in the distances of fields to the well corresponds to a greater well recapture fraction and increased amount of radionuclide recycling.

1. RESPONSE

The response to this RAI demonstrates that using the distribution of distances between a hypothetical well and irrigated fields described in FEP 1.4.07.03.0A, Recycling of Accumulated Radionuclides from Soils to Groundwater (SNL 2008a), is appropriate for calculating well recapture fraction, and that the resulting probability distribution of the well recapture fraction does not underestimate the amount of radionuclide recycling due to irrigation. The response justifies the differences between distances from the hypothetical well to irrigated fields and the actual distances, based on an assessment of the impact of those differences on the well recapture fraction and groundwater concentration. This assessment compares the results from the biosphere-based irrigation recycling model (SNL 2007a) with a more realistic geosphere-based irrigation recycling model, which demonstrates that the impacts of irrigation recycling are overestimated by the biosphere-based irrigation recycling model.

1.1 BIOSPHERE-BASED IRRIGATION RECYCLING MODEL

The screening decision on FEP 1.4.07.03.0A, Recycling of Accumulated Radionuclides from Soils to Groundwater, was based on the analysis performed using a biosphere-based irrigation recycling model (SNL 2007a). A distribution of distances from wells to irrigated fields was developed in this analysis to determine the well recapture fraction. The well recapture fraction represents the fraction of water used for irrigation that is recaptured by the well and is incorporated in the irrigation recycling model using a cumulative probability distribution. The well recapture fraction is a lumped steady-state parameter that accounts in a simplified and conservative way for complex transient physical processes that would occur if irrigation with contaminated groundwater took place within the hypothetical community and the irrigation practice was similar to the one currently used in the Amargosa Desert area. This lumped

parameter was introduced to address the following assumptions about groundwater usage consistent with the regulatory framework:

1. The irrigation takes place within a hypothetical community located at or in the vicinity of the boundary of the accessible environment.

2. All the water used by the hypothetical community is withdrawn from a hypothetical well placed at the point of the highest concentration in the plume (location of the well NC_EWDP-19D). The well location is fixed for all the period of simulation.

3. The hypothetical community uses the groundwater at the rate equal to the annual water demand of 3,000 acre-ft.

Because of the assumptions listed above, a stylized biosphere-based model of irrigation recycling was developed rather than a process model. This stylized model considers one well located in the middle of the contaminant plume pumping at a constant rate equal to 3,000 acre-ft/yr throughout the period of simulation (SNL 2007a). The radionuclide concentrations in the annual water demand volume are calculated based on the radionuclide release rates from the saturated zone at the boundary of the accessible environment and the radionuclide concentrations in the irrigation water recaptured by the well. The well recapture fraction remains constant during the entire period of simulation.

The current irrigation practice in the Amargosa Desert area is significantly more complicated than simulated in the stylized irrigation recycling model. Irrigation takes place at a number of locations in the Amargosa Desert area. A common irrigated field is confined within a quarter mi^2 section and has a round shape. The irrigation well is located approximately in the middle of the field as dictated by the center-pivot irrigation method commonly used in this area. The predominant crop is alfalfa and the water demand of alfalfa is about 5 ft/yr (or 5 acre-ft/acre-yr). The areal photographs of the Amargosa Desert area, which were taken at different times, show that irrigated fields change locations through time. Irrigation at some locations was discontinued and irrigation at other locations was recently introduced. Consequently, applying the existing irrigation practice to the hypothetical community located at the boundary of the accessible environment requires simulating multiple wells and multiple irrigated fields (i.e., at least four simultaneously pumping wells and irrigated fields of 160 acres each, based on the annual water demand of 3,000 acre-ft defined for the hypothetical community) that change place within the community during the simulation period. The distances from the wells to the corresponding irrigated fields are close to zero because the wells are located approximately in the middle of the fields.

The probability distribution developed for the well recapture fraction allowed for incorporating the important features of the current irrigation practice into the stylized irrigation recycling model in a simplified and conservative way. This was done by introducing the probability distributions of the distances from a single hypothetical well to the four irrigated fields (SNL 2007a). The distances to the irrigated fields were used to account in a simplified way for the different locations of the irrigated fields within the hypothetical community boundaries. The multiple locations of the irrigated fields generated using these distributions and shown in

Figure 1 represent all the possible locations at which the irrigation would take place during the different periods of time over the period of simulation if a hypothetical community similar to the Amargosa Desert community existed at this location. Thus, these distances characterize the size of the hypothetical community. It was assumed that the fraction of all the possible locations that fall inside the hypothetical well capture zone during the period of simulation represents the well recapture fraction. This was a simplified way to account for the periods of time during which the irrigation was occurring outside the well capture zone in the stylized model in which the hypothetical well was fixed at one location and could not be moved with the field. The confined aquifer and unconfined aquifer capture zones shown in Figure 1 are for a single realization of the analysis used to quantify uncertainty in the recapture fraction. The capture zone dimensions calculated by the different realizations depend on the values of specific discharge and aquifer thickness averaged over the period of simulation.

The distances between the hypothetical well and the irrigated fields were not intended to represent actual distances. The actual distances from the pumping wells to the corresponding irrigated fields are close to zero because the wells are located approximately in the middle of the fields. Because of the constraints imposed by the stylized approach it was impossible to colocate the irrigated fields with the pumping well in the model. The distances used in the model are representative of potential future irrigated field locations.

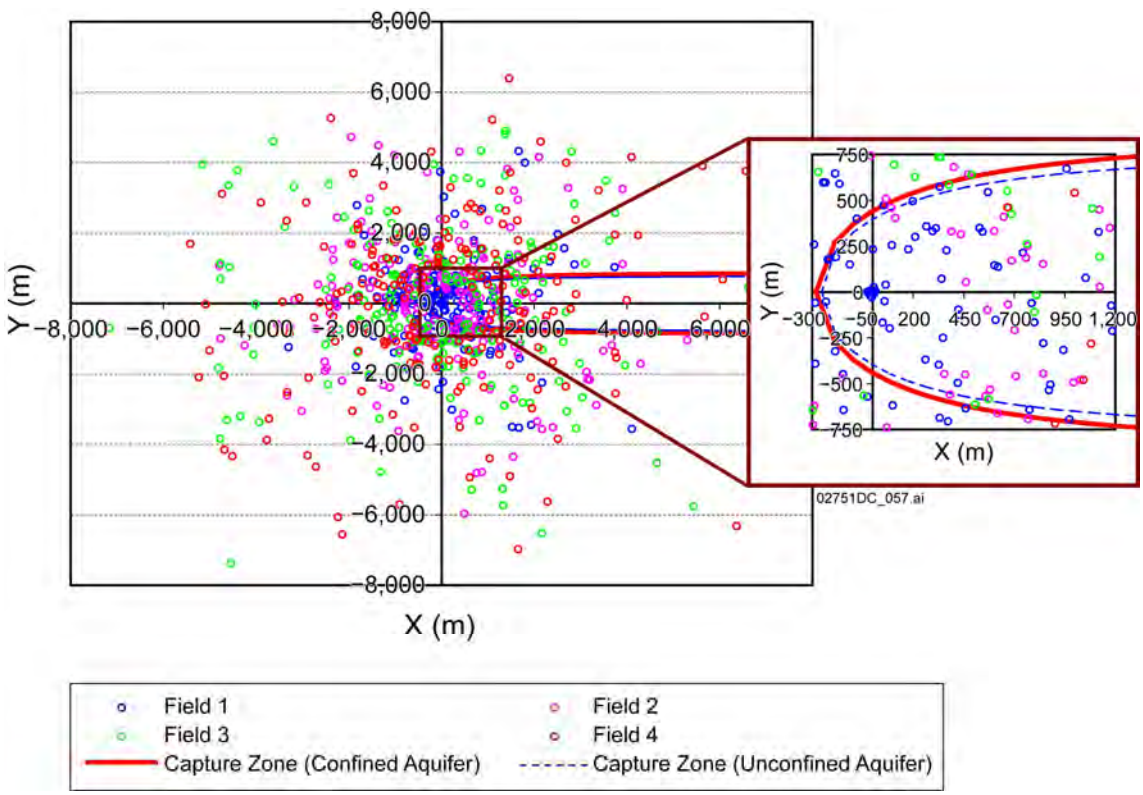

NOTE: Two capture zones are shown in this figure because the capture zone analysis was done for two conceptual models: (1) confined aquifer and (2) unconfined aquifer.

Figure 1. Locations of the Potential Irrigated Fields within the Base Community

The uncertainty in the hypothetical community size (and consequently the uncertainty in the distances distribution) was incorporated by considering two distributions of the distance between the hypothetical well and irrigated fields. One distribution was developed for a base case community and another distribution was developed for a small community. The resulting well recapture fraction probability distribution used in the irrigation recycling model was derived assuming equal probability of base case and small community scenarios. The well recapture fraction is a function of the well capture zone size. The well capture zone dimensions for each realization were calculated based on specific discharge and aquifer thickness averaged over the period of simulation (i.e., average based on the present-day, monsoon, and glacial-transition climate durations and values).

Validation of the recapture fraction analysis described above was accomplished by comparing the estimated value of the recapture fraction with an alternative analysis based on the groundwater budget in the area near the boundary of the accessible environment. In this groundwater-budget approach the well recapture fraction is calculated as the ratio of the present-day annual water demand (3,000 acre-ft/yr) and the present-day outflow of groundwater from Basin 227-A (8,100 acre-ft/yr) (State of Nevada 1971) and is equal to 0.37. Basin 227-A is the hydrographic area (Jackass Flats) with the south boundary approximately located along the boundary of the accessible environment. In order to compare this groundwater-budget approach to the capture-zone approach outlined above, the recapture fraction cumulative distribution function (CDF) had to be recomputed based on present-day values of the hydrogeologic parameters, rather than the time-averaged values over the simulation period of the irrigation recycling model. This was done for both the base case and small community scenarios. The corresponding median values of the new well recapture fraction CDFs are 0.34 and 0.37, respectively, for the base case and small community scenarios, using present-day values of the hydrogeologic parameters. The average of these two median well recapture fractions is 0.355, which compares favorably with the value of 0.37 estimated from the present-day groundwater budget analysis for Basin 227-A.

1.2 GEOSPHERE-BASED IRRIGATION RECYCLING MODEL

The conservatism of the stylized biosphere-based irrigation recycling model (SNL 2007a) can be quantified by comparing the irrigation recycling impacts calculated by this model to the results from an additional analysis that removed most of the conservative limitations associated with this model and which accounts for actual irrigation practices in the Amargosa Desert area. The geosphere-based irrigation recycling model developed in this analysis is a transient three-dimensional flow and transport model that allows for simulating radionuclide transport in the unsaturated zone beneath the irrigated fields and in the saturated zone around the pumping wells. The wells and irrigated field locations within the hypothetical community boundaries change multiple times during the period of simulation based on a stochastically generated representative schedule developed for each field. The pumping and irrigation at each location take place at different periods of time. The number of pumping periods is from 6 to 21. The pumping duration ranges from 25 years to 100 years and is based on the time of residence probability distribution. The pumping occurs continuously at four locations with the total pumping rate of 3,000 acre-ft/yr, but the locations are different. The radionuclide transport in the unsaturated and saturated zones from the previously irrigated fields and from the current

irrigation is tracked by the model and the time-dependent radionuclide concentrations are calculated for each pumping well. This geosphere-based irrigation recycling model simulates the important physical processes and applies actual irrigation practice within the Amargosa Desert area to the location of the boundary of the accessible environment.

1.2.1 Description of the Geosphere-Based Irrigation Recycling Model

The geosphere-based irrigation recycling model simulates the same processes as the biosphere-based irrigation recycling model, but it accounts for transport processes in the saturated zone and provides a more realistic representation of current irrigation practices in the Amargosa Desert area. The geosphere-based model also removes a number of conservative assumptions used in the biosphere-based model. The primary differences between the two models are summarized in Table 1.

Table 1. Representation of the Major Assumptions in the Biosphere-Based and Geosphere-Based Models

Assumption	Biosphere-Based Model	Geosphere-Based Model
Hypothetical pumping well representation	One fully penetrating well located in the middle of contaminant plume during the entire period of simulation	Four partially penetrating pumping wells that change locations within the hypothetical community boundaries multiple times during the period of simulation based on the stochastically generated pumping schedule developed for each well
Irrigation recycling representation	The irrigation recycling is estimated based on steady-state flow and transport and assuming that the pumping well captures the entire contaminant plume.	The recycling is estimated based on transient flow and transport and the assumption regarding the capture zone is not required (it is a part of simulation).
Irrigated field representation	One irrigated field located above the pumping well during the entire period of simulation	Four irrigated fields located above the pumping wells that change locations within the hypothetical community boundaries multiple times during the period of simulation based on the stochastically generated schedule developed for each field
Unsaturated zone representation	Unsaturated zone flow is modeled as a piston flow (flow rate is equal to the percolation rate) and the transport is modeled as one-dimensional advective-dispersive transport that accounts for retardation.	The unsaturated zone is modeled as a transient two-phase (air and water) three-dimensional system. The transport accounts for three-dimensional advection, dispersion, and retardation.
Saturated zone representation	The flow and transport in the saturated zone are not simulated.	The saturated zone is modeled as a transient three-dimensional system. The transport accounts for three-dimensional advection, dispersion, and retardation.

The hypothetical community for the geopshere-based model is assumed to be located at or in the vicinity of the boundary of the accessible environment. This is the same assumption as in the biosphere-based model. Estimates of the irrigation recycling impacts are based on glacial-transition climate conditions because this climate prevails during the 10,000-year period of simulation and is the climatic state at the time of maximum dose at 10,000 years. The modeling domain for the geosphere-based model encompasses the area of primary interest, which is the area occupied by the hypothetical community (see Figure 2). The modeling domain is a parallelogram oriented perpendicular to the flow path, and is 15 km wide (in the direction perpendicular to the flow path), 10 km long (in the direction parallel to the flow path), and 0.55 km deep. The subdomain representing the hypothetical community is smaller than the rectangle representing the entire modeling domain. This was done to avoid boundary effects on the flow and transport at the location of the hypothetical community.

Two different approaches were used to define the shape and boundaries of the subdomain representing the hypothetical community. In one approach, the community is oriented perpendicular to the plume, with a width of 10.4 km perpendicular to the flow (in the east-west direction) and a length of 4.0 km parallel to the flow (in the north-south direction). In the other approach, which is more conservative because the pumping wells more often intersect the contaminated plume, the hypothetical community is confined within a rectangle with dimensions of 7.2 km in the north-south direction (parallel to the flow path) and 5.6 km in the east-west direction (perpendicular to the flow path). The short side of this rectangle is parallel to the boundary of the accessible environment and the total area is 40.3 km^2. This case was chosen as the most reasonable, yet conservative, case for determining the effects of irrigation recycling on the average concentration in the groundwater beneath the hypothetical community (see Section 1.2.2). This hypothetical community rectangle accommodates seven by nine 1/4 mi^2 center-pivot irrigation fields (for a total of 63 fields, each of which is a square, with 800 m on a side—approximately the dimensions of a quarter section). The location of the field does not change during the simulation but the pumping and irrigation schedule does. This is consistent with current patterns of irrigated agriculture in the Amargosa Desert area, where the common irrigated field size is one 1/4 mi^2 section.

The 40.3 km^2 area of the most representative hypothetical community was derived from the areal dimensions of the present-day Amargosa Desert community and its corresponding water usage. The physical boundaries assumed for the present-day Amargosa Desert community include most of the community specific features (residences, new and old fields, and other) but exclude extended empty areas between these features. Most importantly, the present-day Amargosa Desert community boundaries include 95% of all the water uses in the area, which results in an area of about 169.2 km^2. The water use in this delineated area was estimated based on the most recent (2006) Nye County water use permits (State of Nevada 2006). The total water use within the assumed boundaries is 13,191 acre-ft/yr, whereas the total water use in the Amargosa Desert area for the same year is 13,884 acre-ft/yr. Consequently, the water use within the delineated boundaries constitutes 95% of the total water use. Assuming the ratio of water usage in the hypothetical RMEI community (3,000 acre-ft/yr) to the water usage in the Amargosa Desert community (13,191 ac-ft/yr) is the same as the ratio of the area of the hypothetical RMEI community to the area of the Amargosa Desert community (169.2 km^2), the area of the RMEI

community is equal to 38.5 km^2. If this is represented with 63 quarter sections (7 by 9 in a rectangular area) and oriented as described previously, a final value of 40.3 km^2 is used in the geosphere model.

The hydrogeologic framework within the geosphere-based model domain is simplified from the hydrogeologic framework used in the site-scale saturated zone flow model. This is reasonable because in the vicinity of the boundary of the accessible environment most of the flow paths are located in the upper part of the saturated zone and are confined to the alluvial deposits (SNL 2007b, Figure 6-17) and the pumping occurs from the upper part of the saturated zone as well. The geosphere-based irrigation recycling model defines the water table elevations based on the glacial-transition climate conditions. The model consists of two hydrogeologic layers, with the first layer representing the alluvial deposits and the second layer representing the volcanic rocks. The thickness of the alluvial deposits is 310 m and the thickness of the volcanic deposits is 240 m. This is consistent with the thickness of the older alluvial aquifer and Paintbrush volcanic-rock aquifer in the hydrogeologic framework model of the site-scale saturated zone flow model.

The top model boundary in the geosphere-based model represents the land surface, with an elevation of 810 m above mean sea level. This approximately corresponds to the land surface elevation at the middle of the modeling area. The actual surface gradient is not incorporated, as discussed below. This is a reasonable assumption because using a horizontal surface results in a shallower water table upgradient and a deeper water table downgradient. The overall effects from using a horizontal land surface should be negligible while the model implementation becomes significantly simpler. It is assumed that there is no recharge anywhere in the modeling area other than from the irrigated fields, based on the low natural recharge in the vicinity of the accessible environment (SAR Figure 2.3.9-10).

The eastern and western sides of the modeling area and the bottom side are assumed to be no-flow boundaries, because the predominant groundwater flow is from the north of the modeling area to the south. The groundwater flow is defined by specifying corresponding water pressures at these boundaries. The pressures are set equal to the atmospheric pressure at the water table and hydrostatic pressure below the water table. The depth to the water table is defined at the northern and southern boundary based on the glacial-transition climatic conditions. The water table in the middle of the model is approximately 50 m from the surface. This is consistent with the average depth to the water table (49.7 m) used in the biosphere-base model (SNL 2007a). Using these boundary conditions allows for maintaining the same specific discharge through the modeling domain as defined in *Saturated Zone Flow and Transport Model Abstraction* (SNL 2008b, Table 6-5[a] and Section 6.5.2.1[a]).

Note that the water table inside the modeling domain is not used as a boundary as it was in the case of the biosphere-based model. Because the saturated and unsaturated zones are explicitly modeled, the water table location does not need to be specified. The model will calculate the pressures and saturations in both zones at each time step, from which the location of the water table is determined. It will correspond to the first grid block from the surface with full water saturation.

The contaminated plume enters the modeling domain from the north. It is assumed that the concentration of a contaminant is constant and equal to 1 mol/kg within the area defining the contaminant plume. This allows for calculating a steady-state contaminant plume within the modeling domain that is established before the irrigation recycling processes take place within the hypothetical community. The steady-state plume is calculated for nonsorbing and moderately sorbing species. The initial concentration in the well will depend on its location with regard to the contaminant plume. The initial concentration may be 1 mol/kg at the locations within the plume and close to zero in the locations outside the plume. The plume cross-sectional area in the geosphere-based model was defined based on the particle tracks corresponding to the base-case transport model in *Site-Scale Saturated Zone Transport* (SNL 2008c). Note that the particle tracks shown in Figure 6-19 of *Saturated Zone Site-Scale Flow Model* (SNL 2007b) were generated for illustration purposes only and these output data were not suitable for constructing a cross section at the location of well NC_EWDP-19D. An additional transport run for the base-case model that included a large number of particles for better resolution (mean dispersion values were used) was performed specifically for this purpose. Because the model is based on the glacial-transition climate, the upper plume boundary is at the elevation 790 m, which is the water table elevation for the glacial-transition climate. The plume width is approximately 3.2 km, which is about 60% of the width of the hypothetical community described above.

The irrigation-related activities begin within the hypothetical community boundaries as soon as the steady-sate flow and the steady-state plume are established in the modeling domain. It is assumed that four wells are pumped simultaneously at any given moment of time during the simulation period. The number of simultaneously pumping wells is based on the alfalfa irrigation rate. The location of each well is randomly selected within the community boundaries. During the period of simulation the same locations can be randomly used multiple times to represent irrigated fields and pumping wells. The duration of pumping at each specific location is defined based on the time of farming residence distribution. All the wells have the same pumping rate (equal to 2,534.5 m^3/day), which corresponds to 750 acre-ft/yr. The total amount pumped from the four wells is based on the total annual water demand (3,000 acre-ft/yr) used in the biosphere-based model (SNL 2007a).

As mentioned above, the irrigated fields in the geosphere-based recycling model occupy a one-quarter square mile, which is based on the common practice in the Amargosa Desert area (SNL 2007a). Each irrigated field is defined above the corresponding pumping well (Figure 2). The pumping well is located approximately in the center of each field. The pumping and irrigation periods were defined for each of the 63 locations. For the 10,000-year assessment period, the minimum number of pumping periods among the 63 field locations was 6 and the maximum was 21. The total pumping duration ranged from 244 to 1,204 years. A percolation rate through the soils and alluvium 0.149 m/yr (SNL 2007a) is specified during the times when the field is irrigated, corresponding to the overwatering rate used to avoid accumulations of salts in agricultural soils. The infiltration rate is set equal to zero during the periods without irrigation. Note that the infiltration rate during the irrigation periods is based on the data for the Amargosa Desert area. This approach allows for defining this boundary condition without modeling precipitation and evapotranspiration processes.

The conceptual representation of the geosphere-based model is shown in Figure 2.

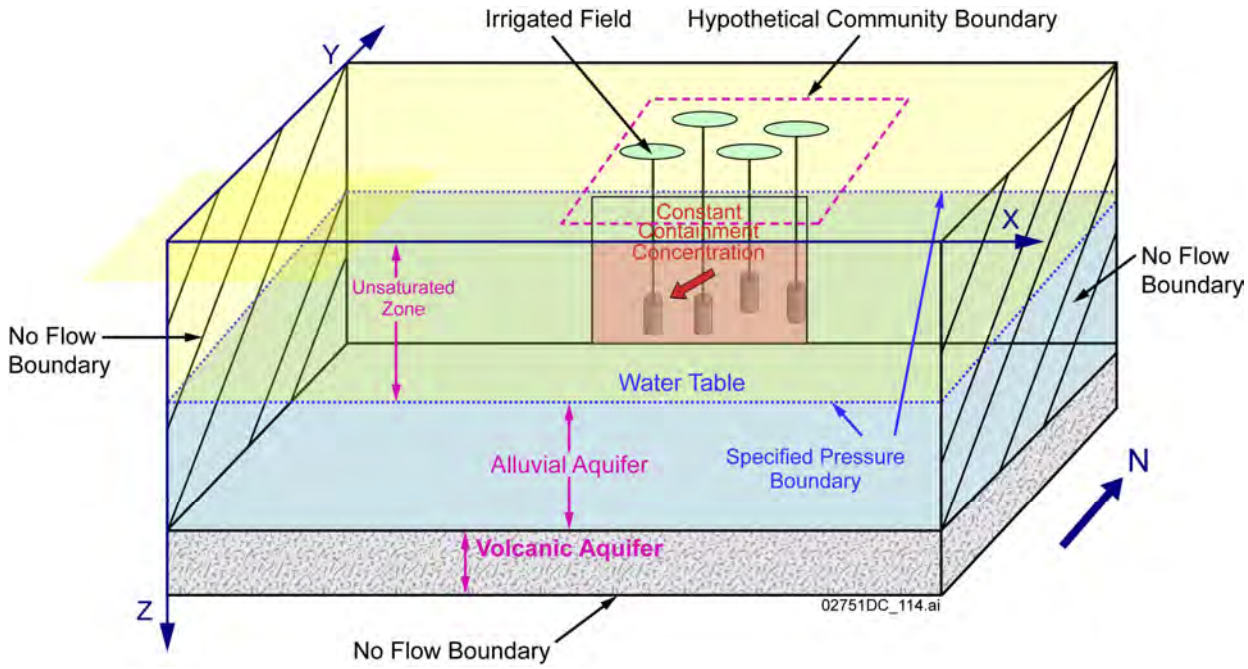

Figure 2. Conceptual Representation of the Geosphere-Based Model

Two processes occur when the well is pumped and the field above the well is irrigated. First, the aquifer around the well undergoes dewatering due to pumping, which results in transient changes in the concentrations in the well water (the plume may start moving towards the pumping well). Second, the water from the irrigated field begins infiltrating through the unsaturated zone. This results in increases in the pressure and saturation under the irrigated field within the unsaturated zone. In the case where the irrigation water is contaminated, the contaminants begin to move through the unsaturated zone with the infiltrating water as well. When the contaminants reach the water table, the concentration in the well begins to increase. When the pumping stops, the flow and the concentrations gradually return to quasi-steady-state conditions unless they are affected by nearby pumping and irrigation processes or the pumping and irrigation at this location resumes.

1.2.2 Results of the Geosphere-Based Irrigation Recycling Model

The irrigation recycling impacts were quantified in the geosphere-based irrigation recycling model by comparing the average concentrations in the pumping wells with and without irrigation recycling. Several sensitivity cases and several approaches for calculating average concentration increase were analyzed, with results ranging from a concentration increase of 1% to a concentration increase of 20%. The differences that distinguished the various sensitivity cases were related to randomness in the pumping schedules and residence time distribution for the 63 possible well locations, differences in the shape and orientation of the hypothetical community with respect to the plume (see Section 1.2.1 for the two different communities considered), and differences in the length of the simulation period (1,000 or 2,000 years). The differences that

distinguished the various approaches used for calculating the average concentration increase in the aquifer beneath the hypothetical community were related to which of the 63 wells were chosen to determine the impact on the average groundwater concentration.

The combination of sensitivity case and concentration approach that was considered to be the most reasonable, yet still conservative, representation of the impacts of irrigation recycling on average contaminant concentrations in the groundwater beneath the hypothetical community results in a concentration increase of 4.9%. This average concentration increase is computed as the average over the 63 concentration increases in the groundwater in the screened intervals of all 63 well locations. For each of the 63 well locations the corresponding concentration increase is computed by comparing the time-averaged concentration with recycling to the time-averaged concentration without recycling in the screened interval. Concentration was averaged over a 1,000-year simulation period, which was found to be a long enough period to estimate the effects of irrigation recycling for a nonsorbing radionuclide. During the 1,000-year period, the four pumping wells move randomly among the 63 possible field locations, according to current irrigation practices and based on a schedule of pumping periods that is derived from the garden residence time distribution in the biosphere model, which has a mean of about 50 years for a pumping period. As described in Section 1.2.1, the community boundaries for this representative case are oriented so that all 63 well locations are either in the plume or capture some of the contamination in the plume for those well locations adjacent to the plume.

As mentioned, the average increase in groundwater concentration for a nonsorbing radionuclide was 4.9% due to the irrigation recycling process. On the other hand, the impact of irrigation recycling with the geosphere-based model for a moderately sorbing radionuclide (1.3 mL/g) was negligible over a 10,000-year time period due to retardation in the unsaturated zone beneath the irrigated fields.

The impacts of irrigation recycling on simulated dose and radionuclide concentrations in the biosphere-based irrigation recycling model, which was the basis of the FEP screening, are larger than for the representative case in the process-level geosphere-based recycling model. For the seismic-ground motion modeling case, which is the dominant modeling case in 10,000 years (SAR Figure 2.4-18a), the mean annual dose derived from the biosphere-based recycling model is 11% higher as an average over the 10,000-year postclosure assessment period with recycling of radionuclides than without recycling (SNL 2007a, Section 6.7). This is the percent increase summed over all radionuclides. In comparison, the increase for a single nonsorbing radionuclide is 4.9% in the representative geosphere-based modeling case. However, given that seismic ground motion is dominated by a single, nonsorbing radionuclide (^{99}Tc) for most of the 10,000-year period (SAR Figure 2.4-26a), the relative impact to dose from irrigation recycling in the geosphere-based model can be derived directly (linearly) from the impacts on concentration in the groundwater. Consequently, the biosphere-based irrigation recycling model used in the screening justification for FEP 1.4.07.03.0A, Recycling of Accumulated Radionuclides from Soils to Groundwater, overestimates the impacts of the irrigation recycling process, relative to the more realistic geosphere-based irrigation recycling model.

1.3 SUMMARY

This RAI questions the distribution of distances between a hypothetical well and irrigated fields developed in *Irrigation Recycling Model* (SNL 2007a). This distribution was used to calculate well recapture fraction, which is one of the major parameters affecting the radionuclide recycling due to irrigation. The conclusions made in *Irrigation Recycling Model* (SNL 2007a) regarding the effects of the radionuclide recycling were used to support the screening decision to exclude FEP 1.4.07.03.0A, Recycling of Accumulated Radionuclides from Soils to Groundwater on the basis of low consequence. This RAI response clarifies that the distribution of distances between a hypothetical well and irrigated fields is a stylized distribution that accounts for the variability in the location of irrigated fields within the biosphere-based irrigation recycling model. The stylized distance distribution in the biosphere-based irrigation recycling model (SNL 2007a) is justified by comparing it to the results of a geosphere-based process-level irrigation recycling analysis that accounts for actual irrigation practice in which the pumping well is located in the middle of the irrigation field as dictated by center-pivot irrigation (the most common method applied in the Amargosa Desert).

The geosphere-based irrigation recycling analysis uses a transient three-dimensional coupled flow and transport model that simulates contaminant transport in the unsaturated zone beneath multiple irrigated fields and in the saturated zone around the pumping wells. It also includes a more realistic representation of transport of recycled contaminants in the saturated zone from beneath the irrigated fields to pumping wells (see response to RAI 3.2.2.1.2.1-3-004). The wells and irrigated field locations within the hypothetical community boundaries change multiple times during the period of simulation based on a stochastically generated representative schedule developed for each field. Radionuclide transport in the unsaturated and saturated zones from the previously irrigated fields and from the current irrigation is tracked by the model. Consequently, the transport distances include all the representative distances associated with the existing irrigation practice, as opposed to the stylized distance approach used in the irrigation recycling model. The geosphere-based model simulates transient flow and transport in a three-dimensional, two-phase (water and air) system that incorporates the unsaturated and saturated zones. The model considers 63 pumping wells and 63 irrigated fields that operate at different time periods within the boundaries of a hypothetical community centered over the contaminant plume.

Two primary conclusions are reached by comparing the results of the process-level geosphere-based model and the simpler biosphere-based model. First, for nonsorbing radionuclides, the representative case in the more realistic geosphere-based model shows an approximately 5% increase in radionuclide concentration as compared to an 11% increase in the biosphere-based model. Secondly, the geosphere-based model shows that sorbing species (those with K_ds equal to 1.3 mL/g or greater) do not reach the water table within the 10,000-year period and are therefore not recycled. These two conclusions from the geosphere-based model show that the stylized distribution of distances in the biosphere-based model is appropriate for the low-consequence screening decision.

2. COMMITMENTS TO NRC

None.

3. DESCRIPTION OF PROPOSED LA CHANGE

None.

4. REFERENCES

SNL (Sandia National Laboratory) 2007a. *Irrigation Recycling Model.* MDL-MGR-HS-000001 REV 00. Las Vegas, Nevada: Sandia National Laboratories. ACC: DOC.20071105.0005; DOC.20080117.0001; LLR.20080414.0002.

SNL 2007b. *Saturated Zone Site-Scale Flow Model.* MDL-NBS-HS-000011 REV 03. Las Vegas, Nevada: Sandia National Laboratories. ACC: DOC.20070626.0004; DOC.20071001.0013.

SNL 2008a. *Features, Events, and Processes for the Total System Performance Assessment: Analyses.* ANL-WIS-MD-000027 REV 00. Las Vegas, Nevada: Sandia National Laboratories. ACC: DOC.20080307.0003; DOC.20080407.0009; DOC.20080722.0002.

SNL 2008b. *Saturated Zone Flow and Transport Model Abstraction.* MDL-NBS-HS-000021 REV 03 AD 02. Las Vegas, Nevada: Sandia National Laboratories. ACC: DOC.20080107.0006.

SNL 2008c. *Site-Scale Saturated Zone Transport.* MDL-NBS-HS-000010 REV 03 AD 01. Las Vegas, Nevada: Sandia National Laboratories. ACC: DOC.20080121.0003.

State of Nevada 1971. *Water for Nevada.* Nevada's Water Resources, Report No. 3. Carson City, Nevada: State of Nevada, Department of Conservation and Natural Resources, Division of Water Resources.

State of Nevada 2006. *Ground Water Pumpage Inventory Amargosa Valley, No. 230 2006*. Carson City, Nevada: State of Nevada, Division of Water Resources. ACC: LLR.20081006.0096.

RAI Volume 3, Chapter 2.2.1.2.1, Third Set, Number 4:

Justify that the assumption on page 6-282 of Sandia National Laboratories (2008) that "radionuclides that reach the water table and are within the well capture zone are returned to the well volume without accounting for transport within the saturated zone" does not underestimate doses at later times. This information is needed to verify compliance with 10 CFR 63.114 (e).

Basis: Accounting for delayed arrival of radionuclides to the well volume would spread radionuclide releases in time. This spread of release could result in higher radionuclide concentrations at the pumping well than estimated using the DOE assumption that each year the recycled water that arrives at the water table makes it to the pumping well. For example, more than a single year release of radionuclides to the water table from recycled water might arrive at the pumping well in a single year at some later time due to delayed transport. It is not clear how dose estimates would be affected by accounting for transport within the saturated zone.

1. RESPONSE

The response to this RAI provides justification for the assumption made in the screening decision for FEP 1.4.07.03.0A, Recycling of Accumulated Radionuclides from Soils to Groundwater (SNL 2008a), that instantaneous transport to the pumping well of the radionuclides that reach the water table and are within the well capture zone does not underestimate doses at later times. The justification is based on the comparison of the results from the biosphere-based model in *Irrigation Recycling Model* (SNL 2007a) and the results from a process-level geosphere-based irrigation recycling model (described in Section 1.2). The geosphere-based model removes many of the conservative simplifications associated with the biosphere-based model and includes transport in the saturated zone. This comparison demonstrates that excluding saturated zone transport from the biosphere-based recycling model does not underestimate doses at later times.

1.1 BIOSPHERE-BASED MODEL

The TSPA model uses the radionuclide concentrations in the groundwater to calculate annual dose to the RMEI from radionuclides released from the geosphere to the biosphere in groundwater. The time-dependent radionuclide concentrations in the groundwater $C_w(t)$ are calculated in the TSPA model as the radionuclide mass fluxes (m_{sz}) (mass per time) exiting the saturated zone at the 18-km boundary of the accessible environment divided by the annual water demand (Q) of 3,000 acre-feet per year. This is schematically presented in Figure 1(a). The biosphere-based irrigation recycling model (SNL 2007a) incorporates additional mass fluxes into the annual water demand due to the irrigation recycling process, as shown in Figure 1(b). These additional mass fluxes from the irrigation return flow are mixed with the annual water demand flow (Q) and represent the irrigation recycling fraction (F_c) of the total annual water demand (Q). The effect of irrigation recycling begins when radionuclide mass in the irrigation return flow reaches the water table. At that time, the concentrations in the representative groundwater volume begin to increase. The diagram shown in Figure 1(b) is simplified to demonstrate the

irrigation recycling process only. Other processes considered in *Irrigation Recycling Model* (SNL 2007a), such as radionuclide removal with soil erosion, are not presented in this diagram.

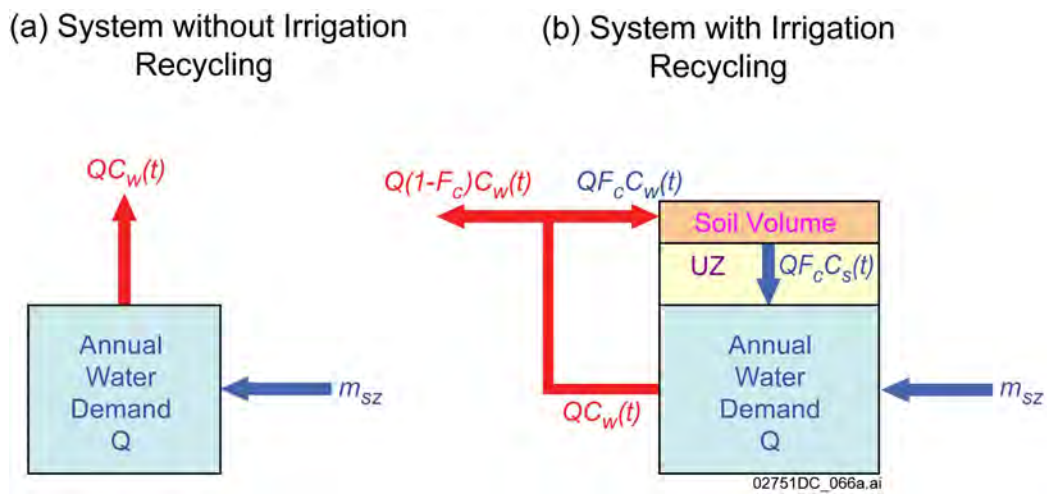

NOTE: UZ = unsaturated zone and $C_s(t)$ = concentration in soil.

Figure 1. Calculation of the Radionuclide Concentrations in the Groundwater with and without Irrigation Recycling

The impact of irrigation recycling to mean annual dose results was calculated as a part of a TSPA sensitivity analysis (SNL 2007a). In this analysis, irrigation recycling results in an 11% increase as an average over the 10,000-year postclosure period for the seismic ground motion modeling case, which is the largest contributor to total mean annual dose summed over all modeling cases (SAR Figure 2.4-18a). Because there is only one major contributor to the total dose (^{99}Tc) for most times (SAR Figure 2.4-26a), the impact on the concentration of ^{99}Tc is approximately the same as the impact on the total dose.

1.2 GEOSPHERE-BASED MODEL

The geosphere-based irrigation recycling model is a process model that removes many of the conservatisms associated with the biosphere-based model by simulating transient three-dimensional flow and transport in the unsaturated zone beneath the irrigated fields and in the saturated zone around the pumping wells. For example, although the assumption of instantaneous saturated-zone transport in the biosphere-based model is conservative regarding the effect of radioactive decay during transit through the saturated zone, it may not be conservative with respect to other processes that might occur during transport, such as delay and dispersion. In particular, pulses of radionuclide mass returning to a pumping well from different irrigated fields could potentially overlap at certain points in time due to delay and spreading, resulting in a positive interference effect. This limitation is removed in the geosphere-based model, which includes transient three-dimensional transport from multiple irrigated fields.

In the geosphere-based model, described in detail in Section 1.2.1, the locations of the wells and irrigated fields within the hypothetical community boundaries change multiple times during the period of simulation based on a stochastically generated representative schedule developed for

each field. Both the alluvium and underlying volcanic deposits are included in the model, although all wells are completed in the alluvium. The locations of the pumping wells with regard to the irrigated fields and the placements of the well screens correspond to the actual practice used in the Amargosa Desert area. The model simulates multiple fields and multiple pumping wells that operate during different periods of time at the different locations to simulate the spread of concentrations due to the transport in the saturated zone. The radionuclide transport time in the saturated zone includes the transport from all the points at the water table that are within the well capture zones.

Geosphere-based model runs were performed with and without irrigation recycling to quantify the effects of irrigation recycling on radionuclide concentrations in the pumping wells (Section 1.2.2). The impacts on radionuclide concentrations from excluding saturated zone transport are estimated in Section 1.2.2 based on the comparison between the concentrations calculated by the biosphere-based model and the geosphere-based model. As shown in Section 1.2.2, the radionuclide concentrations calculated with the biosphere-based model are conservative.

1.2.1 Description of the Geosphere-Based Irrigation Recycling Model

The geosphere-based irrigation recycling model simulates the same processes as the biosphere-based irrigation recycling model, but it accounts for transport processes in the saturated zone and provides a more realistic representation of current irrigation practices in the Amargosa Desert area. The geosphere-based model also removes a number of conservative assumptions used in the biosphere-based model. The primary differences between the two models are summarized in Table 1.

Table 1. Representation of the Major Assumptions in the Biosphere-Based and Geosphere-Based Models

Assumption	Biosphere-Based Model	Geosphere-Based Model
Hypothetical pumping well representation	One fully penetrating well located in the middle of contaminant plume during the entire period of simulation	Four partially penetrating pumping wells that change locations within the hypothetical community boundaries multiple times during the period of simulation based on the stochastically generated pumping schedule developed for each well
Irrigation recycling representation	The irrigation recycling is estimated based on steady-state flow and transport and assuming that the pumping well captures the entire contaminant plume.	The recycling is estimated based on transient flow and transport and the assumption regarding the capture zone is not required (it is a part of simulation).
Irrigated field representation	One irrigated field located above the pumping well during the entire period of simulation	Four irrigated fields located above the pumping wells that change locations within the hypothetical community boundaries multiple times during the period of simulation based on the stochastically generated schedule developed for each field
Unsaturated zone representation	Unsaturated zone flow is modeled as a piston flow (flow rate is equal to the percolation rate), and the transport is modeled as one-dimensional advective-dispersive transport that accounts for retardation.	The unsaturated zone is modeled as a transient two-phase (air and water) three-dimensional system. The transport accounts for three-dimensional advection, dispersion, and retardation.
Saturated zone representation	The flow and transport in the saturated zone are not simulated.	The saturated zone is modeled as a transient three-dimensional system. The transport accounts for three-dimensional advection, dispersion, and retardation.

The hypothetical community for the geosphere-based model is assumed to be located at or in the vicinity of the boundary of the accessible environment. This is the same assumption as in the biosphere-based model. Estimates of the irrigation recycling impacts are based on glacial-transition climate conditions because this climate prevails during the 10,000-year period of simulation and is the climatic state at the time of maximum dose at 10,000 years. The modeling domain for the geosphere-based model encompasses the area of primary interest, which is the area occupied by the hypothetical community (see Figure 2). The modeling domain is a parallelogram oriented perpendicular to the flow path, and is 15 km wide (in the direction perpendicular to the flow path), 10 km long (in the direction parallel to the flow path), and 0.55 km deep. The subdomain representing the hypothetical community is smaller than the rectangle representing the entire modeling domain. This was done to avoid boundary effects on the flow and transport at the location of the hypothetical community.

Two different approaches were used to define the shape and boundaries of the subdomain representing the hypothetical community. In one approach, the community is oriented perpendicular to the plume, with a width of 10.4 km perpendicular to the flow (in the east-west

direction) and a length of 4.0 km parallel to the flow (in the north-south direction). In the other approach, which is more conservative because the pumping wells more often intersect the contaminated plume, the hypothetical community is confined within a rectangle with dimensions of 7.2 km in the north-south direction (parallel to the flow path) and 5.6 km in the east-west direction (perpendicular to the flow path). The short side of this rectangle is parallel to the boundary of the accessible environment and the total area is 40.3 km^2. This case was chosen as the most reasonable, yet conservative, case for determining the effects of irrigation recycling on the average concentration in the groundwater beneath the hypothetical community (see Section 1.2.2). This hypothetical community rectangle accommodates seven by nine 1/4 mi^2 center-pivot irrigation fields (for a total of 63 fields, each of which is a square, with 800 m on a side—approximately the dimensions of a quarter section). The location of the field does not change during the simulation, but the pumping and irrigation schedule does. This is consistent with current patterns of irrigated agriculture in the Amargosa Desert area, where the common irrigated field size is one 1/4 mi^2 section.

The 40.3 km^2 area of the most representative hypothetical community was derived from the areal dimensions of the present-day Amargosa Desert community and its corresponding water usage. The physical boundaries assumed for the present-day Amargosa Desert community include most of the community specific features (residences, new and old fields, and other) but exclude extended empty areas between these features. Most importantly, the present-day Amargosa Desert community boundaries include 95% of all the water uses in the Amargosa Desert area, which results in an area of about 169.2 km^2. The water use in this delineated area was estimated based on the most recent (2006) Nye County water use permits (State of Nevada 2006). The total water use within the assumed boundaries is 13,191 acre-ft/yr, whereas the total water use in the Amargosa Desert area for the same year is 13,884 acre-ft/yr. Consequently, the water use within the delineated boundaries constitutes 95% of the total water use. By assuming the ratio of water usage in the hypothetical RMEI community (3,000 acre-ft/yr) to the water usage in the Amargosa Desert community (13,191 acre-ft/yr) is the same as the ratio of the area of the hypothetical RMEI community to the area of the Amargosa Desert community (169.2 km^2), the area of the RMEI community is equal to 38.5 km^2. If this is represented with 63 quarter sections (7 by 9 in a rectangular area) and oriented as described previously, a final value of 40.3 km^2 is used in the geosphere model.

The hydrogeologic framework within the geosphere-based model domain is simplified from the hydrogeologic framework used in the site-scale saturated zone flow model. This is reasonable because in the vicinity of the boundary of the accessible environment most of the flow paths are located in the upper part of the saturated zone and are confined to the alluvial deposits (SNL 2007b, Figure 6-17), and the pumping occurs from the upper part of the saturated zone as well. The geosphere-based irrigation recycling model defines the water table elevations based on the glacial-transition climate conditions. The model consists of two hydrogeologic layers, with the first layer representing the alluvial deposits and the second layer representing the volcanic rocks. The thickness of the alluvial deposits is 310 m and the thickness of the volcanic deposits is 240 m. This is consistent with the thickness of the older alluvial aquifer and Paintbrush volcanic-rock aquifer in the hydrogeologic framework model of the site-scale saturated zone flow model.

The top model boundary in the geosphere-based model represents the land surface, with an elevation of 810 m above mean sea level. This approximately corresponds to the land surface elevation at the middle of the modeling area. The actual surface gradient is not incorporated, as discussed below. This is a reasonable assumption because using a horizontal surface results in a shallower water table upgradient and a deeper water table downgradient. The overall effects from using a horizontal land surface should be negligible while the model implementation becomes simpler. It is assumed that there is no recharge anywhere in the modeling area other than from the irrigated fields, based on the low natural recharge in the vicinity of the accessible environment (SAR Figure 2.3.9-10).

The eastern and western sides of the modeling area and the bottom side are assumed to be no-flow boundaries because the predominant groundwater flow is from the north of the modeling area to the south. The groundwater flow is defined by specifying corresponding water pressures at these boundaries. The pressures are set equal to the atmospheric pressure at the water table and hydrostatic pressure below the water table. The depth to the water table is defined at the northern and southern boundary based on the glacial-transition climatic conditions. The water table in the middle of the model is approximately 50 m from the surface. This is consistent with the average depth to the water table (49.7 m) used in the biosphere-based model (SNL 2007a). Using these boundary conditions allows for maintaining the same specific discharge through the modeling domain as defined in *Saturated Zone Flow and Transport Model Abstraction* (SNL 2008b, Table 6-5[a] and Section 6.5.2.1[a]).

Note that the water table inside the modeling domain is not used as a boundary as it was in the case of the biosphere-based model. Because the saturated and unsaturated zones are explicitly modeled, the water table location does not need to be specified. The model will calculate the pressures and saturations in both zones at each time step, from which the location of the water table is determined. It will correspond to the first grid block from the surface with full water saturation.

The contaminated plume enters the modeling domain from the north. It is assumed that the concentration of a contaminant is constant and equal to 1 mol/kg within the area defining the contaminant plume. This allows for calculating a steady-state contaminant plume within the modeling domain that is established before the irrigation recycling processes take place within the hypothetical community. The steady-state plume is calculated for nonsorbing and moderately sorbing species. The initial concentration in the well will depend on its location with regard to the contaminant plume. The initial concentration may be 1 mol/kg at the locations within the plume and close to zero in the locations outside the plume. The plume cross-sectional area in the geosphere-based model was defined based on the particle tracks corresponding to the base-case transport model in *Site-Scale Saturated Zone Transport* (SNL 2008c). Note that the particle tracks shown in Figure 6-19 of *Saturated Zone Site-Scale Flow Model* (SNL 2007b) were generated for illustration purposes only and these output data were not suitable for constructing a cross section at the location of well NC-EWDP-19D. An additional transport run for the base-case model that included a large number of particles for better resolution (mean dispersion values were used) was performed specifically for this purpose. Because the model is based on the glacial-transition climate, the upper plume boundary is at the elevation 790 m, which is the water table elevation for the glacial-transition climate. The plume width is

approximately 3.2 km, which is about 60% of the width of the hypothetical community described above.

The irrigation related activities begin within the hypothetical community boundaries as soon as the steady-sate flow and the steady-state plume are established in the modeling domain. It is assumed that four wells are pumped simultaneously at any given moment of time during the simulation period. The number of simultaneously pumping wells is based on the alfalfa irrigation rate. The location of each well is randomly selected within the community boundaries. During the period of simulation, the same locations can be randomly used multiple times to represent irrigated fields and pumping wells. The duration of pumping at each specific location is defined based on the time of farming residence distribution. All the wells have the same pumping rate (equal to 2,534.5 m^3/day), which corresponds to 750 acre-ft/yr. The total amount pumped from the four wells is based on the total annual water demand (3,000 acre-ft/yr) used in the biosphere-based model (SNL 2007a).

As mentioned above, the irrigated fields in the geosphere-based recycling model occupy a one-quarter square mile section, which is based on the common practice in the Amargosa Desert area (SNL 2007a). Each irrigated field is defined above the corresponding pumping well (Figure 2). The pumping well is located approximately in the center of each field. The pumping and irrigation periods were defined for each of the 63 locations. For the 10,000-year assessment period, the minimum number of pumping periods among the 63 field locations was 6 and the maximum was 21. The total pumping duration ranged from 244 years to 1,204 years. A percolation rate through the soils and alluvium of 0.149 m/yr (SNL 2007a) is specified during the times when the field is irrigated, corresponding to the overwatering rate used to avoid accumulations of salts in agricultural soils. The infiltration rate is set equal to zero during the periods without irrigation. Note that the infiltration rate during the irrigation periods is based on the data for the Amargosa Desert area. This approach allows for defining this boundary condition without modeling precipitation and evapotranspiration processes.

The conceptual representation of the geosphere-based model is shown in Figure 2.

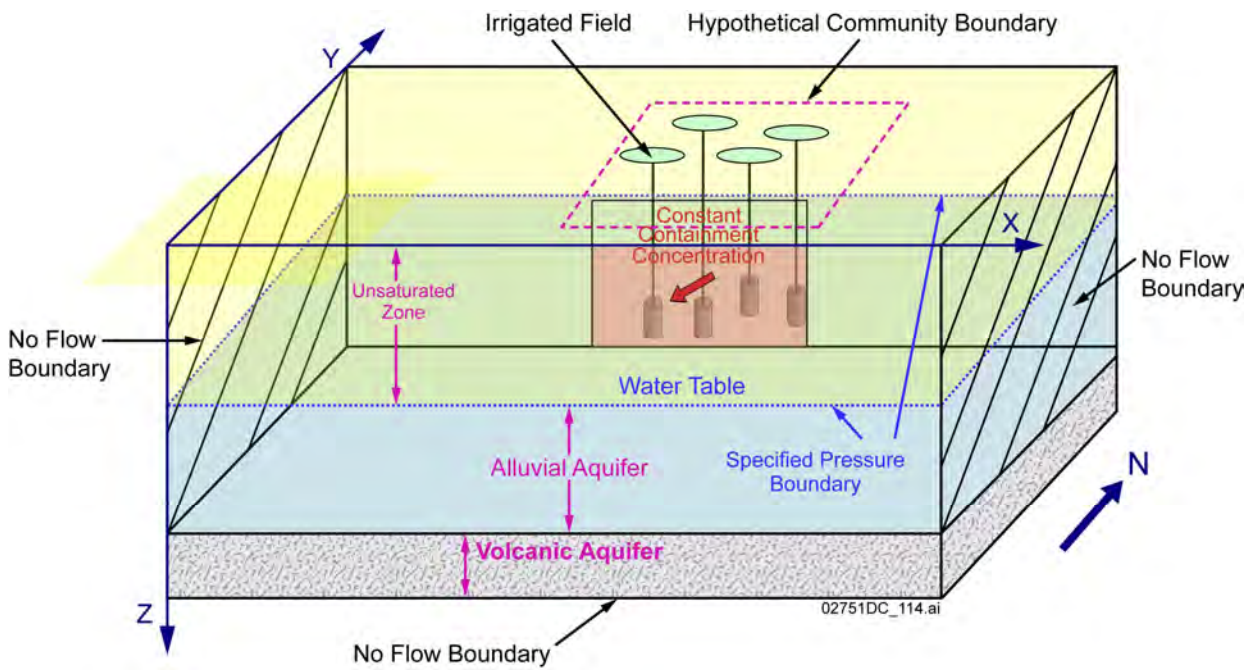

Figure 2. Conceptual Representation of the Geosphere-Based Model

Two processes occur when the well is pumped and the field above the well is irrigated. First, the aquifer around the well undergoes dewatering due to pumping, which results in transient changes in the concentrations in the well water (the plume may start moving towards the pumping well). Second, the water from the irrigated field begins infiltrating through the unsaturated zone. This results in increases in the pressure and saturation under the irrigated field within the unsaturated zone. In the case where the irrigation water is contaminated, the contaminants begin to move through the unsaturated zone with the infiltrating water as well. When the contaminants reach the water table, the concentration in the well begins to increase. When the pumping stops, the flow and the concentrations gradually return to some quasi steady-state conditions unless they are affected by nearby pumping and irrigation processes or the pumping and irrigation at this location resumes.

1.2.2 Results of the Geosphere-Based Irrigation Recycling Model

The irrigation recycling impacts were quantified in the geosphere-based irrigation recycling model by comparing the average concentrations in the pumping wells with and without irrigation recycling. Several sensitivity cases and several approaches for calculating average concentration increase were analyzed, with results ranging from a concentration increase of 1% to a concentration increase of 20%. The differences that distinguished the various sensitivity cases were related to randomness in the pumping schedules and residence time distribution for the 63 possible well locations, differences in the shape and orientation of the hypothetical community with respect to the plume (see Section 1.2.1 for the two different communities considered), and differences in the length of the simulation period (1,000 or 2,000 years). The differences that distinguished the various approaches used for calculating the average concentration increase in

the aquifer beneath the hypothetical community were related to which of the 63 wells were chosen to determine the impact on the average groundwater concentration.

The combination of sensitivity case and concentration approach that was considered to be the most reasonable, yet still conservative, representation of the impacts of irrigation recycling on average contaminant concentrations in the groundwater beneath the hypothetical community results in a concentration increase of 4.9%. This average concentration increase is computed as the average over the 63 concentration increases in the groundwater in the screened intervals of all 63 well locations. For each of the 63 well locations the corresponding concentration increase is computed by comparing the time-averaged concentration with recycling to the time-averaged concentration without recycling in the screened interval. Concentration was averaged over a 1,000-year simulation period, which was found to be a long enough period to estimate the effects of irrigation recycling for a nonsorbing radionuclide. During the 1,000-year period, the four pumping wells move randomly among the 63 possible field locations, according to current irrigation practices and based on a schedule of pumping periods that is derived from the garden residence time distribution in the biosphere model, which has a mean of about 50 years for a pumping period. As described in Section 1.2.1, the community boundaries for this representative case are oriented so that all 63 well locations are either in the plume or capture some of the contamination in the plume for those well locations adjacent to the plume.

As mentioned, the average increase in groundwater concentration for a nonsorbing radionuclide was 4.9% due to the irrigation recycling process. On the other hand, the impact of irrigation recycling with the geosphere-based model for a moderately sorbing radionuclide (1.3 mL/g) was negligible over a 10,000-year time period due to retardation in the unsaturated zone beneath the irrigated fields.

The impacts of irrigation recycling on simulated dose and radionuclide concentrations in the biosphere-based irrigation recycling model, which was the basis of the FEP screening, are larger than for the representative case in the process-level geosphere-based recycling model. For the seismic-ground motion modeling case, which is the dominant modeling case in 10,000 years (SAR Figure 2.4-18a), the mean annual dose derived from the biosphere-based recycling model is 11% higher as an average over the 10,000-year postclosure assessment period with recycling of radionuclides than without recycling (SNL 2007a, Section 6.7). This is the percent increase summed over all radionuclides. In comparison, the increase for a single nonsorbing radionuclide is 4.9% in the representative geosphere-based modeling case. However, given that seismic ground motion is dominated by a single, nonsorbing radionuclide (^{99}Tc) for most of the 10,000-year period (SAR Figure 2.4-26a), the relative impact to dose from irrigation recycling in the geosphere-based model can be derived directly (linearly) from the impacts on concentration in the groundwater. Consequently, the biosphere-based irrigation recycling model used in the screening justification for FEP 1.4.07.03.0A, Recycling of Accumulated Radionuclides from Soils to Groundwater, overestimates the impacts of the irrigation recycling process, relative to the representative case in the more realistic geosphere-based irrigation recycling model.

1.3 SUMMARY

The response to this RAI provides justification for the assumption made in the screening decision for FEP 1.4.07.03.0A, Recycling of Accumulated Radionuclides from Soils to Groundwater (SNL 2008a), that instantaneous transport to the pumping well of the radionuclides that reach the water table and are within the well capture zone does not underestimate doses at later times. Instantaneous transport ignores any effects related to delayed transport or spreading of releases, or other possible positive interference effects, which could possibly result in nonconservative concentrations in the pumping well. The justification for not including these types of effects is based on a comparison of the results from the biosphere-based model in *Irrigation Recycling Model* (SNL 2007a), which provides the basis of the screening decision for FEP 1.4.07.03.0A, with the results of a geosphere-based process-level irrigation recycling analysis.

The geosphere-based irrigation recycling analysis uses a transient three-dimensional coupled flow and transport model that simulates contaminant transport in the unsaturated zone beneath multiple irrigated fields and in the saturated zone around the pumping wells. It also includes a more realistic distance distribution between the wells and fields, based on actual center-pivot irrigation practices (see response to RAI 3.2.2.1.2.1-3-003). The wells and irrigated field locations within the hypothetical community boundaries change multiple times during the period of simulation based on a stochastically generated representative schedule developed for each field. The radionuclide transport in the unsaturated and saturated zones from the previously irrigated fields and from the current irrigation is tracked by the model. Consequently, this process-based model accounts for possible interference effects related to transport delay or spreading of releases from any of the irrigated fields in the hypothetical community, as opposed to the instantaneous transport assumption used in the irrigation recycling model. The geosphere-based model considers 63 pumping wells and 63 irrigated fields that operate at different time periods within the boundaries of a hypothetical community centered over the contaminant plume.

Two primary conclusions are reached by comparing the results of the process-level geosphere-based model and the simpler biosphere-based model. First, for nonsorbing radionuclides, the representative case in the more realistic geosphere-based model shows an approximately 5% increase in radionuclide concentration as compared to an 11% increase in the biosphere-based model. Secondly, the geosphere-based model shows that sorbing species (those with K_ds equal to 1.3 mL/g or greater) do not reach the water table within the 10,000-year period and are therefore not recycled. These two conclusions from the geosphere-based model show that the assumption of instantaneous saturated-zone transport in the biosphere-based model is appropriate for the low-consequence screening decision for FEP 1.4.07.03.0A.

2. COMMITMENTS TO NRC

None.

3. DESCRIPTION OF PROPOSED LA CHANGE

None.

4. REFERENCES

SNL (Sandia National Laboratories) 2007a. *Irrigation Recycling Model.* MDL-MGR-HS-000001 REV 00. Las Vegas, Nevada: Sandia National Laboratories. ACC: DOC.20071105.0005; DOC.20080117.0001; LLR.20080414.0002.

SNL 2007b. *Saturated Zone Site-Scale Flow Model.* MDL-NBS-HS-000011 REV 03. Las Vegas, Nevada: Sandia National Laboratories. ACC: DOC.20070626.0004; DOC.20071001.0013.

SNL 2008a. *Features, Events, and Processes for the Total System Performance Assessment: Analyses.* ANL-WIS-MD-000027 REV 00. Las Vegas, Nevada: Sandia National Laboratories. ACC: DOC.20080307.0003; DOC.20080407.0009; DOC.20080722.0002.

SNL 2008b. *Saturated Zone Flow and Transport Model Abstraction*. MDL-NBS-HS-000021 REV 03 AD 02. Las Vegas, Nevada: Sandia National Laboratories. ACC: DOC.20080107.0006.

SNL 2008c. *Site-Scale Saturated Zone Transport.* MDL-NBS-HS-000010 REV 03 AD 01. Las Vegas, Nevada: Sandia National Laboratories. ACC: DOC.20080121.0003.

State of Nevada 2006. *Ground Water Pumpage Inventory Amargosa Valley, No. 230 2006*. Carson City, Nevada: State of Nevada, Division of Water Resources. ACC: LLR.20081006.0096.

RAI Volume 3, Chapter 2.2.1.2.1, Third Set, Number 6:

State the assumed temperature of the drip shield in the analyses that were used to exclude this FEP from the performance assessment model. Provide the rationale for the assumed temperature. Provide the creep equations (creep strain as a function of time and applied stress) used to estimate the amount of creep strain of Titanium Grades 7 and 29 at the considered temperature. This information is needed to verify compliance with 10 CFR 63.114 (e), (f).

Basis: The assumed temperature of the drip shield in the analyses that DOE used to exclude this FEP from the performance is not clear from the supporting documentation. In Sandia National Laboratories (2008, p. 6-565), DOE stated that "a reasonably bounding drip shield exposure temperature" of 300°C was used in the analysis of creep of metallic materials in the drip shield. The document cited in Sandia National Laboratories (2008), Bechtel SAIC Company (2005), and Safety Analysis Report chapter 2.3.6.8.5 for the analysis of drip shield creep referred to a drip shield temperature of 150°C.

1. RESPONSE

The assumed temperature of the drip shield in the analyses that were used to exclude this FEP from the performance assessment model is 150°C. The following discussion demonstrates that the creep equation used for predicting mechanical deformation at 150°C bounds behavior expected at 300°C. This occurs by removing some conservatism in the analytical approach to calculate the creep at 150°C and applying more realistic estimates for creep rate at 300°C.

1.1 INTRODUCTION

The analysis of the drip shield creep deformation and stability (BSC 2005) was conducted assuming the temperature of the drip shield to be 150°C. The mechanical and creep properties of Titanium Grade 24 and Titanium Grade 7 were calculated for 150°C and used in the analysis. The rationale for using 150°C is provided in *Creep Deformation of the Drip Shield* (BSC 2005, Section 3.2.4). Additional rationale is provided to demonstrate that equations to predict creep rates at 150°C include conservatisms that bound drip shield response at higher temperatures up to 300ºC. The value of 300°C reasonably bounds the range of expected drip shield temperatures.

The creep equations for Titanium Grades 7 and 24 at 150°C are developed in *Creep Deformation of the Drip Shield* (BSC 2005, Equations I-15 and I-22, respectively). The creep equation for Titanium Grade 7 is:

$$\varepsilon = 1.02 \times 10^{-20} \sigma^{8.81} t^{0.28} \qquad \text{(Eq. 1)}$$

and the equation for Titanium Grade 24 (29) is:

$$\varepsilon = 3.40 \times 10^{-35} \sigma^{12.15} t^{0.25} \qquad \text{(Eq. 2)}$$

where ε is creep strain, σ is stress in megapascals, and t is time in hours.

The analysis of creep of the drip shield was conducted for a design in which the drip shield frame components (i.e., the support beams and bulkheads) are manufactured from Titanium Grade 24. In the current version of the drip shield design the material of these frame components is changed to be Titanium Grade 29. The original analyses are considered adequate because Titanium Grade 24 has very similar properties and can be assumed to be analogous to Titanium Grade 29. Titanium Grades 24 and 29 are both based upon an extra-low-interstitial version of Titanium Grade 5 (Ti-6Al-4V) with the addition of a platinum group metal (PGM) to improve corrosion performance. In the case of Titanium Grade 24, this addition is palladium; while for Titanium Grade 29, it is ruthenium. Microstructurally, there should be effectively no difference between the two materials, as the two PGM additions behave similarly in titanium. In terms of mechanical properties, while the minimum allowable yield strength is slightly lower for Titanium Grade 29, the mechanical properties of the material used for the drip shield (e.g., alpha-beta processed + solution anneal + artificial aging) are well in excess of the minimum properties for the Titanium Grade 24 specification upon which the analyses are currently based. As such, for the purposes of the creep analysis of the drip shield, the two materials can be considered to be effectively identical.

1.2 DISCUSSION

This response uses a reasonably bounding drip shield temperature of 300ºC, and a review of the derivation of Equations 1 and 2, to show that the previous analyses (BSC 2005) performed using these creep equations developed for 150°C are representative of drip shield creep response for higher temperatures that may occur with reasonable likelihood.

1.2.1 Drip Shield Temperature

The combination of temperatures greater than 150ºC and loading to a significant percentage of yield stress for drip shield components can only occur with complete or mostly complete drift collapse within the first few hundred years after repository closure. Waste package temperature can be used as a surrogate for drip shield temperature because waste packages are always slightly hotter than drip shields. Temperature histories are available for the hottest waste package in the base case thermal loading arrangement used for total system performance assessment (TSPA), and for two bounding thermal loading arrangements; all of these histories assume complete drift collapse concurrent with waste emplacement (SNL 2008, Figure 6.4.2-28). For the base case, with early drift collapse, the duration of temperatures greater than 150°C cannot exceed approximately 600 years (estimated from SNL 2008, Figure 6.4.2-28). For the bounding cases this limit is approximately 1,000 years. These durations are reduced if the seismic event initiating drift collapse occurs at some time after repository closure because generated heat decreases with time.

The probability of the hottest waste package exceeding 300°C, due to seismically induced drift collapse, is less than 10^{-4} per repository realization (SNL 2008, Section 6.5.1). (The probability of 10^{-4} is the probability that one or more waste packages will see temperatures greater than 300°C, on a per-repository realization basis, considering epistemic uncertainties on rubble

volume and effective thermal conductivity, as well as the aleatory uncertainty on seismic event frequency and magnitude.) Thus, a reasonably bounding temperature of 300ºC may be used in the discussion of creep of drip shield materials, representing a situation with low probability (less than 10^{-4} per repository realization) and short duration (on the order of a few years or less). For this bounding case, a temperature of 250ºC cannot persist longer than approximately 200 years, while 200ºC cannot persist longer than 500 years (SNL 2008, Figure 6.4.2-28). In summary, drip shield stability analyses have been performed at 150ºC for 10,000 years, although this condition will not persist beyond approximately 1,000 years under the collapsed drift scenario. The possibility of higher temperatures (up to a reasonably bounding value of 300ºC) is associated with significantly lower probability and decreased duration.

1.2.2 Creep Equations Developed for 150ºC

Titanium creep Equations 1 and 2 for 150°C were derived using conservative assumptions (BSC 2005, Sections I-3.3 and I-4.2) and are reasonably representative at higher temperatures. The temperature effect on creep properties was accounted for twice in these equations. The creep coefficients were first rescaled for the reduction in yield strength associated with the increase in temperature from room temperature to 150°C. This rescaling produced the same creep for the same value of tensile stress scaled by the yield strength (the expression used is presented in BSC 2005, Section I-3.2). Whereas the ratio of tensile stress to yield strength is related to creep, titanium creep may also exhibit differences related to grain size and other aspects of the state of the material, thus rescaling the creep equations used at low temperature via the yield strength expression alone may not adequately capture the impact which temperature will have on the creep behavior. Accordingly, to avoid under-estimating creep deformation, the creep equations were also modified to explicitly account for the kinetic effect at higher temperature using the activation energy equation (BSC 2005, Equation I-12):

$$\varepsilon(\sigma,t,T) = \varepsilon_{RT}(\sigma,t)\frac{e^{-\frac{Q}{RT}}}{e^{-\frac{Q}{RT_{RT}}}} \qquad \text{(Eq. 3)}$$

where ε is strain after time t at absolute temperature T for stress σ; ε_{RT} is strain after time t at room temperature T_{RT} (i.e., 293 K) for stress σ; Q is the activation energy (30 kJ/mol); and $R = 8.31$ J/mol K is the gas constant. The physically-based form of this equation was recognized by Dutton (1996, Equations 5 and 7) and compared to published experimental data for surrogates (BSC 2005, Sections I-2, I-3.3, and I-3.4). The comparisons showed that the temperature-corrected creep expressions derived for Titanium Grade 7 in *Creep Deformation of the Drip Shield* (BSC 2005, Section I-3) over-predict the creep strain as a function of time for analogous materials.

The discussion above shows that rescaling to the yield stress, and application of the activation-energy equation, contribute redundant conservatism to the derived expressions of creep strain as a function of time for 150ºC. These equations (BSC 2005, Equations I-15 and I-22 for Titanium Grades 7 and 24, respectively) were used to calculate time-dependent drip shield deformation. Note that the activation-energy equation was used alone, without rescaling

due to the temperature induced reduction of yield stress, as a more realistic extrapolation of creep rate laws for Titanium Grades 7 and 24 to 150ºC, for investigation of stress relaxation (BSC 2005, Equations I-14 and I-20).

Applying Equation (3) with Q = 30 kJ/mol increases creep strain by a factor of 44 from room temperature to 150ºC, for Titanium Grades 7 and 24 (BSC 2005, for example dividing Equation I-21 by Equation I-19). Rescaling to the yield stress at 150ºC results in an overall increase in the predicted creep strain by a multiple of 2,094 relative to the room temperature creep strain for Titanium Grade 7 and a multiple of 465 for Titanium Grade 24. For Titanium Grade 7, the rescaling factor is calculated by dividing equation I-15 by Equation I-8, and for Titanium Grade 24, by dividing Equation I-22 by Equation I-19 (BSC 2005, Attachment I).

1.2.3 Creep Response at 300°C

To demonstrate that Equations 1 and 2 produce representative results at higher temperatures, modified equations are developed for 300ºC using the more realistic, less conservative approach based on the activation-energy equation alone, and compared with the previous results. The development begins with the same room temperature equations used to derive Equations 4 and 5 (BSC 2005, Equations I-8 and I-19):

$$\varepsilon = 4.87 \times 10^{-24} \sigma^{8.81} t^{0.28} \qquad \text{(Eq. 4)}$$

$$\varepsilon = 7.31 \times 10^{-38} \sigma^{12.15} t^{0.25} \qquad \text{(Eq. 5)}$$

These equations over estimate creep rate compared to independent estimates at room temperature from Ankem and Wilt (2006). For example, for stress equal to 90% of yield (276 MPa and 828 MPa for Titanium Grades 7 and 24, respectively at room temperature) (BSC 2005, Table 5.2-1), accumulated strain at 10,000 years is 103% and 56% for Titanium Grades 7 and 24, respectively, using Equations 4 and 5. These strains significantly exceed predictions by Ankem and Wilt (2006) for Titanium Grades 7 and 24 surrogates, of 81% and 7.4%, respectively (Sections 4.1.2 and 4.2.3).

Prior to initiation of tertiary creep the strain rate decreases with temperature above approximately 150ºC, from dynamic strain aging (Dutton 1996, Section 5.1; BSC 2005, Figure I-4). For the same tensile loading the rate of strain accumulation decreases from approximately 150ºC, up to temperatures of 300ºC or higher. The behavior has been reported for higher purity grades, from different types of tests, by multiple investigators (Dutton 1996, pp. 8 to 10). The behavior will occur in the drip shields for the stress conditions and strain levels predicted. Accordingly, the conservative approach used previously (BSC 2005, Sections I-3 and I-4) to develop creep equations for simulating drip shield deformation (but not for simulating stress relaxation) at 150ºC, is inappropriate for 300ºC. For this response a different approach is used to develop creep equations for 300ºC, for comparison to the equations used by *Creep Deformation of the Drip Shield* (BSC 2005) for calculating creep deformation. Equation 3 is used for temperature extrapolation to 300ºC, without rescaling to the yield stress.

Using Equation 3 with Equations 4 and 5, the creep equations for Titanium Gradse 7 and 24 for 300°C (573 K) are respectively:

$$\varepsilon = 2.01 \times 10^{-21} \sigma^{8.81} t^{0.28} \quad \text{(Eq. 6)}$$

$$\varepsilon = 3.01 \times 10^{-35} \sigma^{12.15} t^{0.25} \quad \text{(Eq. 7)}$$

Equations 1 and 2, which are the conservative approximations of creep strain for Titanium Grades 7 and 24 used for analyses at 150°C, predict greater strains than Equations 6 and 7. Equation 1 overstates Equation 6 by approximately a factor of 5; Equation 3 overstates Equation 7 by about 13%. Accordingly, although the drip shield creep calculations were carried out using creep equations estimated for 150°C, the margin of conservatism in Equations 1 and 2 is sufficient that the results of these calculations provide reasonable representation of creep response at 300°C.

2. COMMITMENTS TO NRC

None.

3. DESCRIPTION OF PROPOSED LA CHANGE

None.

4. REFERENCES

Ankem, R. and Wilt, T. 2006. *A Literature Review of Low Temperature (<0.25*T_{mp}) Creep Behavior of α, α-β, and β Titanium Alloys*. San Antonio, Texas: Center for Nuclear Waste Regulatory Analyses.

ASTM International 2006. *Standard Specification for Titanium and Titanium Alloy Strip, Sheet, and Plate*. Standard B265-06a. West Conshohocken, Pennsylvania: ASTM International.

BSC (Bechtel SAIC Company) 2005. *Creep Deformation of the Drip Shield*. CAL-WIS-AC-000004 REV 0A. Las Vegas, Nevada: Bechtel SAIC Company. ACC: DOC.20050830.0007.

SNL (Sandia National Laboratories) 2008. *Postclosure Analysis of the Range of Design Thermal Loadings.* ANL-NBS-HS-000057 REV 00. Las Vegas, Nevada: Sandia National Laboratories. ACC: DOC.20080121.0002.

RAI Volume 3, Chapter 2.2.1.2.1, Third Set, Number 7:

Show that uncertainty regarding the extent to which the creep strains of Titanium Grade 7 and Grade 29 vary with temperature is adequately accounted for in the creep analysis. This information is needed to verify compliance with 10 CFR 63.114 (e), (f)

Basis: The temperature-dependence of creep is typically quantified by the activation energy for creep, which generally corresponds to the activation energy of the rate-limiting creep deformation mechanism. Literature reviews of low-temperature (less than about one-fourth of the melting temperature) creep of titanium (e.g. Dutton, 1996; Ankem and Wilt, 2006) suggest that there is significant uncertainty regarding the nature of the rate-limiting creep deformation mechanisms (e.g. dislocations thermally overcoming interstitial barriers, intrinsic lattice resistance, nucleation and growth of deformation twins) and, in turn, the activation energy for creep. A broad range of values for the activation energy of creep of titanium has been reported in the literature (e.g. Kiessel and Sinnott, 1953; Stetina, 1969; Thompson and Odegard, 1973)

1. RESPONSE

The temperature dependence of creep processes is a function of the operative creep mechanisms, which in turn, are defined to a large degree by the material's microstructure. The activation energy selected by the project, and the resulting expressions for creep strain and strain rate, conservatively describe the creep response of the titanium alloys of the drip shield and bound the uncertainty.

1.1 TREATMENT OF TEMPERATURE VARIATION IN THE DRIP SHIELD CREEP CALCULATIONS

The temperature of the drip shield is assumed to be 150°C for temperature-dependent material properties (Assumption 3.2.4 in *Creep Deformation of the Drip Shield* (BSC 2005)) for the entire post-closure period of performance. This temperature overestimates drip shield temperature for most of the 10,000 year period following repository closure in the Nominal Scenario. The waste package temperature in an open drift remains below 150°C for approximately 97% of the 10,000 years following repository closure (SNL 2008, Figure 6.3-76[a]), and the drip shield temperature is less than the waste package temperature. In addition, the drip shield temperature of 150°C is considered appropriate for the case of potential drift collapse, which could accompany a low-probability seismic event. In this case, the drip shield could be partially or completely surrounded by rubble. *Multiscale Thermohydrologic Model* (SNL 2008, Section 6.3.17[a] and Figure 6.3-82[a]) was used to conduct a parameter study of the impact of thermohydrologic parameters on the in-drift environment. The results show that the peak waste package temperature in a collapsed drift for the base case, with low thermal conductivity rubble is greater than 200°C for a very brief period of time—less than 200 years—and the waste package temperature drops below 150°C within approximately 600 years after drift collapse for the low thermal conductivity rubble case, even for the "hottest" waste package considered in the

parameter study. These results are for the case of a collapse occurring coincident with the closure of the repository. Given that the drip shield temperature is defined by the waste package temperature (and will generally be slightly lower), it follows that 150°C overestimates the drip shield temperature and is a reasonable value for evaluation of material properties in a collapsed drift over 94% of the 10,000-year period for the worst case scenario of the hottest waste package with an early drift collapse. The relatively short time the drip shield temperature is above 150°C in the worst case scenario will have a negligible effect on analysis of the creep response of the drip shield over the 10,000-year period.

1.2 DISCUSSION OF THE APPROACH TAKEN IN *CREEP DEFORMATION OF THE DRIP SHIELD* RELATIVE TO THE ACTIVATION ENERGIES FOR CREEP DEFORMATION FROM THE LITERATURE

As discussed in the RAI basis statement, a wide range of values for the activation energy of creep of titanium has been reported in the literature. In the study by Kiessel and Sinnott (1953), commercially pure titanium was evaluated (no information on the microstructure or derived expressions for creep strain or strain rate as a function of time is provided) and an activation energy for creep of 138 kJ/mol is given. Stetina (1969) also evaluated commercial purity titanium, presenting an activation energy for creep of 154 kJ/mol at 150°C, but again, no information was provided on either the microstructure or strain rates/creep strains observed. Thompson and Odegard (1973) evaluated Ti-5Al-2.5Sn (Titanium Grade 6, an α-phase alloy) as bar stock, alpha forged, and beta forged. An activation energy for creep of 37 ± 9 kJ/mol was reported. As indicated by Ankem and Wilt (2006) and Dutton (1996), the creep behavior of a material is a function of the operative mechanisms acting to control the creep process, which is a strong function of the microstructure of the material (e.g., grain size, phase structure, etc.). Therefore, drawing conclusions based on a direct comparison of these literature values for activation energy with no information about the material (other than its composition) is not appropriate.

The analysis of creep of the drip shield was conducted for a design according to which the drip shield frame components (e.g., the support beam and the bulkhead) are manufactured of Titanium Grade 24. In the subsequent version of the drip shield design the material of the frame components was changed to Titanium Grade 29. However, the original analyses are considered adequate because Titanium Grade 24 has been shown to be analogous to Titanium Grade 29. Titanium Grades 24 and 29 are both based upon an extra-low-interstitial version of Titanium Grade 5 (Ti-6Al-4V) with the addition of a platinum group metal (PGM) to improve corrosion performance. In the case of Titanium Grade 24, this addition is palladium, while for Titanium Grade 29, it is ruthenium. Microstructurally, there effectively is no difference between the two materials, as the two PGM additions behave similarly in titanium. In terms of mechanical properties, while the minimum allowable yield strength is slightly lower for Titanium Grade 29 (see Table 1 in ASTM B265-06a), the mechanical properties of the drip shield (e.g., alpha-beta processed + solution annealed + artificial aging) will be well in excess of the minimum properties for the Titanium Grade 24 specification, upon which the analyses are currently based. As such, for the purposes of the creep analysis of the drip shield, the two materials are conservatively considered to be identical.

Assumption 3.2.15 of *Creep Deformation of the Drip Shield* (BSC 2005) states that the activation energy for creep for both Titanium Grades 7 and 24 (and therefore Grade 29) is assumed to be 30 kJ/mol. The change in creep rate (or creep strain) due to increase in temperature predicted assuming a creep activation energy of 30 kJ/mol is compared with experimental results in the literature for an alpha phase alloy analogous to Titanium Grade 7 (Kiessel and Sinnott 1953, Figure 12), the results of which are presented in Figure I-3 of *Creep Deformation of the Drip Shield* (BSC 2005). The comparison indicates that the assumed value (30 kJ/mol) provides a good approximation of the temperature effect. Further validation that the calculated creep strains are appropriate (and conservative) is presented in Section I-3.1 of *Creep Deformation of the Drip Shield* (BSC 2005) in which the room temperature creep strains calculated using the expressions developed in that report were illustrated as being comparable to a second set of relevant literature data (Drefahl et al. 1985). This observation further demonstrates the conservative nature of the expressions used in the project analysis, as the material evaluated in the second study had a grain size of 1,000 microns, whereas the grain size of the material used in project data (for Titanium Grade 7) is on the order of 30 microns. Note, as illustrated in the literature (Ankem and Wilt 2006), the creep rate is a strong function of grain size, increasing with increasing grain size.) The change in creep strain due to an increase in temperature for Titanium Grade 5, analogous to Titanium Grade 29, is presented in Figure I-11 of *Creep Deformation of the Drip Shield* (BSC 2005), where the expressions developed in that report are again demonstrated to capture the temperature effect on the creep behavior of an alloy analogous to Titanium Grade 29. Thus the selected drip shield temperature and Titanium Grades 7 and 29 creep activation energies result in expressions for creep strain and strain rate, which conservatively describe the creep response of the drip shields and bound creep activation energy uncertainties.

2. COMMITMENTS TO NRC

None.

3. DESCRIPTION OF PROPOSED LA CHANGE

None.

4. REFERENCES

Ankem, R. and Wilt, T. 2006. *A Literature Review of Low Temperature (<0.25*T_{mp}) Creep Behavior of α, α-β, and β Titanium Alloys*. San Antonio, Texas: Center for Nuclear Waste Regulatory Analyses.

ASTM International 2006. *Standard Specification for Titanium and Titanium Alloy Strip, Sheet, and Plate*. Standard B265-06a. West Conshohocken, Pennsylvania: ASTM International.

BSC (Bechtel SAIC Company) 2005. *Creep Deformation of the Drip Shield*. CAL-WIS-AC-000004 REV 0A. Las Vegas, Nevada: Bechtel SAIC Company. ACC: DOC.20050830.0007.

Drefahl, K.; Wincierz, P.; Zwicker, U.; and Delarbre, P. 1985. "230,000 h Creep Properties of Titanium Produced from Electrolytic and Sponge Material and TiAl6V4 Alloy at 20°C." *Titanium Science and Technology: Proceedings of the Fifth International Conference on Titanium, Congress-Center, Munich, FRG, September 10-14, 1984. [4]*. 2387-2394. Oberrursel, West Germany: Deutsche Gesellschaft fur Metallkunde.

Kiessel, W.R. and Sinnott, M.J. 1953. "Creep Properties of Commercially Pure Titanium." *Journal of Metals, 5,* (2), 331-338. New York, New York: American Institute of Mining and Metallurgical Engineers.

SNL (Sandia National Laboratories) 2008. *Multiscale Thermohydrologic Model*. ANL-EBS-MD-000049 REV 3 ADD 2. Las Vegas, NV: Sandia National Laboratories. ACC: DOC.20080201.0003; LLR.20080403.0162.

Stetina, K. 1969. "Comments on 'On the Deformation Mechanisms in Alpha-Titanium Below 0.4 T_M.'" *Scripta Metallurgica, 3,* 57-58.

Thompson, A.W. and Odegard, B.C. 1973. "The Influence of Microstructure on Low Temperature Creep of Ti-5Al-2.5Sn." *Metallurgical Transactions, 4*, (4), 899-908. New York, New York: Metallurgical Society of American Institute of Mining, Metallurgical, and Petroleum Engineers.

RAI Volume 3, Chapter 2.2.1.2.1, Third Set, Number 8:

Show that the creep analysis has adequately accounted for the effect of alloy microstructure on the extent of creep strain for Titanium Grades 7 and 29. This information is needed to verify compliance with 10 CFR 63.114 (e), (f).

Basis: The extent to which a titanium alloy creeps at a particular temperature and applied stress level depends upon the microstructure of the material. For instance, previous investigations (e.g. Drefahl et al, 1985; Ankem, Greene, and Singh, 1994; Aiyangar et al, 2005) have shown that the amount of creep deformation and the creep deformation mechanisms (e.g. dislocation slip, deformation twinning) in α-titanium alloys, such as Titanium Grade 7, depend upon the grain size of the material. The amount of creep strain may increase significantly with increasing grain size for the same alloy at the same applied stress level. Similar investigations (e.g. Thompson and Odegard, 1973; Miller, Chen, and Starke, Jr., 1987) have shown that the microstructure has a significant effect on the creep deformation in two-phase α-β titanium alloys, such as Titanium Grade 29.

1. RESPONSE

The creep response of both alpha titanium alloys (e.g., Titanium Grade 7) and alpha-beta titanium alloys (e.g., Titanium Grade 29) is a strong function of their microstructure. In the analysis of the creep response of the drip shield (BSC 2005), expressions were developed for Titanium Grades 7 (Section I-3) and 24 (Section I-4) to predict the creep strain as a function of time. Titanium Grade 24 is equivalent mechanically to Titanium Grade 29 as both alloys are essentially Ti-6Al-4V with the addition of a platinum group metal (palladium in the case of Titanium Grade 24 and ruthenium in the case of Titanium Grade 29). A fixed drip shield temperature of 150°C is assumed for all time in that report, and is used in the calculations below. Note: The appropriateness of this assumed temperature is demonstrated in the response to RAI 3.2.2.1.2.1-3-006.) As will be demonstrated, the expressions utilized in the aforementioned analyses provide a highly conservative representation in the case of both alloys and thus have adequately accounted for the effects of microstructure.

1.1 CAPTURING THE EFFECT OF MICROSTRUCTURE ON THE CREEP OF TITANIUM GRADE 7

In alpha titanium alloys, grain size has a large impact on the creep behavior of the material (Ankem and Wilt 2006). As the grain size is increased, the resulting creep strain increases as a function of time at a given stress. The expressions used to describe the creep strains in *Creep Deformation of the Drip Shield* (BSC 2005) were compared to literature data for a coarse grained alpha titanium alloy (Drefahl et al. 1985). This comparison was used as a validation exercise and is presented in Section I-3.1 of *Creep Deformation of the Drip Shield* (BSC 2005). In this comparison, the derived expressions predicted Titanium Grade 7 creep strains that were comparable to the literature values for the coarse grained alpha titanium alloy. This observation demonstrates the conservative nature of the expressions used in the project analysis for capturing the behavior of alpha titanium alloys such as Titanium Grade 7, as the material evaluated in the

example taken from the study by Drefahl et al. (1985) had a grain size of 1,000 microns, whereas the material used in Yucca Mountain Project experiments (for Titanium Grade 7) is on the order of 30 microns. Utilizing the expressions presented in the literature (Ankem and Wilt 2006, p. 4-4), the creep strain after 27 years (the time interval used in the reference) should be over 15 times larger for an alloy with 1,000 micron grains than one with 30-micron grains.

1.2 CAPTURING THE EFFECT OF MICROSTRUCTURE ON THE CREEP OF TITANIUM GRADE 29

For a given combination of temperature and applied stress, alpha-beta titanium alloys are far more resistant to creep than alpha alloys. This is clearly demonstrated in the data summarized by Ankem and Wilt (2006) while exploring surrogate materials for Titanium Grades 7 and 29. Note that the yield strength of Titanium Grade 29 is approximately three times larger than that of Titanium Grade 7, so when comparing the creep behavior at 50% of the yield strength of Titanium Grade 7, that corresponds to approximately 16% of the yield strength of Titanium Grade 29.

To demonstrate the conservatism of the approach taken in *Creep Deformation of the Drip Shield* (BSC 2005), the creep properties predicted for material used by the Project in experimental studies (Titanium Grade 29 which had been alpha-beta processed, solution annealed, and aged) was compared to literature data of a similar material with a comparable thermomechanical history, and therefore a comparable microstructure. Odegard and Thompson (1974) evaluated aged Ti-6Al-4V (Titanium Grade 5—effectively identical to Titanium Grades 24 and 29 in terms of their creep behavior when subjected to similar thermomechanical processing), at a stress of 60% of the yield strength of the material and ambient temperature, which resulted in a creep strain of approximately 2×10^{-5} after 1,000 hours. In *Creep Deformation of the Drip Shield* (BSC 2005), expressions are provided for creep at room temperature, as well as for an increased temperature of 150°C (the relationship used to correct for increased/decreased temperature is also provided). If the creep strain is calculated for the same stress level as used by Odegard and Thompson (1974) using the room temperature expressions and assumed room temperature yield strength of 828 MPa presented in *Creep Deformation of the Drip Shield* (BSC 2005, Equation I-19), a creep strain of 2.4×10^{-4} is obtained. However, as the DOE conservatively assumes that the drip shield temperature is 150°C for all time, the value obtained utilizing the expression developed for a temperature of 150°C (BSC 2005, Equation I-22) is the more appropriate one to compare the literature values obtained at room temperature to (i.e., the creep analysis performed in BSC 2005 never considers that the temperature is anything other than 150°C). Using the expressions derived by the DOE at 150°C and the assumed yield strength of 683 MPa, a creep strain of 1.06×10^{-2} is obtained after 1,000 hours. Thus, for a given thermomechanical history and microstructure, it can be seen that the values obtained via the expressions derived in *Creep Deformation of the Drip Shield* (BSC 2005) are clearly a highly conservative representation of the creep strain as a function of time for Titanium Grade 29, particularly when the assumed temperature is considered.

1.3 SUMMARY

The creep behavior of both of the titanium alloys proposed for the drip shield is controlled to a large degree by their microstructure. As has been illustrated above, the expressions derived for the creep strains as a function of time for Titanium Grades 7 and 29 in *Creep Deformation of the Drip Shield* (BSC 2005) offer a highly conservative estimate of the creep behavior of both materials. As such, the impact that alloy microstructure will have on the creep properties of the drip shield has been adequately addressed in the analysis.

2. COMMITMENTS TO NRC

None.

3. DESCRIPTION OF PROPOSED LA CHANGE

None.

4. REFERENCES

Ankem, R. and Wilt, T. 2006. *A Literature Review of Low Temperature (<0.25*T_{mp}) Creep Behavior of α, α-β, and β Titanium Alloys*. San Antonio, Texas: Center for Nuclear Waste Regulatory Analyses.

BSC (Bechtel SAIC Company) 2005. *Creep Deformation of the Drip Shield*. CAL-WIS-AC-000004 REV 0A. Las Vegas, Nevada: Bechtel SAIC Company. ACC: DOC.20050830.0007.

Drefahl, K.; Wincierz, P.; Zwicker, U.; and Delarbre, P. 1985. "230,000 h Creep Properties of Titanium Produced from Electrolytic and Sponge Material and TiAl6V4 Alloy at 20°C." *Titanium Science and Technology: Proceedings of the Fifth International Conference on Titanium, Congress-Center, Munich, FRG, September 10-14, 1984. 4.* 2387-2394. Oberrursel, West Germany: Deutsche Gesellschaft fur Metallkunde.

Odegard, B.C. and Thompson, A.W. 1974. "Low Temperature Creep of Ti-6Al-4V." *Metallurgical Transactions*, 5, (5), 1207-1213. New York, New York: Metallurgical Society of American Institute of Mining, Metallurgical, and Petroleum Engineers.

RAI Volume 3, Chapter 2.2.1.2.1, Third Set, Number 9:

Show that the creep analysis has adequately accounted for the potential hydrogen uptake into Titanium Grades 7 and 29. Hydrogen may be generated by corrosion reactions on the titanium alloy surfaces. This information is needed to verify compliance with 10 CFR 63.114 (e), (f).

Basis: In the screening analysis for the FEP 2.1.03.04.0B Hydride Cracking of the Drip Shields, DOE stated that hydrogen generated from corrosion reactions may be absorbed into the drip shield titanium alloys (Sandia National Laboratories, 2008, FEP 2.1.03.04.0B). Previous investigations (e.g. Gao and Dexter, 1987; Paton and Thompson, 1982) have shown that increasing the hydrogen content in Ti-6Al-4V and Ti-5Al-2.5Sn may significantly increase the amount of creep deformation. According to the DOE analysis (Sandia National Laboratories, 2008, FEP 2.1.03.04.0B), titanium alloys may absorb greater than 100 parts per million hydrogen in 10,000 years.

1. RESPONSE

1.1 HYDROGEN CONCENTRATIONS ANTICIPATED WITHIN THE DRIP SHIELD MATERIALS

In order for hydrogen uptake by the drip shield to take place, atomic hydrogen must be generated at the drip shield surface due to the cathodic reaction supporting any general corrosion which occurs. The generation of atomic hydrogen on the drip shield surface can take place only if the water reduction reaction (or hydrogen evolution reaction) is a viable cathodic reaction. If water reduction does take place on the metal surface, adsorbed hydrogen will be produced on the surface of the drip shield, and a certain portion of that will be absorbed into the material. This hydrogen must then be able to diffuse into the material, which does not occur at an appreciable rate unless the temperature is greater than 80°C (SNL 2008, p. 6-418). The hydrogen concentrations that will exist within the drip shield materials during the post-closure period of performance will not be sufficiently large to have a detrimental impact on their creep performance.

Three environments were utilized experimentally to define the corrosion performance of titanium under seepage conditions (where general corrosion is anticipated to take place). These include simulated acidic water (SAW), simulated concentrated water (SCW), and simulated dilute water (SDW). The pH values at room temperature for these solutions are 2.8 to 3.9, 10.1 to 10.8, and 8.4 to 10.2, respectively (SNL 2007a, Corrected Table 7), and will not change significantly from 25°C to 90°C. Based upon these values, the reversible potential for hydrogen production, defined as $-1.98\times10^{-4} \times T$ (in K) $\times$ pH ($-0.059 \times$ pH at room temperature) in volts (V) versus the normal hydrogen electrode (NHE) is:

- -0.17 to $-0.23V_{NHE}$ for SAW, -0.61 to $-0.65V_{NHE}$ for SCW, and -0.50 to $-0.61V_{NHE}$ for SDW at 30°C

- −0.18 to −0.26V_{NHE} for SAW, −0.67 to −0.71V_{NHE} for SCW, and −0.55 to −0.67V_{NHE} for SDW at 60°C

- −0.20 to −0.28V_{NHE} for SAW, −0.73 to −0.78V_{NHE} for SCW, and −0.60 to −0.73V_{NHE} for SDW at 90°C.

In order for the water reduction to be a viable cathodic reaction, the electrode potential must be more negative than the reversible potential at a given pH value. Comparing the experimentally determined open circuit potentials for Titanium Grade 7 in these environments (SNL 2007a, Tables 19 and 20), it can be seen that the open circuit potential is, for all cases, more positive than the reversible potential of the water reduction reaction. As such, hydrogen production at the metal surface is not a thermodynamically viable cathodic reaction; the viable cathodic reaction would be oxygen reduction, which would support the corrosion reaction/passive current density on the metal surface. This is consistent with Yucca Mountain Project data for Titanium Grades 7 and 29 exposed to a series of environments similar to those described above at temperatures as high as 150°C where no hydrogen uptake was observed after an exposure period of 1008 hours. Thus, hydrogen uptake will not occur as general corrosion progresses in the anticipated seepage environments, and as such, hydrogen embrittlement due to general corrosion will not take place.

In the basis statement of this RAI, it is noted that an analysis is made in FEP 2.1.03.04.0B (SNL 2008), which suggested that Titanium Grade 29 may absorb greater than 100 parts per million hydrogen in 10,000 years. The analysis which is referenced in that FEP is taken from *Hydrogen-Induced Cracking of the Drip Shield* (SNL 2007b). In performing that analysis, highly conservative assumptions were made. First, the hydrogen absorption efficiency was assumed to be equivalent to what occurs under highly acidic conditions where the protective passive oxide film on the surface of the titanium had been compromised. Second, it was assumed that the only cathodic reaction rate supporting the anodic dissolution of titanium was the hydrogen evolution reaction, an assumption which, as illustrated above, is thermodynamically unrealistic. The sole purpose of that analysis was to provide an upper bound of the hydrogen concentration which could be present to demonstrate the large margin associated with the statement that HIC would not take place. As such, the assumptions used in the HIC analysis (SNL 2007b) are not applicable to the environmental conditions which are actually anticipated to exist for the drip shield.

1.2 IMPLICATIONS OF ANTICIPATED HYDROGEN CONCENTRATIONS ON THE CREEP PROPERTIES OF THE DRIP SHIELD

Appreciable hydrogen will not be introduced into drip shield materials under the anticipated in-drift conditions. The hydrogen contents, then, will likely remain equivalent to the as received concentrations, which have been on the order of 50ppm for the Titanium Grades 7 and 29 materials tested to date. Gao and Dexter (1987) explored the effect of hydrogen on the creep behavior of Ti-6Al-4V (equivalent to Titanium Grade 29 without the ruthenium addition); hydrogen concentrations from 80 to 720 ppm were evaluated. The study demonstrated that there was little impact of 80 ppm hydrogen on the creep behavior of the material. Based upon their results, it is reasonable to conclude that there would be even less of an effect on the creep behavior at the hydrogen concentrations relevant to materials evaluated to date by the Project. In

another literature study (Paton and Thompson 1982), hydrogen concentrations of 111, 186, and 303 ppm were evaluated in an alpha-forged Ti-5Al-2.5Sn alloy. The results from that study indicated that the lowest concentration they evaluated (i.e., 111ppm) had a negligible impact on creep, and that as the hydrogen concentration was increased to 186 ppm, while short term creep strains were increased, long term creep strains (projected for >2,000 hours (Paton and Thompson 1982, Figure 1) were actually lower than that observed for samples with 111 ppm hydrogen. This reduction in creep strain at long times was hypothesized to be the result of obstruction by hydrides in the lattice and by the remaining dissolved hydrogen.

As discussed above, the typical hydrogen concentration in materials evaluated by the project has been on the order of 50 ppm. Thus, based upon the literature discussed in the RAI basis, the hydrogen concentrations that will exist within the drip shield materials will not be sufficiently large to have a detrimental impact on the creep performance, and in fact may reduce creep strains in the long term.

2. COMMITMENTS TO NRC

DOE commits to update the LA as described in Section 3. The change to be made to the LA will be included in a future LA update.

3. DESCRIPTION OF PROPOSED LA CHANGE

The pH values shown in SNL 2007a, Table 7 and SAR Table 2.3.6-1 are incorrect. The pH of the corrosion test solutions have been corrected (SNL 2007a, Corrected Table 7). This same correction will be made to SAR Table 2.3.6-1. In addition, the minimum and maximum values for the parameters shown in the table have been added.

Table 2.3.6-1. Test Solution Compositions

Ion		SDW (mg/L)	SCW (mg/L)	SAW (mg/L)	SSW (120°C) (mg/L)	BSW-11 (mg/L)
K^+	Minimum	3.58×10^1	1.35×10^3	3.25×10^3	—	5.89×10^4
	Average	3.69×10^1	3.48×10^3	3.51×10^3	1.70×10^5	6.04×10^4
	Maximum	3.94×10^1	4.96×10^3	3.86×10^3	—	6.19×10^4
Na^+	Minimum	3.30×10^2	3.36×10^4	3.92×10^4	—	9.45×10^4
	Average	4.10×10^2	3.99×10^4	4.22×10^4	5.84×10^5	9.75×10^4
	Maximum	4.68×10^2	4.36×10^4	4.36×10^4	—	1.01×10^5
Mg^{2+}	Minimum	0.00	0.00	4.99×10^1	—	0.00
	Average	6.62	5.68×10^{-2}	5.31×10^1	0	0.00
	Maximum	2.75×10^1	2.35×10^{-1}	5.72×10^1	—	0.00
Ca^{2+}	Minimum	0.00	1.11	4.95×10^1	—	6.40×10^{-1}
	Average	1.29×10^1	1.90	6.73×10^1	0	6.75×10^{-1}
	Maximum	4.51×10^1	2.74	9.65×10^1	—	7.09×10^{-1}

Table 2.3.6-1. Test Solution Compositions (continued)

Ion		SDW (mg/L)	SCW (mg/L)	SAW (mg/L)	SSW (120°C) (mg/L)	BSW-11 (mg/L)
F^-	Minimum	0.00	1.03×10^3	0.00	—	3.80×10^3
	Average	9.39	1.26×10^3	2.68×10^2	0	3.83×10^3
	Maximum	3.02×10^1	1.48×10^3	7.75×10^2	—	3.85×10^3
Cl^-	Minimum	5.83×10^1	5.42×10^3	2.21×10^4	—	1.13×10^5
	Average	1.12×10^2	6.47×10^3	2.25×10^4	1.54×10^5	1.16×10^5
	Maximum	1.36×10^2	7.56×10^3	2.77×10^4	—	1.18×10^5
NO_3^-	Minimum	4.04×10^1	6.04×10^3	2.37×10^4	—	1.28×10^5
	Average	2.23×10^2	6.77×10^3	2.47×10^4	1.58×10^6	1.31×10^5
	Maximum	7.54×10^2	7.45×10^3	2.53×10^4	—	1.33×10^5
SO_4^{2-}	Minimum	1.55×10^2	1.21×10^4	4.35×10^4	—	1.17×10^4
	Average	2.32×10^2	1.52×10^4	6.00×10^4	0	1.22×10^4
	Maximum	2.96×10^2	1.92×10^4	6.95×10^4	—	1.28×10^4
HCO_3^-	Minimum	1.10×10^1	1.18×10^4	0.00	—	2.82×10^2
	Average	2.09×10^2	2.95×10^4	3.06×10^{-1}	0	3.87×10^2
	Maximum	5.39×10^2	4.28×10^4	9.51×10^{-1}	—	4.92×10^2
Si	Minimum	0.00	1.60×10^1	2.60×10^1	—	4.17×10^2
	Average	6.52	4.39×10^1	4.52×10^1	0	6.16×10^2
	Maximum	2.21×10^1	1.07×10^2	6.77×10^1	—	8.14×10^2
pH	Minimum	8.4	10.1	2.8	5.5	11.0
	Average	9.5	10.4	3.3	6.25	11.1
	Maximum	10.2	10.8	3.9	7	11.2

4. REFERENCES

Gao, G.Y. and Dexter, S.S. 1987 “Effect of Hydrogen on Creep Behavior of Ti-6AI-4V Alloy at Room Temperature.” *Metallurgical Transactions A*. Vol. 18A, 1125-1130.

Paton, N.E. and Thompson, A.W. 1982. “Creep of Hydrogen-Charged Ti-5Al-2.5Sn at Room Temperature.” *Metallurgical Transactions A.* Vol. 13A, 1531-1532.

SNL (Sandia National Laboratories) 2007a, *General and Localized Corrosion of the Drip Shield*. ANL-EBS-MD-000004 REV 02 ADD 01 ERD 02. Las Vegas, Nevada: Sandia National Laboratories.ACC: ACC: DOC.20060427.0002; DOC.20070807.0004; DOC.20071003.0019; LLR.20080423.0006; DOC.20081209.0001

SNL 2007b. *Hydrogen-Induced Cracking of the Drip Shield.* ANL-EBS-MD-000006 REV 02 ADD 01. Las Vegas, Nevada: Sandia National Laboratories. ACC: DOC.20060306.0007; DOC.20070807.0005; DOC.20081209.0003

SNL 2008. *Features, Events, and Processes for the Total System Performance Assessment: Analyses*. ANL–WIS–MD–000027 REV 00. Las Vegas, Nevada: Sandia National Laboratories. ACC: DOC.20080307.0003; DOC.20080407.0009; LLR.20080522.0166.

RAI Volume 3, Chapter 2.2.1.2.1, Third Set, Number 10:

Define the creep strain/stress threshold, and explain the basis of the creep strain/stress threshold above which failure of the drip shield is assumed. This information is needed to verify compliance with 10 CFR 63.114 (e), (f).

Basis: In Sandia National Laboratories (2008), DOE stated that failure of the drip shield is assumed when the creep strain at any point in the drip shield structure reaches the strain corresponding to the onset of tertiary creep. DOE stated that, based on the literature, the onset of tertiary creep occurs at approximately 15% strain (Sandia National Laboratories, 2008, p. 6-566). In Section 2.3.6.8.5 of the SAR, DOE stated a strain of 10% is assumed to collapse the drip shield. Thus, the creep failure criterion is not clear.

1. RESPONSE

DOE has defined the threshold strain for the onset of tertiary creep as 10% in order to accommodate potential uncertainty and provide additional margin relative to the value of 15% typically reported in the literature. DOE has documented the rationale for the selection of a different (lower, and therefore more conservative) creep strain for the onset of tertiary creep, and hence the point at which the drip shield is assumed to collapse, in Assumption 3.2.9 in *Creep Deformation of the Drip Shield* (BSC 2005) and for FEP 2.1.07.05.0B, Creep of Metallic Materials of the Drip Shield.

As summarized in FEP 2.1.07.05.0B (SNL, 2008, p. 6-566), in the literature the onset of tertiary creep has been demonstrated to occur at a creep strain of approximately 15%. As stated in Assumption 3.2.9 of *Creep Deformation of the Drip Shield* (BSC 2005), the onset of tertiary creep is used to define the point at which the drip shield collapses. As presented in Assumption 3.2.9 of *Creep Deformation of the Drip Shield* (BSC 2005), and then summarized in Section 2.3.6.8.5 of the SAR, DOE has assumed a lower value of 10% strain for the onset of tertiary creep to provide an additional level of conservatism to the analysis of when drip shield collapse occurs due to creep.

The creep equations (BSC 2005, Section 5.3.1) used for analysis of the time-dependent deformation of the drip shield are transient, with monotonically-decreasing creep rate. Such a trend is consistent with observations until a time when the critical creep strain corresponding to onset of tertiary creep is reached (if it is ever reached). Tertiary creep is characterized by accelerated creep strains and precedes failure (creep rupture) of the material. Because tertiary creep was not included in the creep equations, the accumulated calculated creep strain in the structure was compared to the assumed threshold of tertiary creep to assess stability of the structure after a certain period of creep. While the literature has indicated that the transition to tertiary creep takes place at a strain of 15%, to add a degree of conservatism, a value of 10% was used for the calculations presented in *Creep Deformation of the Drip Shield* (BSC 2005). An additional level of conservatism is also provided due to the fact that collapse of the drip shield is assumed to occur when 10% creep strain is reached at any point of the structure. As with reaching a stress sufficient to cause yielding at a given point of a structure does not mean

collapse of a structure, the presence of a sufficiently large stress to result in the onset of tertiary creep for a tensile test/sample does not mean that tertiary creep would initiate in the overall structure or that the structure would collapse. As the structure deforms in response to an applied stress, the stresses will redistribute and relax, and the structure will come to some steady state configuration rather than collapse, as demonstrated in *Creep Deformation of the Drip Shield* (BSC 2005).

2. COMMITMENTS TO NRC

None.

3. DESCRIPTION OF PROPOSED LA CHANGE

None.

4. REFERENCES

BSC (Bechtel SAIC Company) 2005. *Creep Deformation of the Drip Shield.* CAL-WIS-AC-000004 REV 0A. Las Vegas, Nevada: Bechtel SAIC Company. ACC: DOC.20050830.0007.

SNL 2008. *Features, Events, and Processes for the Total System Performance Assessment: Analyses*. ANL–WIS–MD–000027 REV 00. Las Vegas, Nevada: Sandia National Laboratories. ACC: DOC.20040915.0010; DOC.20050419.0001; DOC.20051130.0002; DOC.20060731.0005; LLR.20080311.0066.

RAI Volume 3, Chapter 2.2.1.2.1, Third Set, Number 11:

Provide details of the drip shield creep analysis used for the assessment of creep deformation effects on drip shield performance, i.e., the strain and stress distributions in the drip shield components for 10,000 year simulations associated to the six quasi-static loading cases (SAR Section 2.3.4.5.3.3.2). In addition, for the static and dynamic analyses where the drip shield components experience permanent stresses and strains that exceed the creep failure threshold values, provide explanation why the drip shield system does not experience structural failure. This information is needed to verify compliance with 10 CFR 63.114 (e), (f).

Basis: From the information in the FEP screening document, cited references, and Ankem and Wilt (2006), creep failure of the drip shield may occur for stresses and strains that approach or exceed the stresses and strains at yielding of the titanium alloys. Earlier analysis documented in Bechtel SAIC Company (2004) show that stresses in the drip shield components may approach or exceed yield conditions when subjected to the six static loading cases in the Safety Analysis Report Section 2.3.4.5.3.3.2. However, SAR Section 2.3.4.5.3.1 indicates that the impact of creep on drip shield stability under static load of rubble is not significant.

1. RESPONSE

Strain and stress distributions in the drip shield components for 10,000-year simulations associated to the six quasi-static loading cases are presented in Figures 1 through 30 of this response. Sections 1.1 through 1.3 discuss the processes and mechanisms associated with drip shield structural response to static and dynamic loads. A discussion of these processes relative to titanium creep data provided in Ankem and Wilt is given in Section 1.3.2.

1.1 INTRODUCTION

The analyses presented in *Creep Deformation of the Drip Shield* (BSC 2005) provide an assessment of the creep response of the drip shield following exposure to six different rubble load scenarios,and is referenced in SAR Section 2.3.4.5.3.1. Key assumptions (BSC 2005, Section 3) used in the analysis are summarized here. First, in order to ensure the analyses captured the impact that the temperature profile as a function of time would have on the drip shield, a fixed temperature of 150°C (response to RAI_3.2.2.1.2.1-3-006) was used for all temperature dependent properties (e.g., yield strength, creep rates, etc.) throughout the analyses. General corrosion of the drip shield was addressed by assuming a highly conservative 2-mm loss of cross section for the Titanium Grade 7 and 29 components of the structure for all analyses (i.e., the reduction in cross section was assumed to have already taken place—it does not increase with time). Assuming a 2-mm loss of cross section of all the titanium materials is in effect assuming that, at time zero, a depth of corrosion already exists that is far in excess of what might be achieved in 10,000 years for Titanium Grade 7, and on the order of what might result from a corrosion rate approaching the worst case

scenario for Titanium Grade 29 after 10,000 years. Another conservatism in the approach utilized in *Creep Deformation of the Drip Shield* (BSC 2005) is that there is no threshold stress value at which point creep becomes active—it is calculated for all stresses. This is a highly conservative approach, given that the threshold stress values for Titanium Grade 7 are between 35% and 60% of the yield strength and for Titanium Grade 24 between 25% and 50% of the yield strength (Ankem and Wilt 2006, p. xvi).

An important factor that must be considered in evaluating the creep performance of a structure is recognizing that it is, in fact, a structure—and as such is not equivalent to a tensile test specimen. Thus, evaluating the creep performance must take into account not only the peak loads, but the manner in which loads are initially distributed and later redistributed, the impact that deformation of the structure has on the local stresses and strains, and the influence of objects (e.g., rubble) that might be in contact with the structure. A comprehensive discussion of how each of the aforementioned factors, as well as other issues, was accounted for in the creep analyses discussed here is presented in *Creep Deformation of the Drip Shield* (BSC 2005, Section 5). Practically speaking, the implication of this is that one cannot utilize expressions derived for a tensile specimen as in any way indicative of the overall behavior of a structure. Thus, analyses such as those presented by Ankem and Wilt (2006, Sections 4.1.2 and 4.2.3) are inappropriate for the assessment of the behavior of a complex structure such as the drip shield.

The analysis of creep of the drip shield (BSC 2005) was conducted for a design in which the drip shield frame components (i.e., the support beam and the bulkhead) are manufactured of Titanium Grade 24. In the subsequent version of the drip shield design the material of the frame components was changed to Titanium Grade 29. However, the original analyses are considered adequate because Titanium Grade 24 can be assumed to be analogous to Titanium Grade 29 because both are based upon an extra-low-interstitial version of Titanium Grade 5 (Ti-6Al-4V) with the addition of a platinum group metal (PGM) to improve corrosion performance. In the case of Titanium Grade 24, this addition is palladium, while for Titanium Grade 29, it is ruthenium. Microstructurally, there should be effectively no difference between the two materials, as the two PGM additions behave similarly in titanium. In terms of mechanical properties, while the minimum allowable yield strength is slightly lower for Titanium Grade 29, the mechanical properties of the material that will likely be used for the drip shield (e.g., alpha-beta processed + solution anneal + artificial aging) are well in excess of the minimum properties for the Titanium Grade 24 specification, upon which the analyses are currently based. (The impact assessment for the difference in yield and ultimate strength between Titanium Grades 29 and 24 are provided in *Mechanical Assessment of Degraded Waste Packages and Drip Shields Subject to Vibratory Ground Motion* (SNL 2007, Section 4.1.5). As such, for the purposes of the creep analysis of the drip shield, the two materials are considered to be equivalent.

The details of the drip shield analysis and the results are presented in *Creep Deformation of the Drip Shield* (BSC 2005). The stress and strain distributions for all six load realizations from those analyses are included in this response. The results of the creep simulations indicate that creep deformation for 10,000 years will not cause failure of the drip shield. This conclusion appears to be in contradiction with calculated creep strains based on simple

formulas using the initial stress state in the drip shield (Ankem and Wilt 2006). This response provides the explanation of the apparent discrepancy between the two approaches, and justification of the approach used by the DOE.

The creep failure is typically formulated in terms of strain, and not in terms of stress. If the loading condition is such that stress remains permanent, the time of failure can be estimated based on stress using an expression for creep strain as a function of time. Although the load on the drip shield structure surrounded by rubble is conservatively assumed to be permanent, the stresses in the structure cannot be assumed to be permanent. Thus, time to creep failure cannot be estimated based on stresses. More detailed discussion is provided in Section 1.3. None of the tensile plastic strains after static and dynamic analyses exceed the creep failure threshold values. The discussion provided in this response explains why subsequent creep deformation will not cause structural failure of the drip shield.

1.2 STRESS AND STRAIN DISTRIBUTIONS

Details of the stress and strain distributions in the drip shield calculated after instantaneous deformation (stresses only) and after simulation of 10,000 years of creep (stresses and strains) are shown in Figures 1 to 30. In the analysis, for an assumed temperature of 150°C, the yield strengths for Titanium Grades 7 and 24 were 176 and 683 MPa (BSC 2005, Table 5.2-1), respectively. The average pressure values are presented for six rubble load realizations in Table 1 (BSC 2005, Table 5.2-2).

Table 1. Average Pressure Values on the Drip Shield for Quasi-Static Loading Cases (rock size 0.2 m)

Realization	Pressure (kPa)		
	Left	Top	Right
1	41.54	108.91	58.76
2	19.15	147.07	19.33
3	31.35	154.81	6.69
4	57.23	129.75	128.81
5	69.69	112.73	105.43
6	32.97	113.87	52.19
Average	41.99	127.86	61.87

The results for load realization 1 are in Figures 1 to 5; for load realization 2 are in Figures 6 to 10; for load realization 3 are in Figures 11 to 15; for load realization 4 are in Figures 16 to 20; for load realization 5 are in Figures 21 to 25; and for load realization 6 are in Figures 26 to 30. All of the results are shown in the vertical cross-section normal to the drip shield axis through the middle of the bulkhead and the support beam. Thus, the cross-section includes the portion of the drip shield plates (Titanium Grade 7) and the components of the drip shield frame (Titanium Grade 29). The drip shield stress states and the deformed configurations after instantaneous deformation due to six load realizations presented here are the same as

those calculated and reported in *Structural Stability of a Drip Shield Under Quasi-Static Pressure* (BSC 2004, Attachment II and Figures III-1, III-2, and III-4).

As discussed in *Creep Deformation of the Drip Shield* (BSC 2005, Section 5.4.3) and in Section 1.3, none of the six load realizations fails after 10,000 years of creep. That conclusion is further confirmed by the contour plots of creep shear strains after 10,000 years of creep in Figures 5, 10, 15, 20, 25, and 30. (The effective strain, which is typically compared with the threshold or failure strain in assessment of metal failure, is obtained by multiplying the creep shear strain contoured in the figures by $\sqrt{4/3}$. The discussion of different strain invariants and effective strain is provided in *Mechanical Assessment of Degraded Waste Packages and Drip Shields Subject to Vibratory Ground Motion* (SNL 2007, Section 6.5.1.2.3). The discussion is provided for Alloy 22, but is equally applicable to titanium.) All calculations show the creep strains less than 5% (BSC 2005, Table 5.4-1). Ankem and Wilt recognize a dearth of data specific to creep characterization (onset of creep and rupture strain limit) for Titanium Grades 7 and 24. This is addressed in the DOE model by conservatively establishing the onset of tertiary creep and rupture strain as 10% (BSC 2005, Section 5.4.1.2). Further discussion is located in Sections 1.3.2 and 1.3.3.

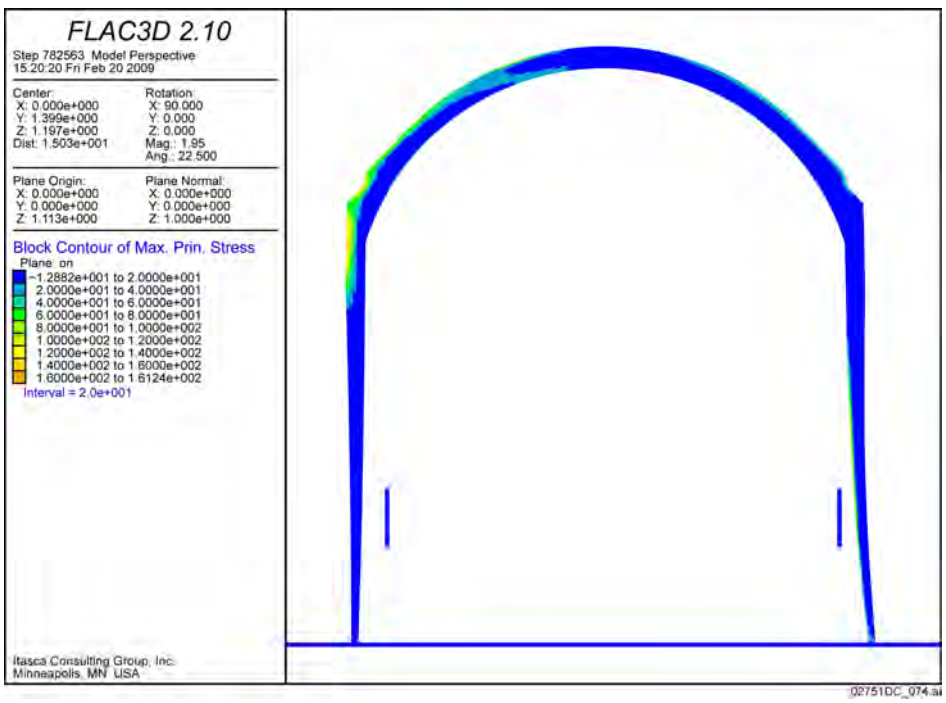

Figure 1. Realization 1: Maximum Principal Stress (MPa) after Instantaneous Deformation

Figure 2. Realization 1: Minimum Principal Stress (MPa) after Instantaneous Deformation

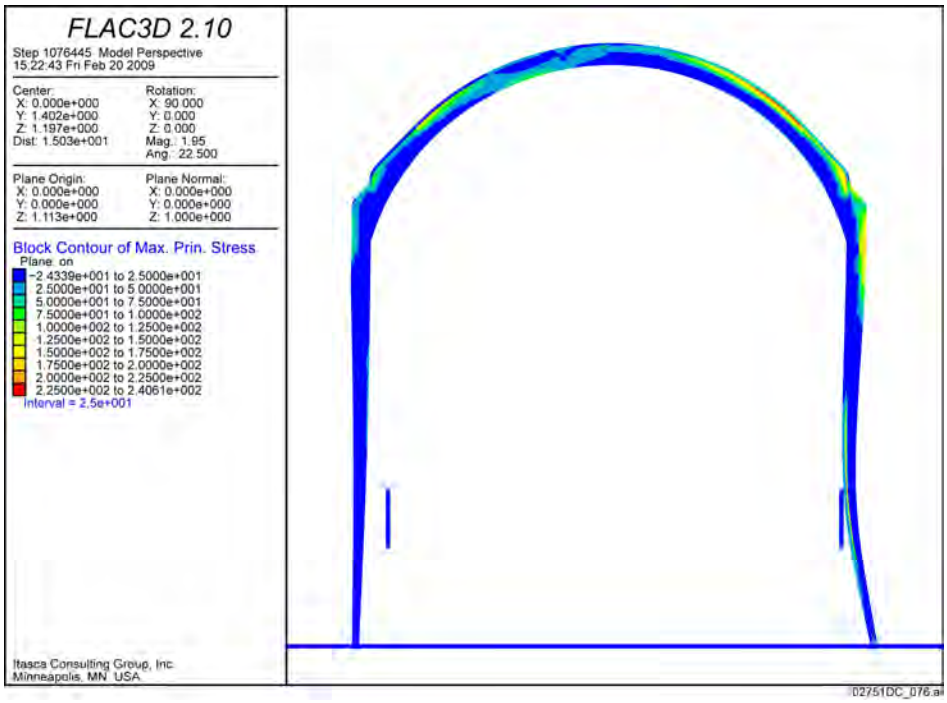

Figure 3. Realization 1: Maximum Principal Stress (MPa) after 10,000 Years of Creep

Figure 4. Realization 1: Minimum Principal Stress (MPa) after 10,000 Years of Creep

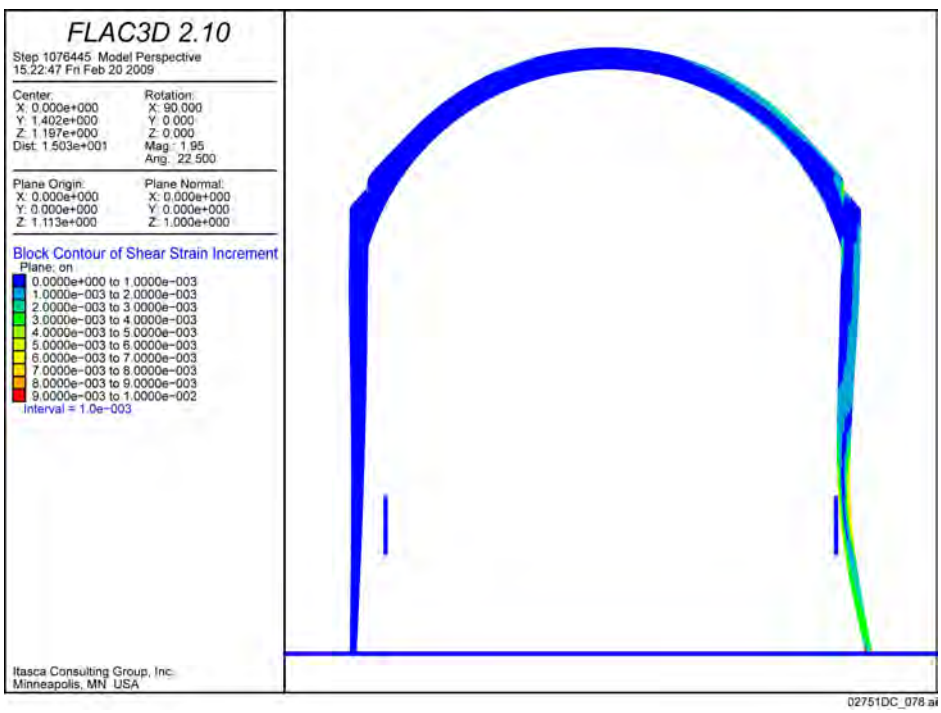

NOTE: The effective strains are obtained by multiplying the shear strains shown in the figure by $\sqrt{4/3}$. For better resolution, the maximum of the contoured range is set to 0.01. The maximum shear strain is 0.037 at the base of the right leg.

Figure 5. Realization 1: Creep Shear Strain after 10,000 Years of Creep

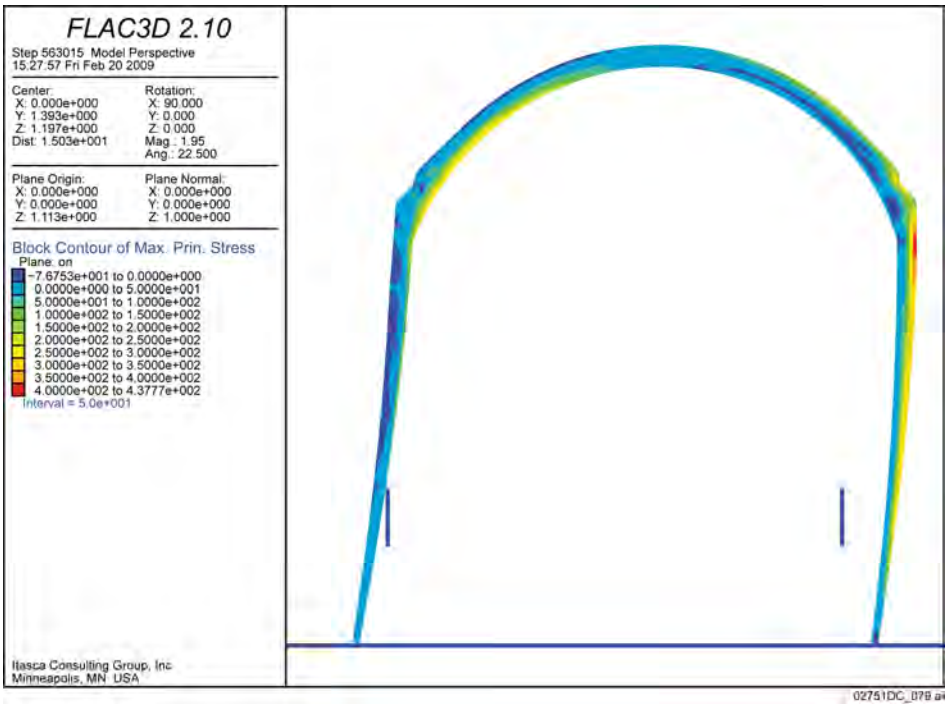

Figure 6. Realization 2: Maximum Principal Stress (MPa) after Instantaneous Deformation

Figure 7. Realization 2: Minimum Principal Stress (MPa) after Instantaneous Deformation

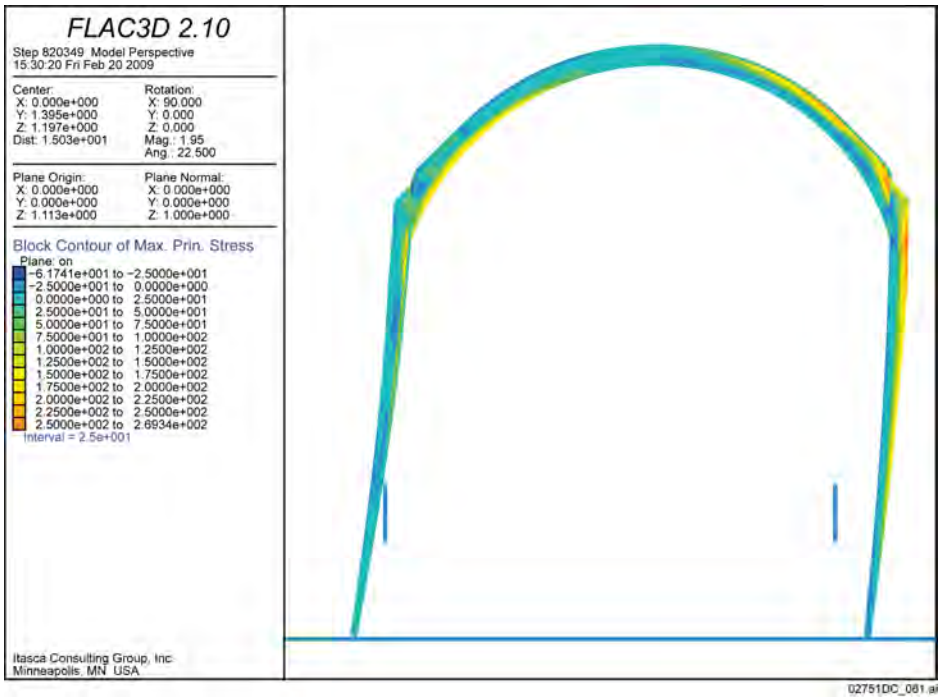

Figure 8. Realization 2: Maximum Principal Stress (MPa) after 10,000 Years of Creep

Figure 9. Realization 2: Minimum Principal Stress (MPa) after 10,000 Years of Creep

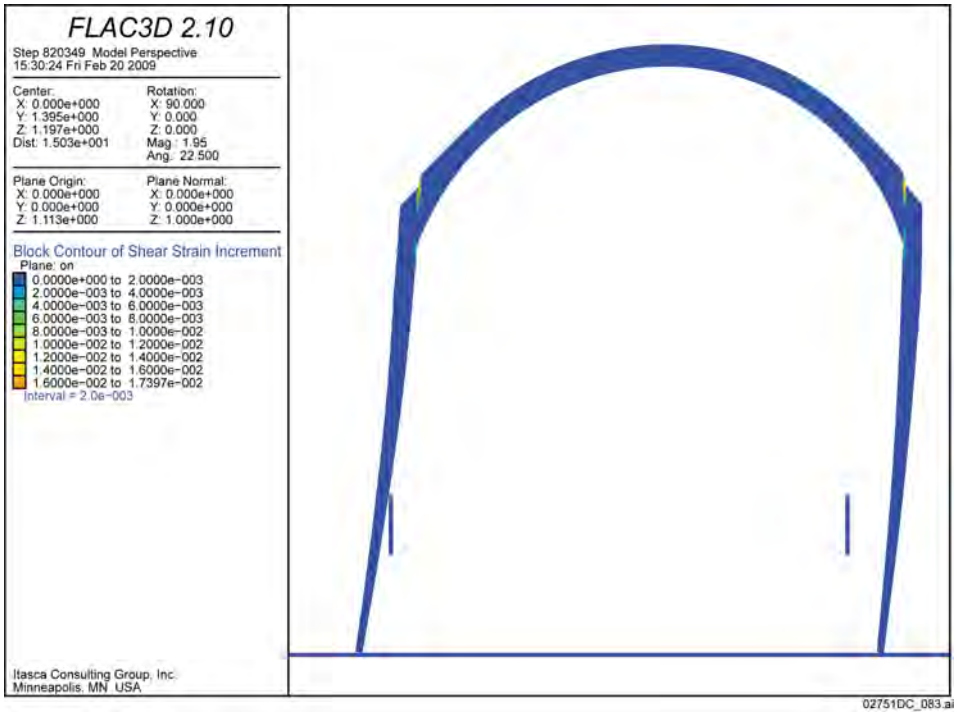

NOTE: The effective strains are obtained by multiplying the shear strains shown in the figure by $\sqrt{4/3}$.

Figure 10. Realization 2: Creep Shear Strain after 10,000 Years of Creep

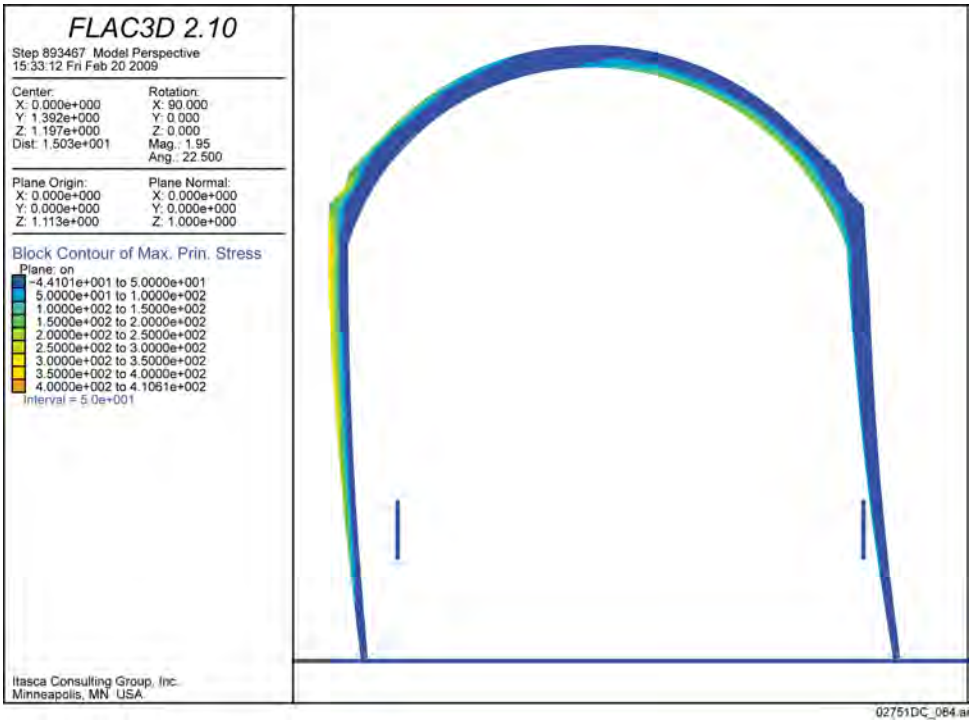

Figure 11. Realization 3: Maximum Principal Stress (MPa) after Instantaneous Deformation

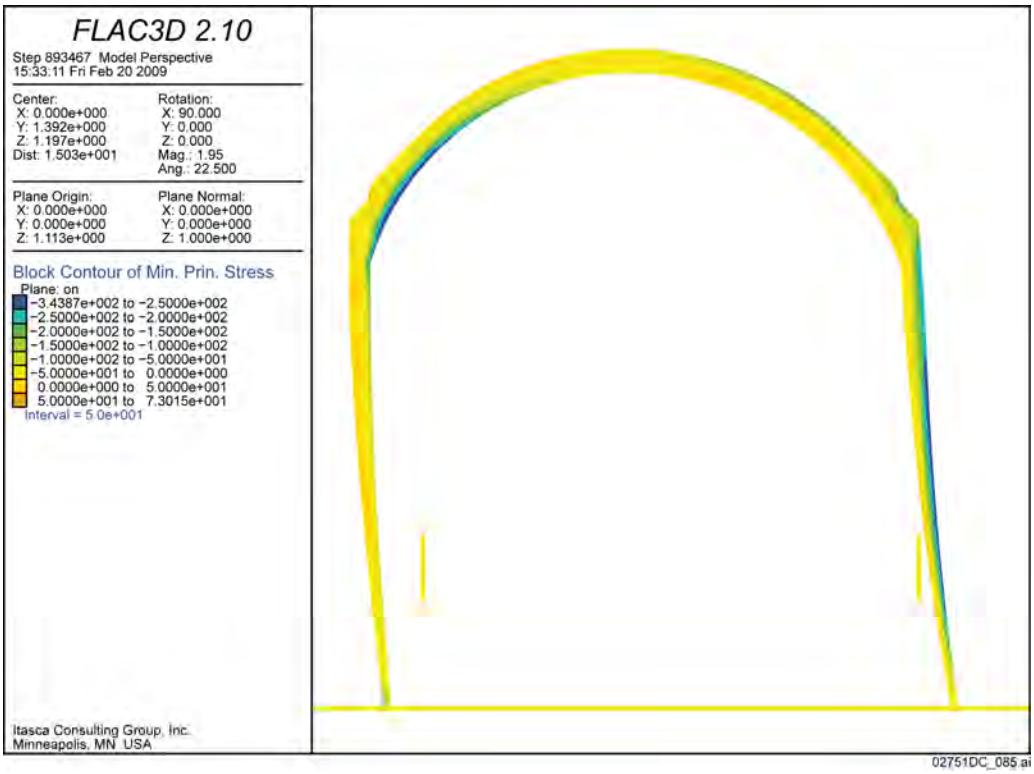

Figure 12. Realization 3: Minimum Principal Stress (MPa) after Instantaneous Deformation

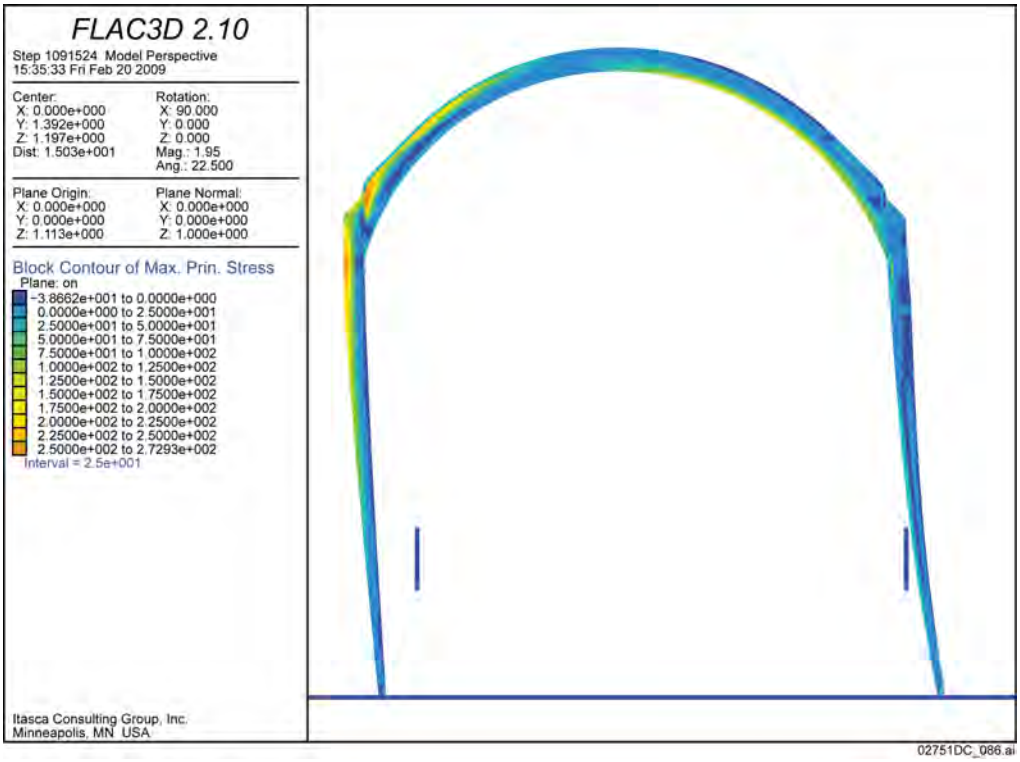

Figure 13. Realization 3: Maximum Principal Stress (MPa) after 10,000 Years of Creep

Figure 14. Realization 3: Minimum Principal Stress (MPa) after 10,000 Years of Creep

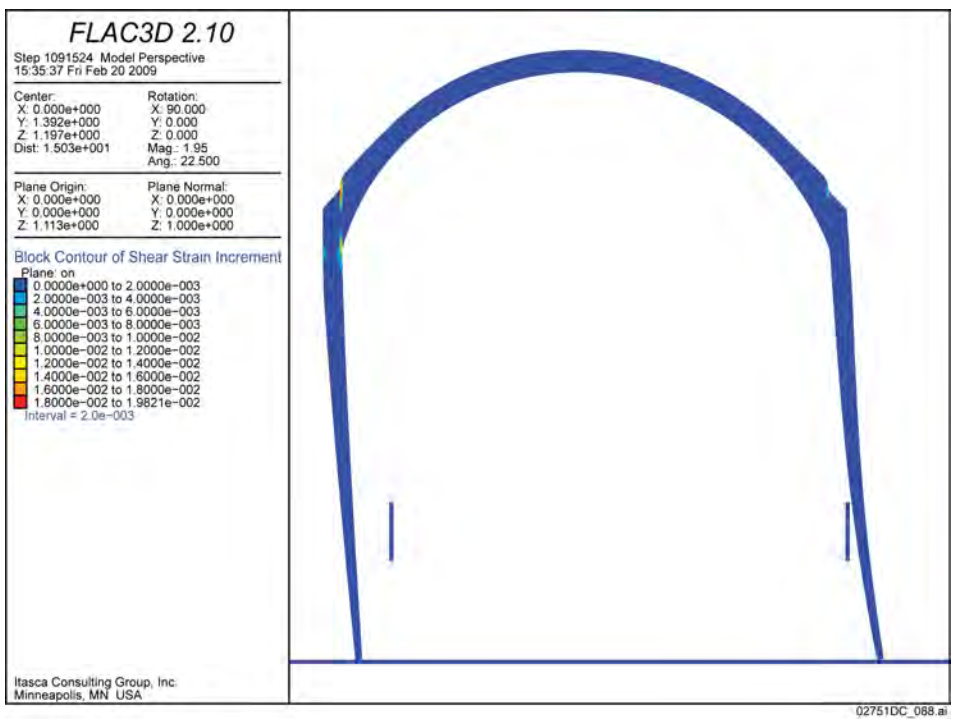

NOTE: The effective strains are obtained by multiplying the shear strains shown in the figure by $\sqrt{4/3}$.

Figure 15. Realization 3: Creep Shear Strain after 10,000 Years of Creep

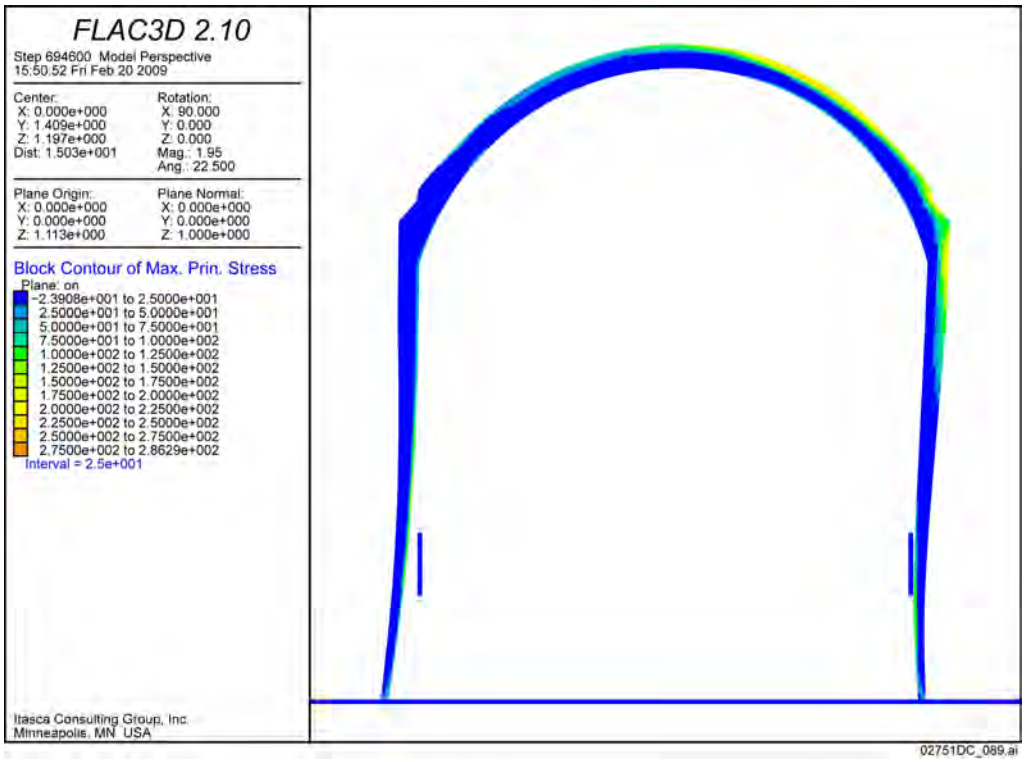

Figure 16. Realization 4: Maximum Principal Stress (MPa) after Instantaneous Deformation

Figure 17. Realization 4: Minimum Principal Stress (MPa) after Instantaneous Deformation

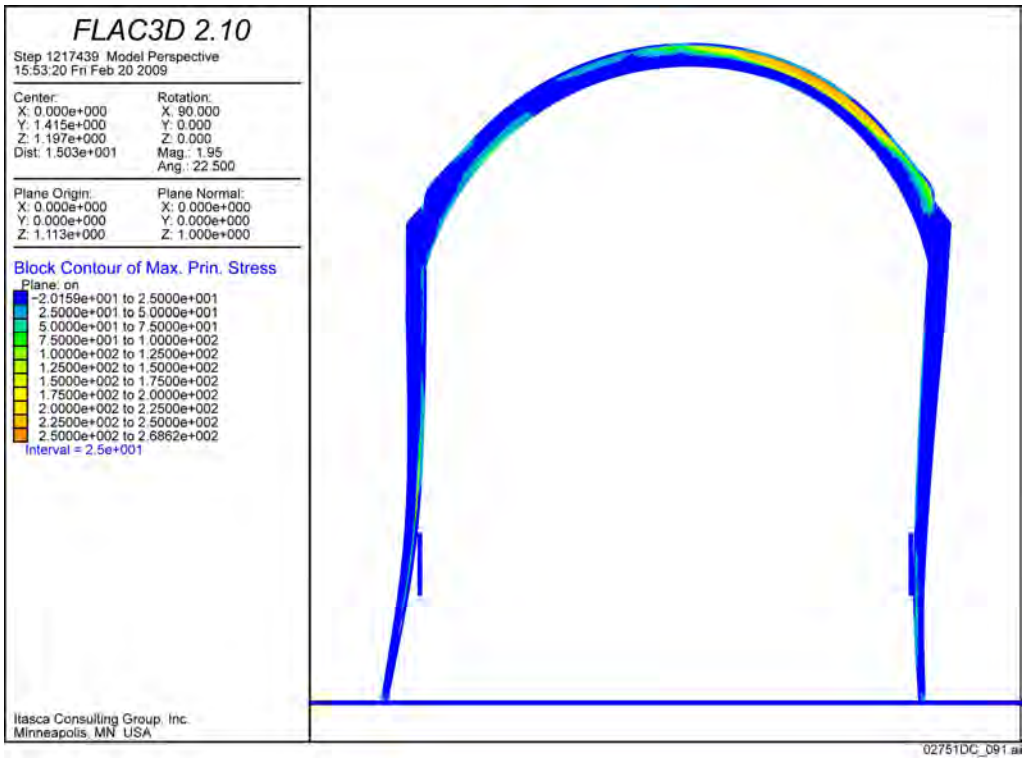

Figure 18. Realization 4: Maximum Principal Stress (MPa) after 10,000 Years of Creep

Figure 19. Realization 4: Minimum Principal Stress (MPa) after 10,000 Years of Creep

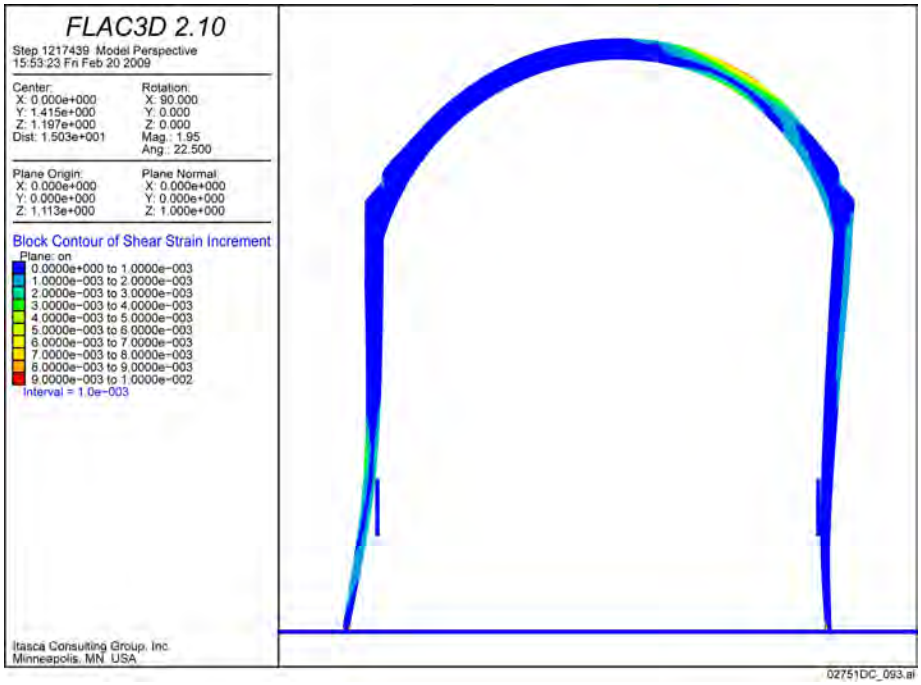

NOTE: The effective strains are obtained by multiplying the shear strains shown in the figure by $\sqrt{4/3}$. For better resolution, the maximum of the contoured range is set to 0.01. The maximum shear strain is 0.027 at the base of the right leg.

Figure 20. Realization 4: Creep Shear Strain after 10,000 Years of Creep

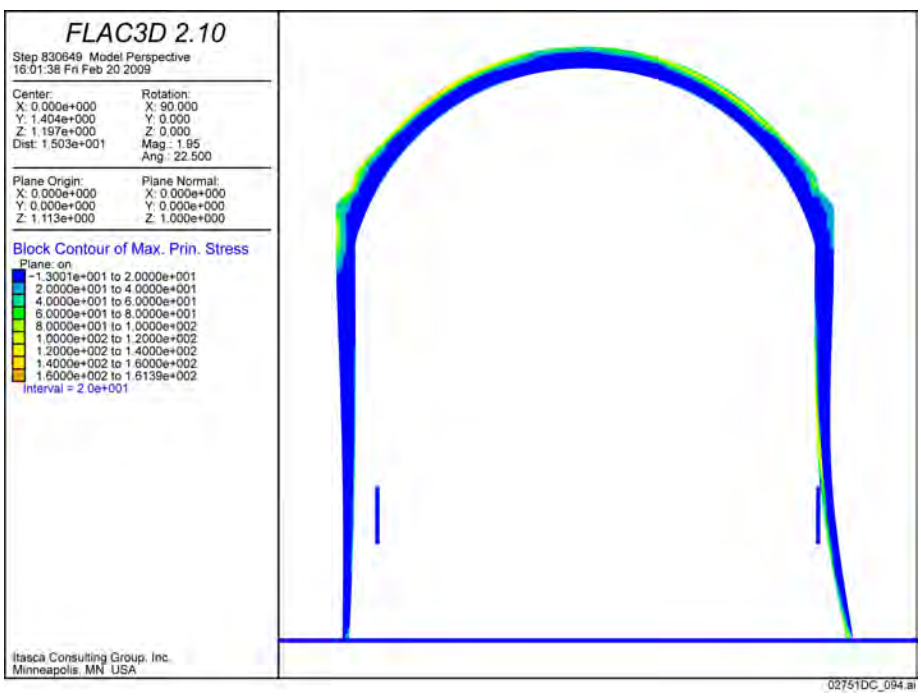

Figure 21. Realization 5: Maximum Principal Stress (MPa) after Instantaneous Deformation

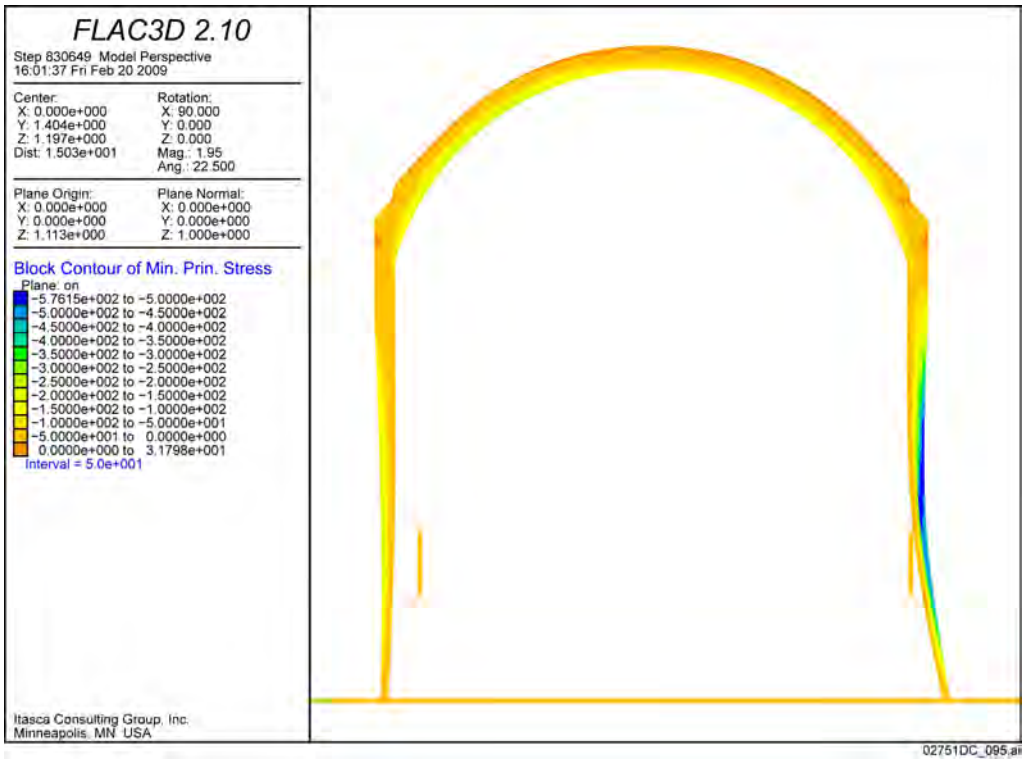

Figure 22. Realization 5: Minimum Principal Stress (MPa) after Instantaneous Deformation

Figure 23. Realization 5: Maximum Principal Stress (MPa) after 10,000 Years of Creep

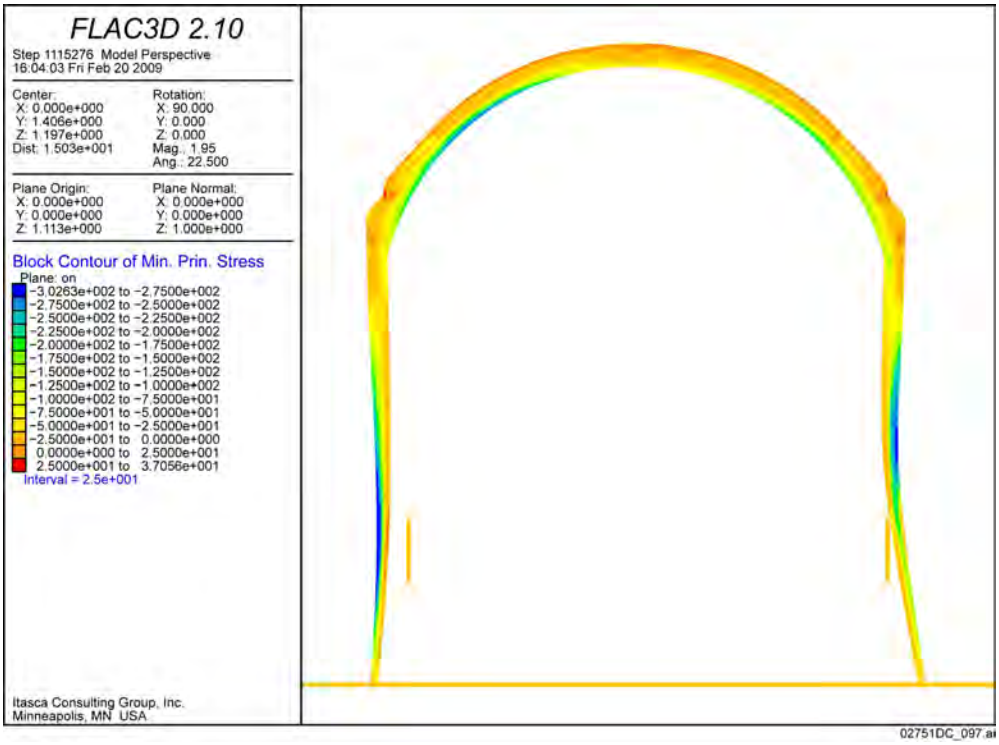

Figure 24. Realization 5: Minimum Principal Stress (MPa) after 10,000 Years of Creep

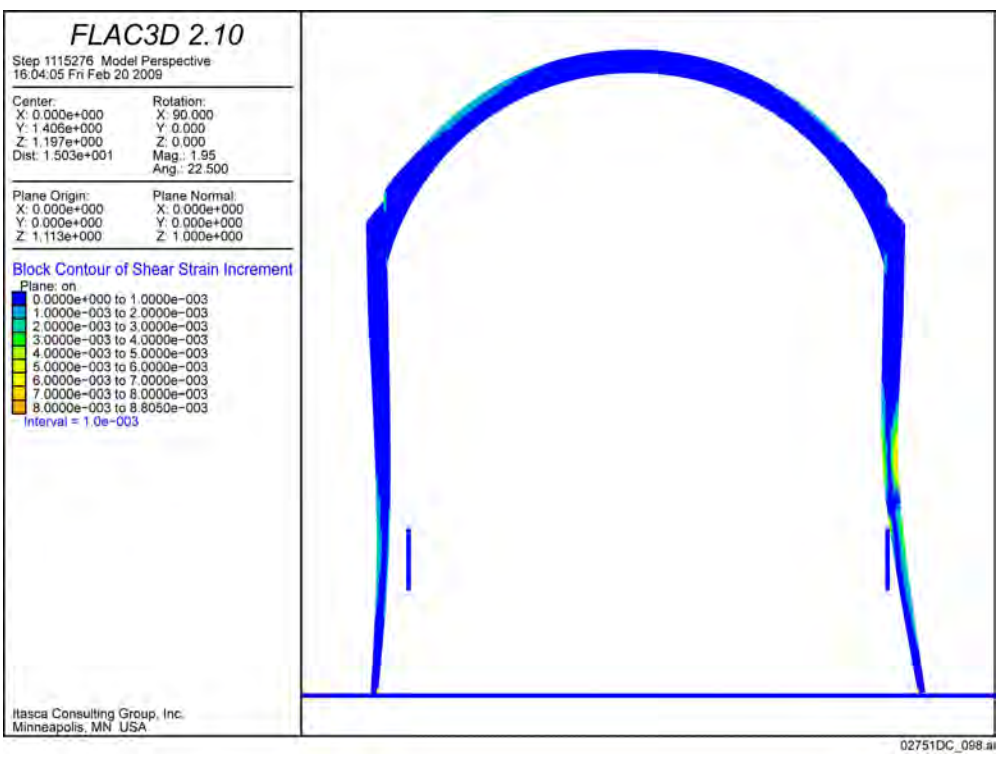

NOTE: The effective strains are obtained by multiplying the shear strains shown in the figure by $\sqrt{4/3}$.

Figure 25. Realization 5: Creep Shear Strain after 10,000 Years of Creep

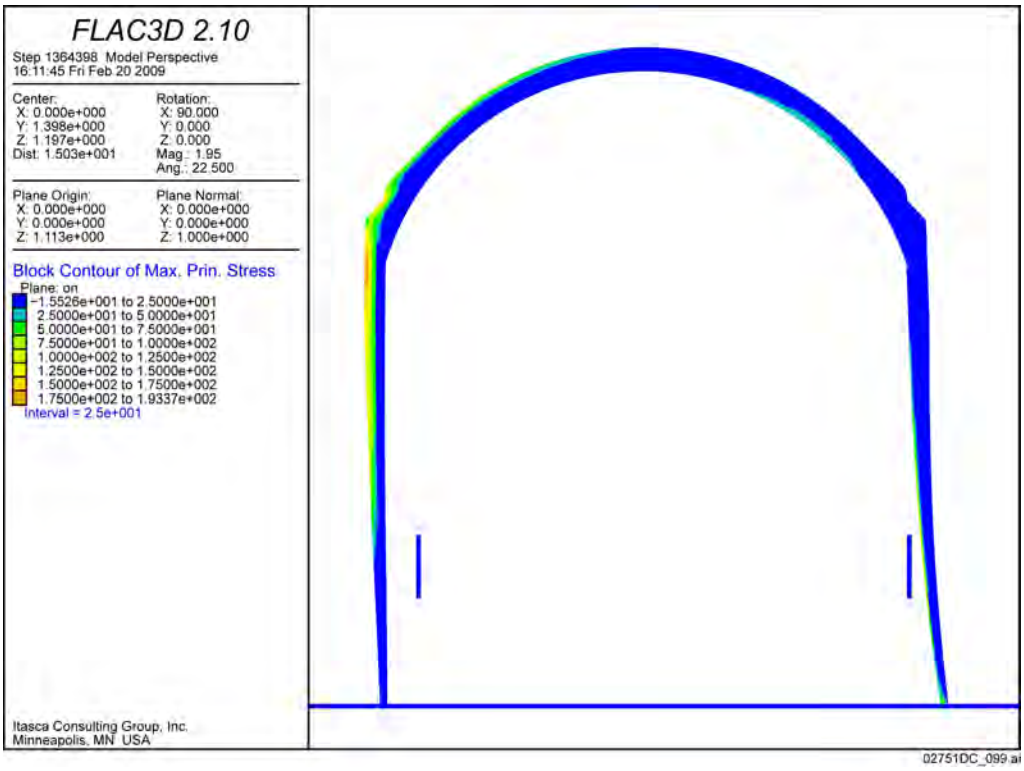

Figure 26. Realization 6: Maximum Principal Stress (MPa) after Instantaneous Deformation

Figure 27. Realization 6: Minimum Principal Stress (MPa) after Instantaneous Deformation

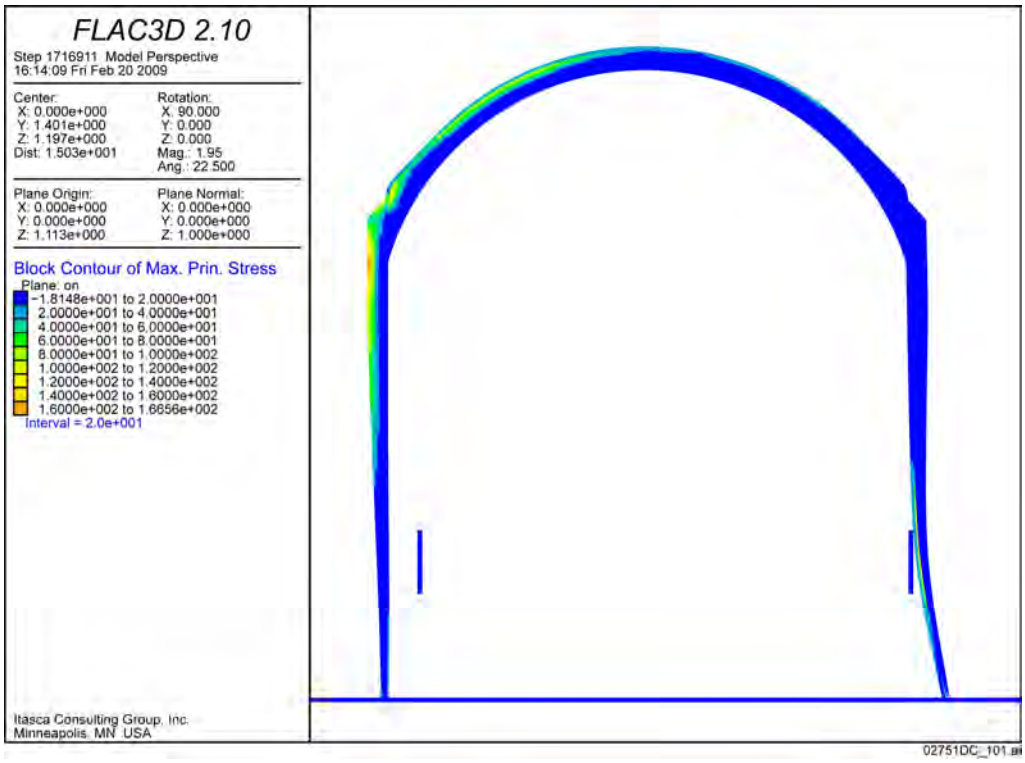

Figure 28. Realization 6: Maximum Principal Stress (MPa) after 10,000 Years of Creep

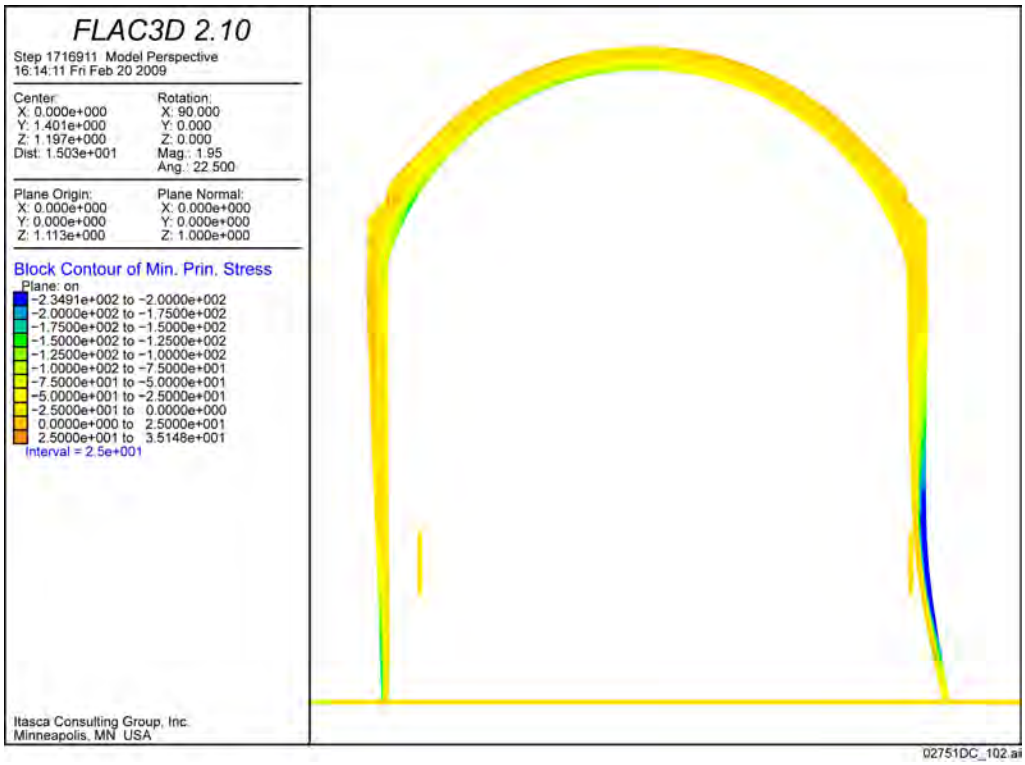

Figure 29. Realization 6: Minimum Principal Stress (MPa) after 10,000 Years of Creep

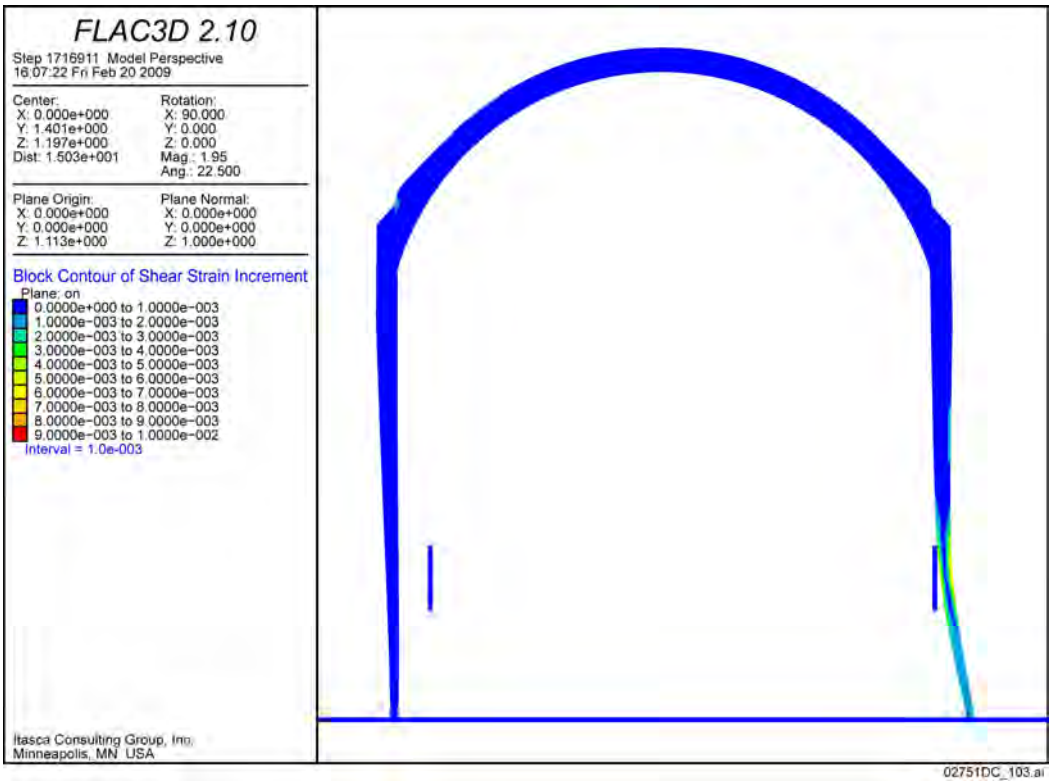

NOTE: The effective strains are obtained by multiplying the shear strains shown in the figure by $\sqrt{4/3}$. For better resolution, the maximum of the contoured range is set to 0.01. The maximum shear strain is 0.026 at the base of the right leg.

Figure 30. Realization 6: Creep Shear Strain after 10,000 Years of Creep

1.3 DISCUSSION

1.3.1 Creep and Relaxation of Drip Shield Stresses Due to Static Rubble Load

The maximum stress in the drip shield after instantaneous deformation due to six load realizations of the rubble load is 438 MPa in realization 2, in the right support beam, near the drip shield shoulder, as shown in Figure 6. That stress is 64% of the Titanium Grade 24 yield strength at 150°C (BSC 2005, Table 5.2-1). Stresses greater than 438 MPa in the drip shield structure under static rubble load are observed only in the case of factor-of-safety calculations (BSC 2004, Figures III-6 through III-20), in which the drip shield stability was analyzed for rubble load when the rubble density was increased 2.5, 3, and 4 times. In the case in which rubble density increased by four times, stresses in the components of the drip shield frame reach and exceed the yield strength of Titanium Grade 24 (BSC 2004, Figures III-17 and III-19). However, the drip shield still reaches the stable configuration (i.e., it reaches equilibrium before strains anywhere in the structure exceed the rupture strains). Because the objective of simulating the cases for increased rubble density was to estimate factor of safety of the drip shield with respect to failure for static rubble load and short-term loading conditions, those cases were not analyzed for creep deformation.

Drip shield stability for six load realizations was evaluated and factor-of-safety calculations were carried out, using a very conservative assumption that all loads applied on the drip shield structure are independent of deformation of the drip shield. Because the drip shield is surrounded by rubble, which is exerting the load on the drip shield, the loads on the drip shield will change as it deforms. (For example, as the drip shield leans on one side, the pressure of the rubble on the drip shield will increase on the side toward which the drip shield leans, while the pressure on the other side will decrease.) The increase in stress arching effect in the rubble and reduction in the rubble vertical load on the drip shield crown were conservatively not considered in all analyses. (Stress arching is the effect by which the stresses in a granular material above a structure are transferred by frictional forces to the abutments, not directly as a dead weight on the structure.) However, the change in the horizontal loads due to rubble back pressure on the drip shield legs as the drip shield leans (i.e., interaction between the drip shield and the rubble accumulated along the drip shield legs) is essential to realism and is evaluated explicitly (BSC 2005, Section 5.4).

Drip shield stability due to creep deformation of titanium was analyzed with and without interaction between the drip shield and rubble accumulated along the drip shield legs (BSC 2005). (Interaction means accounting for change in the rubble pressure on the drip shield legs as the drip shield deforms.) In both cases, the initial equilibrium was calculated assuming no interaction. Different assumptions of interactions were used during the creep part of simulation. The case without interaction between the drip shield and rubble was simulated for illustration purposes only, because it represents very conservative (and unrealistic) loading conditions. For example, rubble load realization 2, for the same initial stress distribution with a maximum of 438 MPa, results in drip shield collapse after 10,000 years of creep when interaction with rubble is not represented (BSC 2005, Figures 5.4-6 and 5.4-7), but remains in a stable configuration when back pressure of rubble along the drip shield legs is accounted for (e.g., Figures 8 through 10). The initial stress state at the onset of creep deformation generally (without considering loading type and boundary conditions) is an inappropriate method for the assessment of the potential for material failure due to creep, even if used as an approximation only. The reason is that despite the fact that active loads on the structure could be permanent, the stresses in the structure will change as a result of creep deformation. As shown in Figures 6 and 8 for rubble load realization 2, the maximum stress has decreased from 438 MPa, after instantaneous deformation, to 269 MPa (which is not at the same location as that of the initial maximum stress), after 10,000 years of creep deformation. The stress history at the point on the drip shield support beam with maximum stress of 438 MPa after instantaneous deformation due to static rubble load is shown in Figure 31. Time-dependent deformation of titanium under loading and boundary conditions of the drip shield surrounded by rubble actually result in relatively quick relaxation of the maximum stress, such that stress drops over approximately 500 years from 438 to 250 MPa. During the remaining time to 10,000 years, the stress at that location gradually increases to 265 MPa. Thus, at that point the stress drops from 64% to 39% of the yield stress. The creep rate, $\dot{\varepsilon}$, which is power function of stress, σ, i.e.:

$$\dot{\varepsilon} \propto \sigma^n \qquad \text{(Eq. 1)}$$

is very sensitive to stress change. A conservative (i.e., ensuring that creep rates are overestimated for different stress levels) fit to experimental data (BSC 2005, Equation I-22) indicates that $n = 12.15$. Consequently the change in stress from 438 to 265 MPa results in a decrease in creep rate of three orders of magnitude.

The creep deformation not only changes the maximum stresses in the structure, but it also changes the stress distribution. While the maximum stress after the instantaneous deformation was in the support beams, the creep deformation caused the maximum stress to migrate into the bulkhead near its connection with the right support beam.

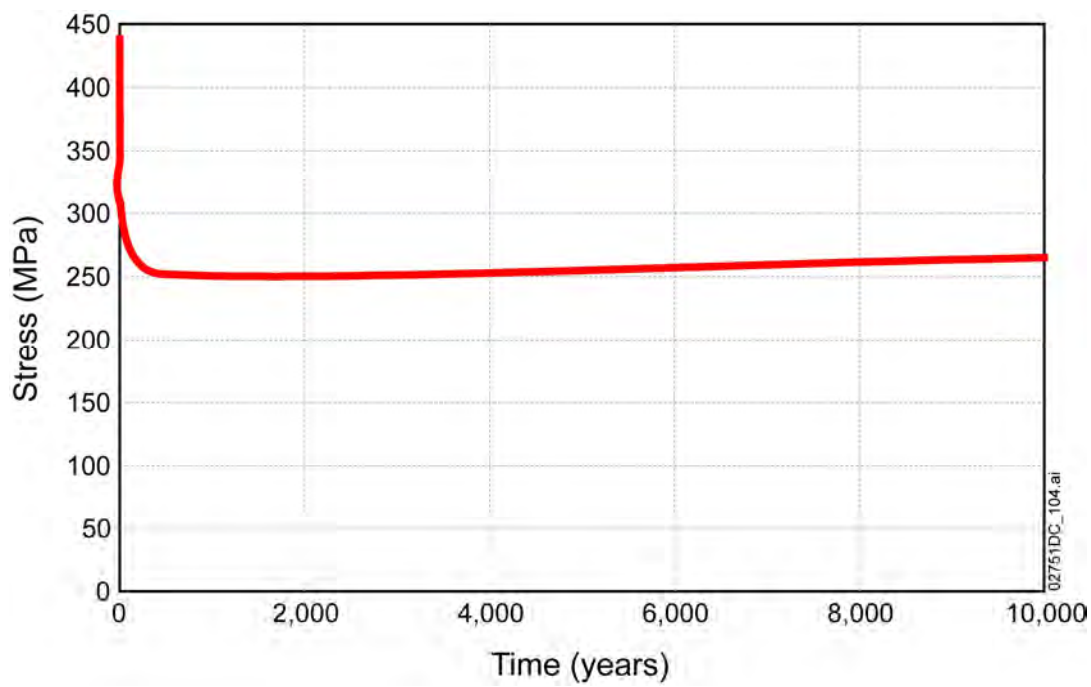

Figure 31. Stress History at the Point with the Maximum Stress of 438 MPa in Load Realization 2

1.3.2 Comparison with Ankem and Wilt (2006)

The creep equation for Titanium Grade 24 at 150°C used in the simulations of creep deformation of the drip shield (BSC 2005, Equation I-22) is:

$$\varepsilon = 3.40 \times 10^{-35} \sigma^{12.15} t^{0.25} \qquad \text{(Eq. 2)}$$

where σ is stress in megapascals, and t is time in hours. Using Equation 2, the creep strain after 10,000 years due to the maximum stress of 438 MPa for load realization 2 is predicted to be 41%. Clearly, this creep equation predicts greater creep strains than those predicted by Ankem and Wilt (2006, p. 4-16) (i.e., 15% of creep strain at stress equal to 90% of the yield stress) (615 MPa for yield stress of 683 MPa, BSC 2005, Table 5.2-1). However, this simple calculation (i.e., using Equation 2) cannot be used to assess the drip shield creep strain because the formula is derived by fitting a line to the test results for a straight specimen subject to uniaxial tension at a given load (and corresponding engineering stress), in which

the applied force is constant and independent of the deformation. The simple formula in Equation 2, and formulas in Ankem and Wilt (2006, Tables 4-1 and 4-5) are applicable to calculation of creep strain only when the loading and boundary conditions are such that engineering stress does not change with time. That certainly is not the case for the drip shield surrounded by rubble. For example, in rubble load realization 2 the maximum stress drops to 250 MPa in less than 500 years. The creep strain after 10,000 years, calculated using Equation 2 for a stress of 250 MPa is only approximately 0.05%.

The other extreme loading condition, compared to the loading condition with constant load, is when the stress is initialized in a beam with fixed ends (such as might exist in a dent caused by rock block impact). In this case, even if the stress is greater than the yield strength, the time-dependent response of the titanium will not cause additional deformation because imposed boundary conditions prevent the deformation. Instead, time-dependent creep internal to the beam will result in relaxation of stresses, or gradual stress reduction with time.

Thus, the initial stress cannot be generally used for estimation of the creep strain as a function of time because it leads to significant overestimation of the creep strain. Although the creep equations used in the analysis of drip shield creep deformation are more conservative than the creep equations recommended by Ankem and Wilt (2006), the estimated creep strains are smaller than the creep strain corresponding to onset of tertiary creep (and, thus, drip shield collapse) because the actual evolution of stresses during deformation is accounted for in the analysis.

1.3.3 Creep and Relaxation of Drip Shield Stresses after Seismically Induced Drift Collapse

When the drip shield is surrounded by the rubble, either resulting from gradual accumulation of rubble in which the drip shield maintains its initial undeformed configuration (i.e., the six static load realizations) or after strong seismic ground motions, that cause both drift collapse and deformation of the drip shield due to its interaction with the rubble during shaking (SNL 2007, Figure 6-63), the rubble acts on the drip shield as an active load but it also provides kinematic constraint. To be able to assess the potential for drip shield failure due to creep deformation and to estimate the time when failure will occur, it is necessary to carry out creep simulations and compare the predicted strains with the strain threshold for onset of tertiary creep. Such analyses have been completed for the six static load realizations (BSC 2005; Figures 1 to 30) and they indicate relatively small creep strains, typically equal to or less than 2%, for 10,000 years (BSC 2005, Table 5.4-1), while the failure strain criterion is established to be 10% (even though the literature indicates that it should be about 15%, see response to RAI 3.2.2.1.2.1-3-010). Where greater strains (in all cases less than 5%) are calculated (i.e., realizations 1, 4, and 60), they are localized at the base of the drip shield leg and are inconsequential to overall drip shield stability and integrity. These calculations show that, even for the conservative assumption of rubble acting as a dead weight on the drip shield crown, creep deformation with time makes the rubble along the drip shield legs act more as a kinematic constraint and less as an active load.

The creep deformation of the drip shield after strong seismic ground motions (cases shown in SNL 2007, Figures 6-60 to 6-62) was not simulated. The typical maximum creep strain that was calculated for static load realizations was less than 2% (Figures 1 to 30). Most likely the maximum creep strain will not accumulate at the location of the maximum strain after seismic loading. During seismic ground shaking the drip shield will be subjected to very complex loading. The permanent, plastic strains do not accumulate at a steady rate. The peak strains are achieved typically during the time of strongest shaking, before the end of seismic shaking. Subsequently the loads that cause maximum plastic strain decrease due to the transient nature of the seismic load. Also, deformation and strain due to contact of a metal structure with fixed and stiff boundaries will result in a reduction of the interaction load. (If a large load develops at the contact between a structure and rigid boundary, the load will decrease as the structure deforms and conforms to the shape of the rigid boundary.) Thus, the cross section with greatest plastic strains at the end of seismic shaking is probably not the location of the greatest active load. However, even adding the maximum creep strain calculated for the static rubble load to the maximum plastic strains from dynamic simulations will not change the characterization of any of the cases (SNL 2007, Section 6.4.4, Figures 6-61 to 6-63, and Table 6-146) from “stable” to “failed”. Note that the failure criterion requires tensile strain. Thus, some cases (SNL 2007, Table 6-146) are characterized as “stable” even though the strains are relatively large (e.g., SNL 2007, Figure 6-62) because those large strains are compressive.

1.4 SUMMARY

The completed creep calculations show relatively small creep strains over 10,000 years. Although the creep equations used in the calculations are more conservative than those used by Ankem and Wilt (2006), the DOE model does not predict creep failure in 10,000 years. The reason is that both static and dynamic loading conditions in the drip shield structure are more complex than uniaxial tension with constant load, which Ankem and Wilt (2006) used to calculate the creep strains as function of time. Conclusions about the stability of drip shields after static and dynamic analyses are not affected by consideration of the subsequent creep deformation because of the stress reduction associated with that deformation.

The analyses shown in BSC (2005) demonstrate that the drip shield can withstand static loads from rockfall, and associated creep deformation, and remain structurally stable. Analyses presented in SAR 2.3.4.5.3.3.2 demonstrate that the drip shield can withstand a range of dynamic loads imposed by seismic excitation of rubble loads. The drip shield creep deformation in these cases does not compromise the drip shield primary role of diverting seepage.

As discussed in the responses to this set of RAIs, the model of creep deformation of the drip shield is appropriate and conservative. The basis for exclusion of FEP 2.1.07.05.0B is appropriate as demonstrated in the response to this RAI by relatively small strain and lack of failure.

2. COMMITMENTS TO NRC

None.

3. DESCRIPTION OF PROPOSED LA CHANGE

None.

4. REFERENCES

Ankem, R. and Wilt, T. 2006. *A Literature Review of Low Temperature (<0.25*Tm) Creep Behavior of* α, $\alpha-\beta$ *and* β *Titanium Alloys.* San Antonio Texas: CNWRA.

BSC (Bechtel SAIC Company) 2004. *Structural Stability of a Drip Shield Under Quasi-Static Pressure*. 000-00C-SSE0-00500-000-00A. Las Vegas, Nevada: Bechtel SAIC Company. ACC: ENG.20040830.0032; ENG.20080312.0017.

BSC 2005. *Creep Deformation of the Drip Shield*. CAL-WIS-AC-000004 REV 0A. Las Vegas, Nevada: Bechtel SAIC Company. ACC: DOC.20050830.0007.

Drefahl, K., Wincierz, P., Zwicker, U., and Delarbre, P. 1985. "230,000 h creep properties of titanium produced from electrolytic and sponge material and TiAl6V4 alloy at 20°C." *Titanium Science and Technology* (G. Lutjering, U. Zwicker and W. Bunk, editors), Deutsche Gesellschaft fur Metallkunde E.V., Germany. TIC: 257549.

Dutton, R. 1996. *A Review of the Low-temperature Creep Behavior of Titanium.* AECL_11544. Pinawa, Manitoba, Canada: Whiteshell Laboratories, Atomic Energy of Canada Limited. TIC: 231204.

SNL (Sandia National Laboratories) 2007. *Mechanical Assessment of Degraded Waste Packages and Drip Shields Subject to Vibratory Ground Motion*. MDL-WIS-AC-000001 REV 00. Las Vegas, Nevada: Sandia National Laboratories. ACC: DOC.20070917.0006; DOC.20080623.0002; DOC.20081021.0001.